5-9-2024

Vascular Electrophysiology and Pathogenic Consequences of Cardiovascular KATP Channel Mutations

Alex Hanson
Washington University in St. Louis

WASHINGTON UNIVERSITY IN ST. LOUIS

Division of Biology and Biomedical Sciences
Molecular Cell Biology

Dissertation Examination Committee:
Colin Nichols, Chair
Robert Mecham, Co-Chair
Daniel Link
Jonathan Silva
Amber Stratman

Vascular Electrophysiology and Pathogenic Consequences of Cardiovascular K_{ATP} Channel Mutations

by
Alex Michael Hanson

A dissertation presented to
Washington University in St. Louis
in partial fulfillment of the
requirements for the degree
of Doctor of Philosophy

May 2024
St. Louis, Missouri

Table of Contents

List of Figures

List of Tables

Acknowledgements

I take great pleasure in thanking Colin Nichols, my research mentor, for his belief in my ability to succeed in his lab, even when I was a medical student who had never stepped foot in a basic science laboratory. During my time in his lab, I grew more than I could have imagined at the outset, and I learned some lessons from Colin that I will take with me forever – in research, and in life. In particular, he helped me realize the value of being practical, and recognizing that learning often happens with your hands, not just your head.

I cannot thank Conor McClenaghan enough for his outpouring of time and energy, regardless of how much he had on his own plate. He taught me how to patch-clamp, how to run a PCR, how to passage cells, and above all how to think like a scientist. I also appreciated his humor and levity, especially when things were hard.

I am grateful to the rest of the Nichols lab members, who are a great community of colleagues – every one of them is generous with their time, eager to help others even if they are in the middle of something, and know how to have a good time. In particular, I would like to thank Theresa Harter, as well as Rob Tryon, for their work over the years managing the lab. They have a knack for knowing the answer to any possible question, and the lab would not function without the work they do.

I would like to thank KC Weng for helping me learn hiPS cell culture and cardiomyocyte differentiation. I thank him and Eve Angsutararux for all their help over at the Silva lab during the past five years.

My sincere thanks to Bob Mecham, Jon Silva, Amber Stratman, and Dan Link for their positive criticism and feedback during our committee meetings. Each one of them has helped shape this project, and provided invaluable guidance on how to spend my time more wisely during the past several years. Additionally, I would like to thank Jon Silva for welcoming me into his lab, as well, which allowed me take my work in exciting new directions.

I am grateful to the WUSM MSTP for supporting my development over the years, and for enabling me to pursue my training as a scientist.

I would not have made it to, let alone through, graduate school without the support of my Mom and Dad, all three of my sisters, and both of my brothers.
Finally, I want to thank Renée, who has supported me during the lowest moments, and motivated and inspired me to reach the highest ones.

Alex Michael Hanson

Washington University in St. Louis
May 2024

ABSTRACT OF THE DISSERTATION

Vascular Electrophysiology and

Pathogenic Consequences of Cardiovascular K_{ATP} Channel Mutations

by

Alex Michael Hanson

Doctor of Philosophy in Biology and Biomedical Sciences

Molecular Cell Biology

Washington University in St. Louis, 2024

Professor Colin G. Nichols, Chair

The complex cardiovascular disorder Cantú Syndrome (CS) arises from gain-of-function (GoF) mutations in either *KCNJ8* or *ABCC9*, the genes encoding the Kir6.1 and SUR2 subunits of cardiovascular ATP-sensitive potassium (K_{ATP}) channels, respectively. CS involves an array of cardiovascular pathologies, including cardiac hypertrophy and hypercontractility, low systemic vascular resistance, and excessively compliant, dilated, and tortuous vessels. Together, the latter features exemplify the hypomyotonic and hyperelastic components of CS vasculopathy. It was recently established that CS vasculopathy drives the associated cardiac pathologies, which are observed even in the absence of cardiac K_{ATP} GoF. In this thesis, I carried out experiments to determine the molecular mechanisms by which K_{ATP} function is altered by several pathogenic CS mutations in distinct structural domains of the TMD2 domain of SUR2: Y985S (YS), G989E (GE), M1060I (MI), R1154Q (RQ), and R1154W (RW). I showed that the cluster of YS/GE/MI substitutions, as well as RQ and RW, augmented Mg^{2+}-nucleotide activation of the K_{ATP} channel. I also tested the responses of these channel variants to

inhibition by the sulfonylurea drug glibenclamide, a potential pharmacotherapy for CS. RQ and RW, which are the two most common CS-associated mutations, significantly decreased glibenclamide potency. CRISPR/Cas9 genome engineering was used to introduce SUR2[R1150Q], the equivalent of human SUR2[R1154Q], to the mouse *ABCC9* gene. As previously seen in mice carrying the CS-associated SUR2[A478V] and Kir6.1[V65M] mutations, both heterozygous and homozygous RQ animals exhibited enlarged hearts, elevated cardiac output, and hypotension, but, surprisingly, there was almost complete loss of SUR2-dependent K_{ATP} in homozygous RQ ventricles. The introduced mutation is located in a putative exon splicing enhancer site at the 3' end of exon 27. Sequencing of SUR2 cDNA from mouse tissues revealed not only the full-length *ABCC9* transcript, but also a novel in-frame deletion of 93 bases (corresponding to the 31 amino acids encoded by exon 28), the latter being present in ~40% and ~90% of transcripts from hetero- and homozygous tissues, respectively. Recombinant expression of SUR2A protein lacking exon 28 resulted in non-functional channels. To determine whether this phenomenon is present in humans, I used RQ and RW CS patient-derived human induced pluripotent stem cells (hiPSCs) to generate novel hiPSC-cardiomyocyte (hiPSC-CM) and hiPSC-vascular smooth muscle cell (hiPSC-VSMC) models for CS. hiPSC-CMs and hiPSC-VSMCs carrying the RQ mutation showed only full-length *ABCC9* transcripts. This was consistent with my analysis of *ABCC9* RNA from primary tissues that had been surgically removed from an RQ patient. Together, these data suggest that aberrant *ABCC9* splicing is specific to the murine model. I then carried out the first electrophysiological analysis of control hiPSC-VSMCs, demonstrating that membrane potential and functional expression of voltage-

gated K^+ (K_v) and L-type Ca^{2+} currents (LTCCs) are very similar to those I measured in native mouse arterial VSMCs, validating hiPSC-VSMCs as an electrical model of human VSMCs. Functional K_{ATP} expression in hiPSC-VSMCs was also consistent with previous studies on native mouse VSMCs, and pinacidil sensitivity demonstrated SUR2 expression. However, both basal and pinacidil-activated K_{ATP} currents were considerably larger in RQ and RW hiPSC-VSMCs. Consistent with lack of cell-autonomous modulation of K_v and LTCCs that I demonstrated in native arterial VSMCs isolated from CS mice, K_{ATP} GoF in hiPSC-VSMCs resulted in membrane hyperpolarization, explaining the hypomyotonic basis of CS vasculopathy. Consistent with the hyperelastic component of CS, increased compliance and dilation was observed in isolated aortae from CS mice, which was associated with increased elastin mRNA expression in these vessels. I then found increased elastin mRNA in CS hiPSC-VSMCs. These results show that increased elastogenesis is driven by genetic K_{ATP} overactivity in the context of CS vasculopathy, which is therefore a cell-autonomous consequence of membrane hyperpolarization.

Chapter 1: Introduction

1.1 K_{ATP} Channels – Discovery, Structure, and Function

1.1.1 Discovery of K_{ATP} Channels

Early in the 1980s, pioneering patch-clamp experiments on cardiomyocytes isolated from guinea pig and rabbit hearts revealed characteristic potassium currents inhibited by ATP. The molecular mediators of these currents were deemed ATP-sensitive K^+ (K_{ATP}) channels, marking the first reported characterization of K_{ATP} (Noma, 1983).

In the following years, plasmalemmal K_{ATP} channels were observed in multiple tissues, including pancreatic β-cells (Ashcroft, Harrison, & Ashcroft, 1984), skeletal muscle (Spruce, Standen, & Stanfield, 1985), neurons (Ashford, Sturgess, Trout, Gardner, & Hales, 1988), smooth muscle (Beech, Zhang, Nakao, & Bolton, 1993), kidney (Hunter & Giebisch, 1988), and epithelial cells (Kunzelmann et al., 1989).

1.1.2 K_{ATP} Channel Structure and Genetic Basis

K_{ATP} channels are hetero-octameric complexes comprising four pore-forming Kir6 subunits, each of which is in association with one regulatory SUR subunit (Figure 1.1) (C. G. Nichols, Singh, & Grange, 2013). Kir6 subunits are encoded by *KCNJ8* (Kir6.1) and *KCNJ11* (Kir6.2), and SUR subunits are encoded by *ABCC8* (SUR1) and *ABCC9* (SUR2) (Figure 1.1A), which are members of the ATP binding cassette (ABC) family of membrane proteins (C. G. Nichols et al., 2013). The architecture of Kir6.1 and Kir6.2 is conserved with other Kir channels, with two transmembrane helices (M1 and M2), as well as a bridging extracellular loop that forms the narrow, ion-selective portion of the pore (Kuo et al., 2003; Tao, Avalos, Chen, & MacKinnon, 2009). Like other *ABCC* family members, SUR proteins contain two six-helix transmembrane domains, TMD1 and TMD2 (Bryan, Vila-Carriles, Zhao, Babenko, & Aguilar-Bryan, 2004). However, in addition, SUR proteins also contain an additional N-terminal TMD0 domain, which comprises 5 transmembrane helices that are key for functional expression of Kir6 (Bryan et al., 2004). SUR proteins

also have two nucleotide binding folds (NBDs): the first (NBD1) between TMD1 and TMD2, and the second (NBD2) after TMD2 (Figure 1.1B), in the cytoplasmic C-terminus (C. G. Nichols, 2006; C.G. Nichols, Koster, Enkvetchakul, & Flagg, 2006).

KCNJ8 and *ABCC9* are adjacent genes on human chromosome 12p12.1 (Chutkow, Simon, Le Beau, & Burant, 1996; Inagaki, Inazawa, & Seino, 1995) while *KCNJ11* and *ABCC8* are located on chromosome 11p15.1 (Inagaki, Gonoi, et al., 1995; Inagaki, Inazawa, et al., 1995) and these subunits are variably expressed to give rise to distinct K_{ATP} channels in different tissues (Figure 1.1) (Flagg et al., 2008; Koster et al., 2006; C. G. Nichols et al., 2013). K_{ATP} heterogeneity is further conferred by variable splicing of SUR isoforms (Chutkow, Makielski, Nelson, Burant, & Fan, 1999; Davis-Taber et al., 2000; Gros et al., 2002); particularly prominent are 2 major splice isoforms of SUR2: SUR2A and SUR2B (Chutkow et al., 1996; Inagaki et al., 1996; Isomoto et al., 1996). K_{ATP} channels in vascular smooth muscle are predominantly composed of Kir6.1 and SUR2B (Aziz et al., 2014; A. Li et al., 2013; C. G. Nichols et al., 2013), whereas SUR2A predominates in cardiac ventricular myocyte K_{ATP} channels (Figure 1.1) (Cole, McPherson, & Sontag, 1991; Suzuki et al., 2002).

1.1.3 Regulation of K_{ATP} Channel Activity

1.1.3.1 Intracellular nucleotides

Free (i.e., not Mg^{2+}-bound) intracellular nucleotides inhibit the K_{ATP} channel, with ATP having the most pronounced effect, although ADP and several other nucleotides are also capable of causing K_{ATP} channel inhibition (Lederer & Nichols, 1989; C. G. Nichols & Lederer, 1990a; Noma, 1983). ATP binds to Kir6.2 in a horseshoe-shaped pocket formed by the residues 182-185 (IFSK) and 332-335 (KFGN) (Lee, Chen, & MacKinnon, 2017). Kir6.1 is slightly less sensitive to ATP inhibition than Kir6.2 (Babenko & Bryan, 2001; Y. Cui, Tran, Tinker, & Clapp, 2002). While K_{ATP} channels are capable of binding to four molecules of ATP, one in each subunit, binding of a single ATP is also sufficient to cause channel closure (Enkvetchakul & Nichols, 2003; Vanoye et al., 2002). Half-maximal

inhibition of rat ventricular K_{ATP} channels has been observed at ATP concentrations in the range of 20-100uM (Findlay, 1988; Lederer & Nichols, 1989; Noma, 1983).

Conversely, magnesium-bound nucleotides activate the K_{ATP} channel – an effect most pronounced for MgADP, but also observed for MgATP (C. G. Nichols & Lederer, 1990b; Proks, de Wet, & Ashcroft, 2013). Activation of K_{ATP} channels by Mg^{2+}-nucleotides is mediated by interactions between the NBDs of the SUR subunit (Gribble, Tucker, & Ashcroft, 1997a; S. Shyng, Ferrigni, & Nichols, 1997). NBD1 interacts with NBD2 to form a MgATP and MgADP binding site potentially capable of MgATP hydrolysis, although the extent to which nucleotide hydrolysis contributes to channel activation remains unclear (Bienengraeber et al., 2000; de Wet et al., 2007; Kuhner et al., 2012; Ortiz, Gossack, Quast, & Bryan, 2013; Ueda, Inagaki, & Seino, 1997; Zingman et al., 2001).

Given that the intracellular ATP:ADP ratio is the major determinant of K_{ATP} channel open probability (P_o), K_{ATP} channels functionally tune membrane voltage (V_m) and cell excitability based on the dynamic metabolic state of the cell (C. G. Nichols et al., 2013).

1.1.3.2 PIP2, pH, and phosphorylation

In addition to the intracellular energy charge, membrane phospholipids such as phosphatidylinositol 4,5-bisphosphate (PIP_2) increase K_{ATP} channel activity via binding to the Kir6 subunits (Baukrowitz et al., 1998; Fan & Makielski, 1997; Quinn, Cui, Giblin, Clapp, & Tinker, 2003; Ribalet, John, Xie, & Weiss, 2005; S. L. Shyng & Nichols, 1998), and this effectively reduces ATP sensitivity of the channel (Enkvetchakul & Nichols, 2003). Accordingly, PIP_2 hydrolysis by phospholipase C (PLC) leads to a reduction in K_{ATP} channel activity (Fan & Makielski, 1997; Hilgemann & Ball, 1996). Moreover, other lipids such as long-chain acyl-coA molecules have also been shown to influence K_{ATP} channel activity (Liu, Hanley, Ray, & Daut, 2001).

K_{ATP} channels also exhibit functional response to intracellular pH, with acidic cytosolic conditions leading to increased K_{ATP} activity (Davies, 1990; Davies, Standen, & Stanfield, 1992; Xu et al., 2001). As with PIP_2, low pH leads to decreased ATP sensitivity,

although the precise underlying molecular mechanisms remain unclear (N. Cui et al., 2006; Wu et al., 2002).

K_{ATP} activation has been observed in response to protein kinase A (PKA)-mediated phosphorylation of smooth muscle and pancreatic K_{ATP}, although the exact phosophorylation sites responsible for this functional effect remain unknown (Beguin, Nagashima, Nishimura, Gonoi, & Seino, 1999; Y. F. Lin, Jan, & Jan, 2000). Furthermore, protein kinase C (PKC) is capable of both inhibiting and activating cardiac ventricular K_{ATP} channels at low and high concentrations, respectively (Light, Allen, Walsh, & French, 1995; Light, Sabir, Allen, Walsh, & French, 1996).

1.1.3.3 Pharmacology

Sulfonylurea drugs are classic K_{ATP} channel inhibitors that act primarily via binding with the SUR subunits (Aguilar-Bryan et al., 1995). Indeed, this functional effect is the basis for the naming of these proteins as “sulfonylurea receptors” (i.e., SUR). However, these compounds are also capable of interacting with the Kir6 subunits; initial reports with recombinant pancreatic-type (i.e., Kir6.2/SUR1) K_{ATP} channels helped establish a biphasic dose-response curve for sulfonylurea drugs, pointing to two distinct binding sites that exhibit differing pharmacological affinities (Gribble & Ashcroft, 1999; Gribble, Tucker, & Ashcroft, 1997b; Hansen et al., 2002). Whereas the Kir6 subunits possess a low-affinity binding site, the SUR subunit contains the characteristic high-affinity binding site (Ashfield, Gribble, Ashcroft, & Ashcroft, 1999; Gribble et al., 1997b). However, there are pronounced pharmacological differences between specific SUR isoforms; whereas K_{ATP} channels comprising either SUR1 or SUR2B exhibit high affinity for glibenclamide, glimepiride, repaglinide, and meglitinide, only SUR1-containing channels show high-affinity response to tolbutamide, gliclazide, chlorpropamide, and nateglinide (Reimann, Dabrowski, Jones, Gribble, & Ashcroft, 2003) – a response that is apparently conferred by SUR1 residue S1237, as indicated by chimera studies and cryo-EM structural reports (Ashfield et al., 1999; Hambrock, Loffler-Walz, Russ, Lange, & Quast, 2001; Hansen et al., 2002; G. M. Martin, Kandasamy, DiMaio, Yoshioka, & Shyng, 2017).

An array of pharmacological K_{ATP} channel activators exists, including SUR2-selective drugs such as pinacidil, minoxidil, nicorandil, and Cromakalim, and SUR1- and SUR2B-selective drugs such as diazoxide (Giblin, Cui, Clapp, & Tinker, 2002; Mannhold, 2004). The specific binding sites underlying these effects remain undefined, although they appear to be separate from the high-affinity binding site of sulfonylurea drugs (Babenko, Gonzalez, & Bryan, 2000; Hambrock et al., 2001; Loffler-Walz, Hambrock, & Quast, 2002; Moreau, Jacquet, Prost, D'Hahan, & Vivaudou, 2000; Uhde, Toman, Gross, Schwanstecher, & Schwanstecher, 1999).

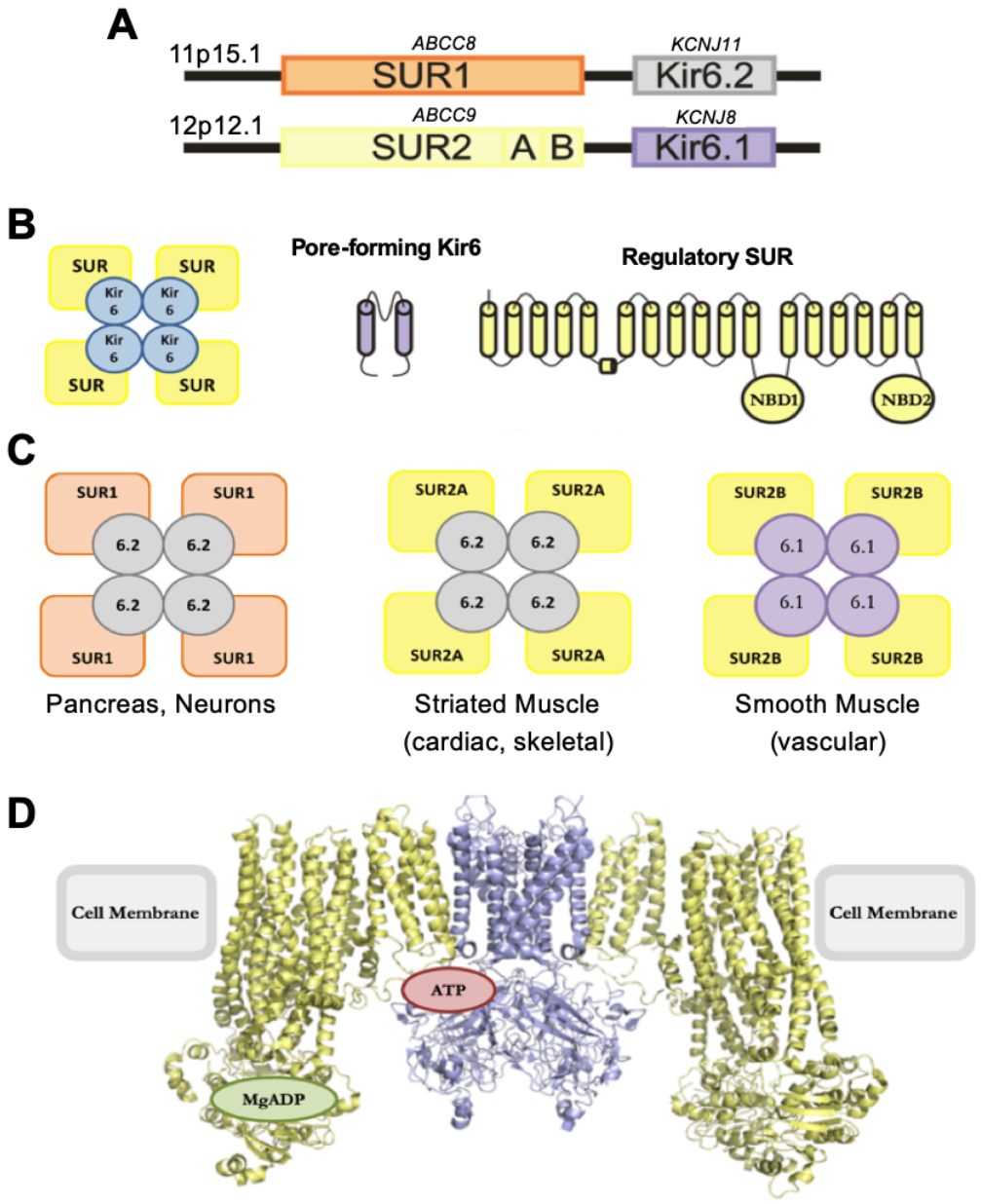

Figure 1.1: Genetic basis, composition, and structure of mammalian K_{ATP} channels. (**A**) Schematic representation of the genes encoding K_{ATP} channels. (**B**) Generic depiction of the hetero-octameric protein complex of the K_{ATP} channel, showing Kir6 tetramer surrounded by four SUR subunits, each containing two nucleotide binding domains (NBD1 and NBD2). (**C**) Illustration of tissue-specific mammalian K_{ATP} channel subunit architecture. (**D**) Cross-section of the K_{ATP} channel structural model, showing the ATP and Mg^{2+}-nucleotide binding sites.

1.2 K_{ATP} Channels in Cardiovascular Myocytes

1.2.1 Cardiomyocytes

Kir6.2 and SUR2A are the predominant isoforms in cardiac ventricular myocyte K_{ATP} channels (Figure 1.1C) (Cole et al., 1991; C. G. Nichols et al., 2013; Suzuki et al., 2002). As with all potassium channels, K_{ATP} channel activation (i.e., opening) in cardiomyocytes leads to K^+ efflux and hyperpolarization of cell membrane potential, which causes action potential shortening and, after 1-15 minutes of maximum K_{ATP} activation, is capable of causing contractile failure (Berlin, Cannell, & Lederer, 1989). Early contractile failure of cardiomyocytes can be delayed or avoided by pharmacological inhibition of K_{ATP} channels or by cellular injection of ATP; therefore, in contrast to the sustained contracture that follows, early contractile failure is due not to SR calcium depletion, but rather to robust activation of cardiac K_{ATP} conductances (Lederer, Nichols, & Smith, 1989). Thus, K_{ATP} channel activity is capable of having dramatic effects on cardiac function, partially as a consequence of being the most highly expressed cardiac ion channel (Foster & Coetzee, 2016a). However, under normal physiological conditions when millimolar ATP levels cause full channel inhibition (Elliott, Smith, & Allen, 1989; Kakei M, 1985; Noma, 1983), K_{ATP} channels appear to play a negligible role in regulating cardiac function, which is supported by findings from genetic knock-out animals (Suzuki et al., 2001; Suzuki et al., 2002) and gain-of-function transgenic animals (Flagg & Nichols, 2001). In general, it is understood that ATP depletion during ischemia causes activation of K_{ATP} channels, which may be cardioprotective by reducing cardiac contractility – a hypothesis that is supported by studies on genetic knock-in mice with cardiac K_{ATP} overactivity (A. J. Nichols, Koster, & Ohlstein, 1990; W. K. Olson et al., 2001; Suzuki et al., 2002).

1.2.2 Vascular Smooth Muscle Cells

K_{ATP} channels in vascular smooth muscle cells (VSMCs) are predominantly composed of Kir6.1 and SUR2B (Figure 1.1C) (Aziz et al., 2014; A. Li et al., 2013; C. G. Nichols et al., 2013). In contrast to other myocytes, contractile VSMCs (i.e., from resistance vessels) exhibit a membrane potential that is relatively depolarized, in the range of ~ -30 to -45 mV, near the activation range for LTCCs (Loutzenhiser, Chilton, & Trottier, 1997; Welsh,

Jackson, & Segal, 1998; Welsh, Nelson, Eckman, & Brayden, 2000). Thus, contractile VSMCs are normally in a partially activated state that is dually responsive to myotonic stimulation or inhibition; small positive membrane voltage (V_m) deflections activate voltage-sensitive LTCCs to increase contractile tone, whereas hyperpolarizing stimuli, such as activation of K^+ channels, shift the V_m away from the activation range of LTC channels, resulting in reduced contractility, in turn causing vasodilation and decreased systemic vascular resistance (Brayden, 2002). Since basal electrical resistance of the VSMC plasma membrane is very high, in the range of 1–10 GΩ, even very small increases in K^+ conductance mediated by only a few K^+ channels can have dramatic effects on VSMC membrane potential and contractility (Nelson, Patlak, Worley, & Standen, 1990). K_{ATP} channels are key determinants of smooth muscle excitability (Bonev & Nelson, 1993; Ko, Han, Jung, & Park, 2008; Nakashima & Vanhoutte, 1995; Nelson, Huang, Brayden, Hescheler, & Standen, 1990; Teramoto, 2006). During hypoxia, activation of vascular K_{ATP} channels is thought to mediate coronary vasodilatory response by the arteries to maintain cardiac blood supply (Daut-J. Maier-Rudolph-W. von Beckerath-N. Mehrke-G. Gunther-K. Goedel-Meinen-L. IN Physiologisches Institut der Technischen Universitat Munchen, 1990). Moreover, K_{ATP} channels play a role in ischemic reperfusion of coronary and cerebral blood vessels (Bari, Louis, & Busija, 1998; Kanatsuka et al., 1992). Several reports have also demonstrated a link between vascular K_{ATP} channel activity and the characteristic vasodilation that occurs in the context of endotoxemia and acidosis (Ishizaka & Kuo, 1996; Kinoshita & Katusic, 1997; Landry & Oliver, 1992).

In contrast to distal resistance vessels, VSMCs that comprise larger, elastic vessels such as the aorta are not understood to be contractile; instead, elastic vessels distend to accommodate cardiac stroke volume during systole, and passively recoil during diastole, thereby delivering a non-pulsatile, laminar flow of blood to distal vessels and capillaries (Wagenseil & Mecham, 2009). This passive function is conferred by the characteristic network of elastic fibers of large proximal vessels, which in turn is produced and deposited by elastogenic VSMCs (Wagenseil & Mecham, 2009). Increased

elastogenesis is a recognized consequence of pharmacological activation of vascular K_{ATP} channels (Fhayli et al., 2019; Hayashi et al., 1994; Knutsen et al., 2018; Tajima, Hayashi, Suzuki, & Nishikawa, 1995). Thus, electrical activity in general, and K_{ATP} activity in particular, are key components of normal VSMC function in elastic vessels as well as resistance vessels, and alterations have been shown to dramatically influence VSMC function in ways that are relevant to disease (Dabertrand et al., 2015; Humphries & Dart, 2015; Jouen-Tachoire, Tucker, & Tammaro, 2021; Welch & Chung, 2022).

1.3 K_{ATP} Channels and Cardiovascular Pathology in Cantú Syndrome

1.3.1 Clinical Features of Cantú Syndrome

Cantú Syndrome (CS) was first described in 1982 in Mexico by Dr. Cantú (Cantu, Garcia-Cruz, Sanchez-Corona, Hernandez, & Nazara, 1982). CS is characterized by a very complex symptomatology (Figure 1.2) predominantly affecting the cardiovascular system, with pathologies including cardiac hypertrophy and hypercontractility, aortic insufficiency, aortic root dilatation, patent ductus arteriosus, pericardial effusion, systemic hypotension, pulmonary hypertension, and striking vascular dilation and tortuosity (Concolino, Formicola, Camera, & Strisciuglio, 2000; Engels et al., 2002; Garcia-Cruz et al., 2011; Garcia-Cruz et al.; Grange, Lorch, Cole, & Singh, 2006; Grange et al., 2019; Kobayashi, Cook, & Williams; Lazalde, Sanchez-Urbina, Nuno-Arana, Bitar, & de Lourdes Ramirez-Duenas, 2000; C. G. Nichols et al., 2013; Robertson et al., 1999; Rosser et al., 1998; Scurr et al.). The latter gross morphological changes to the vasculature correspond to abnormal biomechanical properties, including excessive vascular compliance (Grange et al., 2019; Y. Huang et al., 2018). Thus, CS pathologies encompass a complex array of cardiovascular features, particularly those pertaining to CS vasculopathy.

Although the cardiovascular pathologies are particularly diverse and striking (Figure 1.2A), CS is also characterized by clinical features affecting many other organ systems (Figure 1.2B), including hypertrichosis, lymphedema, distinctive facial features, macrocephaly, skeletal abnormalities, joint hyperextensibility, broncheomalacia, and migraines or severe headache (Concolino et al., 2000; Engels et al., 2002; Garcia-Cruz

et al., 2011; Garcia-Cruz et al.; Grange et al., 2006; Grange et al., 2019; Kobayashi et al.; Lazalde et al., 2000; C. G. Nichols et al., 2013; Robertson et al., 1999; Rosser et al., 1998; Scurr et al.). Neonates with CS are at a high risk for preterm delivery (<37 weeks), and over half of their mothers exhibit polyhydramnios (Grange et al., 2019). Key diagnostic features at birth generally include hypertrichosis, distinctive facial morphology, and macrocephaly (Grange et al., 2019). Developmental delay is often reported in young children, but intellectual disability is not common, and intelligence is typically normal in adult CS patients (Grange et al., 2019). The clinical features of CS arise with highly variable expressivity, even for a given variant within the same family, although underlying mechanisms responsible for such variable expressivity are not understood (Grange et al., 2019) (C. G. Nichols et al., 2013).

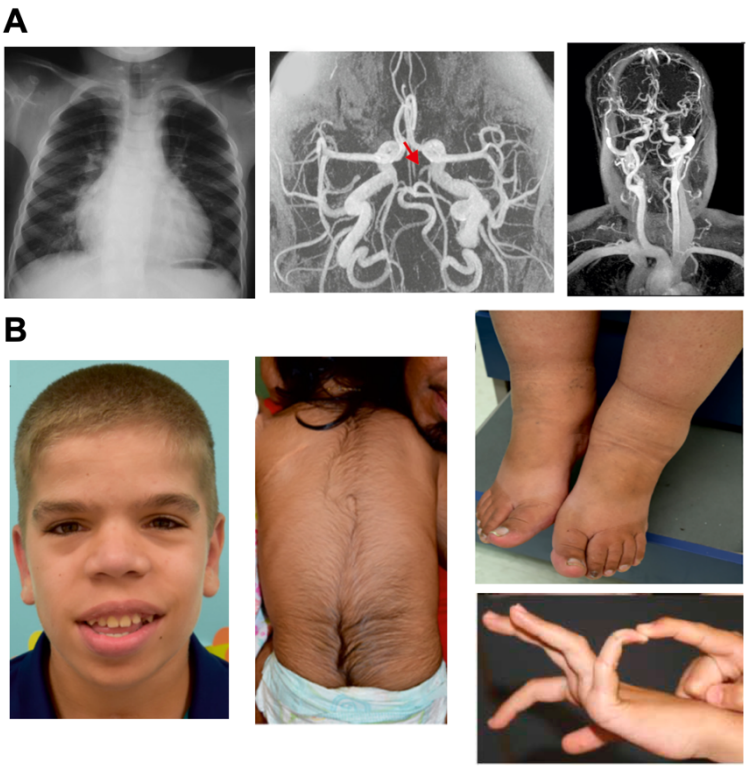

Figure 1.2: Complex clinical features of Cantú Syndrome. (**A**) Characteristic cardiovascular features include cardiac hypertrophy (*left panel*), and vascular dilation, compliance, and tortuosity (*middle and right panels*). (**B**) Extra-cardiovascular features include distinctive facial morphology (*left*), hypertrichosis (*middle*), lymphedema (*top right*), and joint hyperextensibility (*bottom right*).

1.3.2 Genetic Basis and Molecular Mechanism of Cantú Syndrome

K_{ATP} channel activator drugs such as diazoxide and minoxidil have been used systemically to treat congenital hyperinsulinism and refractory hypertension, as well as topically, in the case of minoxidil, to promote hair growth. Characteristic side effects were consistently observed in patients treated with these drugs, including hypertrichosis, pericardial effusion, coarsening of facial features, and edema (Mehta, Mamdani, Shansky, Mahurkar, & Dunea, 1975; Meisheri, Cipkus, & Taylor, 1988; Miki et al., 2005; Pennisi et al., 1977). Based on the striking resemblance of these side effects to classic CS features, it was hypothesized that CS may result from K^+ channel overactivity (Grange et al., 2006).

Various studies soon determined that CS patient mutations arising in *ABCC9* and *KCNJ8* genes confer GoF to recombinant K_{ATP} channels due to differential mechanisms, including elevated channel sensitivity to Mg^{2+}-nucleotide activation and/or diminished sensitivity to ATP inhibition (Brownstein et al., 2013; Cooper, McClenaghan, Chen, Stary-Weinzinger, & Nichols, 2017; Cooper et al., 2014; Cooper, Sala-Rabanal, Lee, & Nichols, 2015; Harakalova et al., 2012; McClenaghan et al., 2018; van Bon et al., 2012). Thus, the diverse array of CS clinical features are all fundamentally driven by GoF of Kir6.1/SUR2 K_{ATP} channels resulting from autosomal dominant missense mutations in *ABCC9* and, less commonly, *KCNJ8*, which may be inherited or arise de novo (Grange et al., 2019). It has recently been established that the cardiovascular features of CS share a primary origin in vascular K_{ATP} GoF, which produces cardiac hypertrophy and hypercontractility arising even in the absence of cardiac K_{ATP} GoF (Y. Huang et al., 2018).

K^+ channels have long held promise as potential cardiovascular therapeutic targets given their ubiquitous, yet often tissue-specific expression, along with their critical roles as modulators of membrane potential and excitability (Humphries & Dart, 2015). Moreover, while very few K^+ channel-selective drugs are currently approved for clinical use in cardiovascular disease, K_{ATP} channel drugs are an exception, which is particularly promising for CS given the array of licensed K_{ATP} channel inhibitors (Humphries & Dart, 2015). However, in spite of this, there are currently no well-established treatments for CS.

Studies from the Nichols and Grange groups support the potential benefit of sulfonylureas as effective inhibitors of genetically overactive K_{ATP} channels (McClenaghan, Huang, Yan, et al., 2020). There is also recent evidence that these drugs may provide clinical benefit in CS patients (A. Ma et al., 2019), although the risk of hypoglycemia caused by "off-target" effects on Kir6.2/SUR1 pancreatic K_{ATP} channels remains a chief concern that limits the widespread clinical use of these drugs in the treatment of CS.

1.3.3 Approaches to Understanding Molecular, Cellular, and Pathophysiological Consequences of CS mutations

1.3.3.1 Heterologous Expression of Recombinant Channels

The use of recombinant complementary DNA (cDNA) for heterologous expression marked a key technological advance that paved the way for protein cloning, sequencing, and functional analysis, yielding breakthroughs in our understanding of structure-function relationships in ion channels (Mathie, Veale, & Holden, 2021; Tapper & George, 2003). The innovation enabled selective expression of ion channel cDNA in amenable cell lines at a time when the study of native channels was especially difficult and often impractical, allowing for in-depth characterization of molecular consequences resulting from pathogenic ion channel mutations (Mathie et al., 2021; Tapper & George, 2003).

In the past decade, heterologous expression of recombinant K_{ATP} channels has provided an invaluable approach for testing whether novel reported *ABCC9* and *KCNJ8* variants from suspected CS patients give rise to channel GoF (Brownstein et al., 2013; Cooper et al., 2017; Cooper et al., 2014; Cooper et al., 2015; Harakalova et al., 2012; McClenaghan et al., 2018; van Bon et al., 2012). Beyond functional confirmation of GoF, studies on recombinant channels have led to deeper understanding of underlying molecular mechanisms, which generally include elevated sensitivity to Mg^{2+}-nucleotide activation, and/or reduced sensitivity to ATP inhibition (Brownstein et al., 2013; Cooper et al., 2017; Cooper et al., 2014; Cooper et al., 2015; Harakalova et al., 2012; McClenaghan et al., 2018; van Bon et al., 2012). Furthermore, recombinant K_{ATP} channels have provided an avenue for characterizing pharmacological consequences of CS

mutations, some of which are capable of reducing sensitivity to K_{ATP} channel inhibitors (Cooper et al., 2017; Cooper et al., 2015), which has direct implications for potential pharmacotherapeutic candidates for the clinical treatment of CS.

However, much of our understanding of CS mutations to-date is based on heterologous expression of nonhuman constructs with analogous mutations in rat and/or mouse genes. While molecular consequences are likely qualitatively or "directionally" consistent with human-specific channels, it is possible that fundamental molecular mechanisms and pharmacology associated with analogous nonhuman constructs may quantitatively diverge from those in human-specific proteins. Moreover, studies on recombinant K_{ATP} channels generally employ heterologous expression of Kir6.2/SUR2A, due to pronounced rundown of vascular-type (i.e., Kir6.1/SUR2B) channels in inside-out excised patch-clamp experiments (Brownstein et al., 2013; Cooper et al., 2017; Cooper et al., 2014; Cooper et al., 2015; Harakalova et al., 2012; McClenaghan et al., 2018; van Bon et al., 2012).

Again, qualitative effects of mutations in Kir6.2/SUR2A channels are likely conserved irrespective of the pore-forming subunit, but it is known that nucleotide-dependent channel activity differs quantitatively between SUR2A and SUR2B, which are identical except for their C-terminal exon (Matsuoka et al., 2000; Reimann, Gribble, & Ashcroft, 2000). Thus, it is reasonable to expect that molecular consequences are not quantitatively identical between channels comprising differing protein composition. Furthermore, conclusions from experiments using heterologously expressed K_{ATP} channels are generally focused in scope, appropriately limited to primary molecular consequences of channel variants expressed in cell lines that are efficient for transfection and patch-clamp (e.g., Cos, HEK, etc.), but which do not functionally resemble VSMCs or other myocytes, precluding in-depth characterization of secondary, downstream effects relevant to cell and tissue function. Thus, while analysis of recombinant channels is a powerful approach for assessing molecular consequences of mutations, it should be used in parallel with other systems for a comprehensive understanding of associated cell-autonomous and pathophysiological consequences.

1.3.3.2 Murine Models

Mouse models have been invaluable for the study of cardiovascular biology and disease in a complex pathophysiological context (Faury et al., 2003; Hawes et al., 2020; Houser et al., 2012; C. L. Huang, 2017; C. J. Lin et al., 2021; Miano, Zhu, & Lowenstein, 2016; Wagenseil et al., 2009). Although much valuable knowledge has been generated from human studies, it is inevitably observational due to obvious ethical issues precluding interventional experimentation on human biology (C. L. Huang, 2017). Nonhuman animal models of cardiovascular disease allow for targeted genetic manipulations and exploratory pharmacological interventions in a physiological setting, and interpretations are often highly translatable to human clinical conditions (C. L. Huang, 2017). Additionally, native cells from animal models provide a valuable approach to study bona fide cardiovascular cells within the vastly complex pathophysiological milieu that involves signaling from other cells, the extracellular matrix (ECM), and circulating hormones, which impact cell function in myriad ways and often play critical pathogenic roles (Faury et al., 2003; C. J. Lin et al., 2021; Schwach & Passier, 2019; Stegemann, Hong, & Nerem, 2005). Specifically, the advent of CRISPR-Cas9 gene editing has heralded major breakthroughs in cardiovascular disease modeling due to its remarkable simplicity and efficiency (Miano et al., 2016). This technology involves a Cas9 endonuclease, a chimeric guide RNA, and a homology directed repair template for precise genome editing (Miano et al., 2016). Many cardiovascular diseases, including a wide array of electrophysiological pathologies, have been studied in CRISPR-Cas9-modified murine models (Miano et al., 2016).

To better understand the pathogenic mechanisms linking CS mutations to cardiovascular pathology *in vivo*, the Nichols group generated novel CS mouse models by using CRISPR-Cas9 to globally introduce the CS-associated SUR2[A478V] (AV) and Kir6.1[V65M] (VM) mutations to the equivalent endogenous murine loci (Y. Huang et al., 2018; McClenaghan, Huang, Yan, et al., 2020). These animals recapitulate CS cardiovascular pathologies, including cardiomegaly, elevated cardiac output, low

systemic blood pressure, and a dilated, compliant vasculature (Y. Huang et al., 2018). Whole-cell patch-clamp recordings from acutely isolated VSMCs revealed elevated basal K_{ATP} conductances, especially in VM mice, explaining the mechanistic basis for vasodilation and lower blood pressure (Y. Huang et al., 2018). Inside-out excised patch-clamp recordings from acutely isolated ventricular cardiomyocytes revealed K_{ATP} GoF for AV animals, but normal cardiac K_{ATP} activity in V65M mice, consistent with prevailing evidence that Kir6.1 (i.e., the protein containing the VM mutation) is not functionally expressed in the myocardium (C. G. Nichols et al., 2013). Importantly, since VM mice have a severe cardiovascular phenotype, this finding indicates that CS cardiac pathologies are driven by vascular K_{ATP} overactivity, highlighting the critical etiological role of CS vasculopathy. CS vascular dysfunction drives cardiac remodeling due to elevated renin-angiotensin signaling and baroreceptor-mediated adrenergic signaling (Y. Huang et al., 2018; McClenaghan, Huang, Matkovich, et al., 2020; McClenaghan, Huang, Yan, et al., 2020). The Nichols group also demonstrated reversal of cardiac hypertrophy and systemic hypotension in AV and VM mice using VSMC-specific genetic knockdown of K_{ATP} channel activity, as well as with chronic glibenclamide administration (McClenaghan, Huang, Yan, et al., 2020). These findings provide further confirmation that vascular K_{ATP} GoF drives CS cardiac pathology, and demonstrates that the hypomyotonic component of CS vasculopathy is reversible with pharmacotherapeutic use of glibenclamide as a CS treatment *in vivo*.

Thus, the advantages of nonhuman animal models have paved the way for great strides in our understanding of the consequences and implications of CS mutations *in vivo*. However, since the physiological context is so profoundly integrated, it precludes dissection of purely cell-autonomous mechanisms from those influenced by the environment within which native VSMCs are embedded. Additionally, the use of nonhuman animal models carries a risk of introducing non-translatable artifacts due to species-based differences in biology, which is a latent possibility that is rarely suspected or accounted for, unless findings are replicated in human cell-based systems (Perlman, 2016; von Scheidt et al., 2017; Zaragoza et al., 2011).

1.3.3.2 Human iPSC-Derived Cardiovascular Cell Models

1.3.3.2.1 Pluripotent Stem Cells

In 1981, nearly coinciding with the time that K_{ATP} channels were being discovered, early reports described cell lines derived from pre-implantation embryos, and exhibited a capacity to generate any cell type in the body – a property known today as pluripotency (M. J. Evans & Kaufman, 1981; G. R. Martin, 1981). These newfound cells, deemed embryonic stem cells (ESCs), transformed the field of developmental biology and marked the beginning of a new era in technologies for genetic engineering (Bradley, Evans, Kaufman, & Robertson, 1984; Doetschman et al., 1987). A couple decades later, it was discovered that somatic cells could be reprogrammed to induce expression of characteristic pluripotency-related genes via fusion with ESCs (Cowan, Atienza, Melton, & Eggan, 2005; Tada, Takahama, Abe, Nakatsuji, & Tada, 2001). These major advances provided intriguing evidence that even terminally differentiated somatic cells could be reprogrammed to a pluripotent state – a revolutionary concept that was previously thought not to be possible. Given the complex ethical nuances of ESC acquisition and study, this notion held great theoretical promise for provision of an essentially unlimited source of pluripotent stem cells.

Landmark reports soon detailed the induction of mouse fibroblasts into ESC-like cells through ectopic overexpression of only four key pluripotency-associated transcription factors: OCT3/4, SOX2, KLF4 and c-MYC (OSKM) (Takahashi & Yamanaka, 2006). These cells were termed induced pluripotent stem cells (iPSCs). In the ensuing year, the same pioneering group showed that the OSKM reprogramming approach could also generate human iPSCs (hiPSCs) (Takahashi et al., 2007). At almost the same time, a separate group demonstrated that this could also be achieved by expressing NANOG and LIN28, in addition to OCT3/4 and SOX2 (Yu et al., 2007). Since then, a wide array of reprogramming methods have been described, and various groups have demonstrated that, with appropriate differentiation conditions, iPSCs are indeed amenable to differentiation into essentially any somatic cell type, via lineage involving all three germ

layers (Karagiannis et al., 2019; Pushp et al., 2021).

iPSCs provide promising avenues for a wide range of applications, from basic scientific study and disease modeling to drug discovery and tissue regenerative therapies (Gahwiler et al., 2021; Karagiannis et al., 2019; Maguire, Xiao, & Xu, 2017; Patsch et al., 2015; Trillhaase, Maertens, Aherrahrou, & Erdmann, 2021). In particular, patient-derived iPSCs represent an invaluable avenue for precision medicine-based approaches, which stem from a recognition that disease mechanisms and therapeutic responses may be influenced by the unique genetic background of an individual (Karakikes, Ameen, Termglinchan, & Wu, 2015). Furthermore, whilst transformed cell lines and nonhuman animal models have contributed significantly to our understanding of human cardiovascular biology and pathogenesis, the need for human cell-based systems is obviated by the degree to which human cell biology is distinct from established nonhuman models (Karakikes et al., 2015; H. Zhang et al., 2021). Thus, human iPSC-derived cells are increasingly being used to shape our understanding of human biology and disease. However, interpretations from such cells must be appropriately informed by the extent of our understanding regarding their resemblance to the relevant native cell type (Karakikes et al., 2015). There is no sufficient set of factors to definitively 'prove' that a hiPSC-derived cell is *bona fide*. However, a range of cellular features may be characterized in parallel to provide reasonable confidence of the degree of phenotypic recapitulation and, of equal importance, functional aspects where hiPSC-derived cells diverge from their native counterparts. Although there is no exhaustive list, such factors may include transcriptomic signatures, metabolomic profiles, cell surface marker expression, characteristic functional responses, and electrophysiology (Karagiannis et al., 2019; Karakikes et al., 2015; Patsch et al., 2015). Collectively, characterization of such factors may lead to a holistic understanding of the extent to which a given hiPSC-derived cell type merits inferences regarding fundamental biology, disease, and medicine.

1.3.3.2.2 hiPSC-Derived Cardiomyocytes

There are substantial functional differences between human cardiomyocytes and those isolated from nonhuman animal models, which include beat rates, Ca^{2+} handling, bioenergetic consumption, myofilament structure, and cardiomyocyte electrophysiology (Karakikes et al., 2015). Therefore, human-based cell models are particularly important for cardiac research. Human iPSC-derived cardiomyocytes (hiPSC-CMs) provide a means to overcome the barriers associated with nonhuman animal models, and require only minimally invasive procedures to provide a theoretically unlimited supply of patient-derived, immortalized human cardiomyocytes (Karakikes et al., 2015). Accordingly, much attention has been dedicated to generation and refinement of hiPSC-CMs (Burridge, Keller, Gold, & Wu, 2012; Collins & Varmus, 2015; Karakikes et al., 2015; Kolanowski, Antos, & Guan, 2017; van Mil et al., 2018). Various independent reports have defined key signaling pathways that promote pro-cardiac programming during cardiomyocyte differentiation, including canonical Wnt signaling, nodal (i.e., Activin/TGF-β) pathways, and bone morphogenetic protein (BMP) (S. M. Evans, Yelon, Conlon, & Kirby, 2010; Noseda, Peterkin, Simoes, Patient, & Schneider, 2011; E. N. Olson, 2006). Recent methodological advances in hiPSC-CM differentiation aim to recapitulate these natural signaling pathways *in vitro* (Kattman et al., 2011; Lian et al., 2012; J. Zhang et al., 2012). While various small molecules and hormones have been reported to help direct hiPSC-CM differentiation (Burridge et al., 2012), tight temporal modulation of Wnt signaling is particularly critical, with optimal pro-cardiac programming associated with an initial 48-hour Wnt activation, followed by a 48-hour window of Wnt inhibition In general, hiPSC-CM differentiation protocols give rise to phenotypically heterogeneous cell populations, necessitating subsequent CM purification – this can be metabolically achieved through glucose deprivation (Tohyama et al., 2013), in addition to a variety of other viable purification methods (Ban et al., 2013; Dubois et al., 2011; Hattori et al., 2010; Uosaki et al., 2011). These approaches to generate hiPSC-CMs have led to insights to prevalent diseases like hypertrophic cardiomyopathy (Lan et al., 2013) and dilated cardiomyopathy (Sun et al., 2012), in addition to various channelopathies, including long-QT syndromes (Davis et al., 2012; Egashira et al., 2012; Itzhaki et al., 2011; Lahti et al., 2012; Matsa et

al., 2011; Moretti et al., 2010; Wang et al., 2014; Yazawa et al., 2011; Zhu et al., 2019) and catecholaminergic polymorphic ventricular tachycardia (Fatima et al., 2011; Jung et al., 2012; Novak et al., 2012).

However, despite these advances, multiple reports have demonstrated substantial phenotypic heterogeneity in differentiated cardiac cell populations, such as distinct electrical characteristics corresponding to atrial-, ventricular- and nodal-like cells (Burridge et al., 2014; J. Ma et al., 2011; Yazawa et al., 2011; J. Zhang et al., 2009; Zwi et al., 2009). Overall, cardiac ion channel expression of hiPSC-CMs largely recapitulates native CMs, including functional expression of depolarizing I_{Na} currents, I_f currents, and L-type Ca^{2+} channels (Davis et al., 2012; J. Ma et al., 2011; Yazawa et al., 2011) and hyperpolarizing K^+ currents such as I_{to}, I_{Ks}, and I_{Kr} (J. Ma et al., 2011; Moretti et al., 2010). However, in contrast to native CMs, hiPSC-CMs generally exhibit essentially negligible I_{K1} current, which is important for repolarization during the cardiac action potential (Karakikes et al., 2015). Furthermore, it remains unclear whether hiPSC-CMs consistently exhibit functional K_{ATP} channel expression (Karakikes et al., 2015), despite this being perhaps the most highly expressed ion channel in native cardiomyocytes (Foster & Coetzee, 2016a). Therefore, although major strides have been made in the use of hiPSC-CMs to study cardiac biology and disease, there remain key challenges in the generation of cells that faithfully recapitulate the electrophysiology of native, adult CMs.

1.3.3.2.3 hiPSC-Derived Vascular Smooth Muscle Cells

Cardiovascular events are often preceded by vascular abnormalities, and thus critical to prevention of cardiovascular deaths is an understanding of fundamental vasculopathic mechanisms arising in VSMCs (Dash, Jiang, Suh, & Qyang, 2015). VSMCs derived from human induced pluripotent stem cells (hiPSCs) offer promise for the study of human-specific, as well as cell-autonomous, mechanisms of cardiovascular disease, and can also provide an approach for pharmacotherapeutic testing (Maguire et al., 2017; Patsch et al., 2015). The latter has generated excitement and is the subject of active, ongoing study in the field of hiPSC-derived 3D tissue engineering (Gahwiler et al., 2021; Trillhaase

et al., 2021). New approaches for differentiation of hiPSCs into vascular smooth muscle cells (hiPSC-VSMCs) are increasingly being used to shape our understanding of vascular biology and fundamental disease mechanisms (Maguire et al., 2017; Oh, Jung, & Yoon, 2021; Patsch et al., 2015). The most robust differentiation protocols employ chemically defined conditions to mimic endogenous developmental signaling cues, and subsequently carry out comprehensive validation of VSMC phenotype through a combination of transcriptomic, metabolomic, proteomic, and bio-functional modalities to holistically characterize cell identity (Ayoubi, Sheikh, & Eskildsen, 2017; Dash et al., 2015; Patsch et al., 2015; Shen, Quertermous, Fischbein, & Wu, 2021). One such protocol was recently developed by the Cowan group, and yields an essentially pure population of hiPSC-VSMCs (Patsch et al., 2015).

hiPSC-VSMCs may represent a very promising approach for the study of fundamental pathogenic mechanisms underlying complex CS cardiovascular pathologies, which share a fundamental etiology of overactive vascular K_{ATP} channels (Y. Huang et al., 2018; McClenaghan, Huang, Yan, et al., 2020). As the vast majority of knowledge to-date has been generated from murine models and heterologous expression of rat/mouse constructs (Brownstein et al., 2013; Cooper et al., 2017; Cooper et al., 2014; Cooper et al., 2015; Harakalova et al., 2012; McClenaghan et al., 2018; van Bon et al., 2012), patient-derived hiPSC-VSMCs may represent an avenue for gaining insight to human-specific, cell-autonomous mechanisms underlying CS vasculopathy. Moreover, many CS-associated mutations have been identified (Grange et al., 2019), and often possess distinct molecular mechanisms (Brownstein et al., 2013; Cooper et al., 2017; Cooper et al., 2014; Cooper et al., 2015; Harakalova et al., 2012; McClenaghan et al., 2018; van Bon et al., 2012), and occasionally affect pharmacological sensitivity to pharmacotherapeutic candidates such as glibenclamide (Cooper et al., 2017; Cooper et al., 2015). It is conceivable that differences may also exist in the downstream cellular consequences of these various mutations. Thus, hiPSC-VSMCs derived from individual CS patients may offer a way to characterize mutation-specific disease mechanisms, and inform personalized approaches to pharmacotherapeutic treatment plans in CS (Collins

& Varmus, 2015).

1.3.4 Major Questions Addressed in this Thesis

The above sections have discussed prior studies of the genetic basis, protein composition, structure, and function of K_{ATP} channels in mammalian tissues, as well as studies revealing that GoF mutations in these channels constitute the molecular basis of the complex, multisystem disorder known as Cantú Syndrome. At the beginning of this project, the use of existing sulfonylurea drugs to treat CS through inhibition of cardiovascular K_{ATP} channels was theoretical, and had not yet been explored in practice. This was mainly due to the clinical risk of potentially life-threatening hypoglycemia, arising from the 'off-target' action of these drugs on pancreatic K_{ATP} channels. The above sections also highlighted that, at the outset of this project, some CS mutations were known to reduce channel sensitivity to glibenclamide, the leading pharmacotherapeutic candidate in CS. Given the distinct genetic bases of pancreatic and cardiovascular K_{ATP} channels, this would be associated with reduced therapeutic effect, yet unaffected hypoglycemic risk. Therefore, understanding pharmacological consequences of particular CS mutations has critical implications for personalized, patient-specific treatment plans for CS. In the longer term, the development of cardiovascular-specific K_{ATP} inhibitors may be informed by deeper understanding of the precise molecular mechanisms by which CS mutations give rise to K_{ATP} channel GoF.

At the beginning of this project, very little was known about how CS mutations give rise to cardiovascular pathologies *in vivo*. Therefore, other members of the Nichols group had generated a CRISPR-Cas9 murine model of the most common CS mutation, SUR2[R1154Q]. However, several strange phenomena had been observed in this mouse model, which were not present in two other murine models also generated by the Nichols group. These unexplained phenomena included: (i) paradoxical cardiac K_{ATP} pharmacology, characterized by diazoxide- rather than pinacidil-sensitive channels; (ii) the discovery of a novel *ABCC9* transcript in RQ mouse cardiomyocytes, and (iii) a phenotype that was unexpectedly mild compared to the two other murine CS models,

given the relative molecular effect of these mutations in recombinant channels. At the time, the basis and implications of these observations were completely unknown. It was also unclear to what extent alternate *ABCC9* splicing was occurring in heterozygous and homozygous animals, and whether it was also present outside the heart, in other SUR2-expressing myocytes. Perhaps most importantly, it was unknown whether alternate *ABCC9* splicing was observed in human CS patients, which could explain the considerable variable expressivity of CS clinical features, even for a given variant within the same family. Regarding CS mouse models more generally, it was also unclear whether cardiovascular K_{ATP} GoF led to any compensatory effects on the functional activity of other vascular ion channels, potentially associated with complex pathophysiological signalling pathways that are stimulated in CS and are known to cause extensive phenotypic changes in cardiovascular cells (Briones et al., 2009). If observed, such compensatory electrophysiological changes would relate directly to the fundamental etiology of CS as a vascular electrical disease, and may also contribute to variable expressivity in CS.

Fundamental to understanding CS etiology is a grasp on cell-autonomous mechanisms, which link molecular K_{ATP} GoF to pathophysiological outcomes *in vivo*. Of particular relevance are such mechanisms in vascular cells, given the emerging evidence at the start of this project that CS vasculopathy is the underlying driver of broader cardiovascular pathologies. However, prior to this project, essentially nothing was known about vascular cell-autonomous pathogenic mechanisms in CS. It was hypothesized that K_{ATP} GoF causes cell hyperpolarization, leading to a hypocontactile vasculature, but this effect on membrane potential had never been demonstrated in any cell model with CS mutations. Even more fundamentally, despite prevailing evidence that vascular K_{ATP} GoF is the etiology of the diverse cardiovascular changes in CS, the molecular effect had never been demonstrated in human vascular cells with CS mutations. Additionally, it was hypothesized that elastogenesis was increased by CS mutations, based on apparently hyperelastic vascular changes in CS (Grange et al., 2019; Y. Huang et al., 2018; Kisilevsky, Kohly, & Margolin, 2019; Leon Guerrero et al., 2016), as well as past

observations from pharmacological studies (Hayashi et al., 1994; Knutsen et al., 2018; Tajima et al., 1995). However, increased elastin levels had never been experimentally demonstrated CS. Human iPSC-VSMCs offered a potential approach for exploring pathogenic vascular cell-autonomous mechanisms in CS. However, the use of this system for the study of a vascular electrical disease such as CS, and vascular disease in general, depends critically on the extent to which these cells recapitulate the electrophysiology of native VSMCs. Prior to this project, no study had assessed the electrophysiology of these cells. Electrical activity is a key component of normal VSMC function, and electrical abnormalities had been shown to dramatically alter VSMC function in ways that are relevant to disease (Dabertrand et al., 2015; Humphries & Dart, 2015; Jouen-Tachoire et al., 2021; Welch & Chung, 2022). Thus, there was a critical imperative to understand the electrophysiology of hiPSC-VSMCs, and how it relates to that of native VSMCs.

The following chapters describe the molecular characterization of several putative CS-associated variants in heterologously-expressed recombinant K_{ATP} channels, including underlying molecular mechanisms and sulfonylurea sensitivity (Ch. 2). Functional effects of the two most common CS mutations (RQ and RW) are characterized in recombinant channels (Ch. 2), murine models (Ch. 3), and patient derived hiPSC-VSMCs (Ch.4). The unexpected phenomena in the RQ mouse are also characterized in-depth (Ch. 3). Functional activity of other (non-K_{ATP}) vascular ion channels in native VSMCs isolated from CS mice is described (Ch. 3). The following chapters also address the question of whether alternate *ABCC9* splicing is occurring in human patients (Ch. 4). The following chapters also contain the first electrophysiological characterization of hiPSC-derived VSMCs (Ch. 4). Functional K_{ATP} expression in hiPSC-CMs is also addressed (Ch. 4). Electrical consequences of CS mutations on K_{ATP} channel activity and membrane potential in CS patient-derived hiPSC-VSMCs are determined, which explain the hypomyotonic component of CS vasculopathy (Ch. 4). The following chapters also describe cell-autonomous hyperelastogenic consequences of CS mutations in patient-

derived hiPSC-VSMCs and CS murine models, explaining the hyperelastogenic basis of CS vasculopathy (Ch. 4).

Chapter 2: Molecular consequences of CS mutations on recombinant K_{ATP} channel activity and pharmacology

Adapted from McClenaghan, Hanson, et al. "Cantu syndrome-associated SUR2 (ABCC9) mutations in distinct structural domains result in K_{ATP} channel gain-of-function by differential mechanisms", *published 2018 in Journal of Biological Chemistry*

Prior to this project, several novel *ABCC9* variants had been reported from suspected CS patients. However, these putative CS-associated mutations had not been functionally characterized. This chapter describes the molecular characterization of these CS-associated variants in heterologously-expressed recombinant K_{ATP} channels.

I identified the spatial cluster of novel CS mutations (M1056I, Y981S, G985E) and conceived the concerted functional characterization of these variants. I carried out $^{86}Rb^{+}$ efflux experiments for the M1056I mutation, and Conor McClenaghan performed $^{86}Rb^{+}$ efflux experiments for the other mutations. I carried out patch-clamp electrophysiology experiments to characterize the R1150Q and M1056I mutations, and the rest were characterized by Conor McClenaghan. Colin Nichols and Conor McClenaghan drafted the paper, and I helped review the manuscript.

2.1 METHODS

2.1.1 Molecular biology and cell culture

Mutations were introduced into a rat SUR2A (pCMV_rSUR2A; GenBank™ accession no. D83598.1) cDNA construct using site-directed mutagenesis and verified by direct Sanger sequencing. The residue numbering refers to the rSUR2A clone, which shares 97% sequence identity with the human sequence and was used to allow for comparison with previous reports of the effects of other CS mutations that also used rSUR2A. Cosm6

cells were cultured in Dulbecco's modified Eagle's medium (DMEM) and transfected using FuGENE 6 (Roche Applied Science) with WT pcDNA3.1_mKir6.2 (0.6 μg; GenBank™ accession no. D50581.1) and WT or mutant pCMV_rSUR2A constructs (1 μg) in addition to 0.2 μg of pcDNA3.1_eGFP for visual detection of successful transfection. To model heterozygous expression of mutant subunits, cells were transfected with WT Kir6.2 along with a 1:1 ratio of WT and mutant rSUR2A (0.5:0.5 μg). Excised patch-clamp recordings were made 48–72 h post-transfection.

2.1.2 $^{86}Rb^+$ efflux assay

Transfected Cosm6 cells were plated in 12-well plates to reach 70–80% confluence on the day of experimenting. Prior to commencing the efflux assay, the culture medium was replaced by DMEM supplemented with 1 μCi/ml $^{86}RbCl$ (PerkinElmer Life Sciences) and incubated for >6 h (37 °C/5% CO_2) to load the cells with the $^{86}Rb^+$ isotope. After the loading incubation, cells were washed with Ringer's solution containing (in mm) 118 NaCl, 10 HEPES, 25 $NaHCO_3$, 4.7 KCl, 1.2 KH_2PO_4, 2.5 $CaCl_2$, and 1.2 $MgSO_4^-$ either alone or supplemented with 2.5 mg/ml oligomycin and 1 mm 2-deoxy-d-glucose to induce metabolic inhibition (MI) and incubated at room temperature for a further 10 min. Cells were then washed three times with Ringer's solution (either with or without MI supplements) before the experiment was commenced. Ringer's solution was added to each well, collected, and replaced at the defined time points (2.5, 5, 12.5, 22.5, and 37.5 min). After the experiment, cells were lysed with 2% SDS to attain the remaining intracellular $^{86}Rb^+$, and sample radioactivity was determined by scintillation counting.

The cumulative $^{86}Rb^+$ efflux at each time point was calculated from the total counts from each sample (including the $^{86}Rb^+$ remaining post-cell lysis). Apparent K_{ATP}-independent efflux rate constants (k_1) were obtained from GFP-transfected cells using Equation 1,

$$\text{efflux} = 1 - e^{-k_1 \cdot t}$$

and K_{ATP}-dependent efflux rate constant (k_2) was obtained from K_{ATP}-transfected cells using Equation 2,

$$\text{efflux} = 1 - e^{((-k_1 \cdot t) + (-k_2 \cdot t))}$$

where k_1 was obtained from GFP-transfected cells (Equation 1) The number of active channels was assumed to be proportional to k_2. In MI conditions a time-dependent divergence from a mono-exponential efflux is observed. This is attributed to inactivation of background efflux mechanisms over time; therefore, in this condition rate constants were derived from exponential functions fit to early time points only (2.5–12.5 min). Efflux-time data shown represents the mean ± S.E. from at least three independent experiments each with multiple replicates ($N \geq 3$, $n \geq 4$). K_{ATP}-dependent flux rate data is shown as mean ± S.D. Statistical significance was determined using Mann-Whitney *U* tests with a *p* value <0.05 deemed statistically significant.

2.1.3 Inside-out excised patch-clamp recordings

Pipettes were made from soda lime glass microhematocrit tubes (Kimble) and had a resistance of 1–2 megohms when filled with pipette solution. The bath and pipette solutions (K_{INT}) contained (in mm): 140 KCl, 10 HEPES, 1 EGTA (pH 7.4 with KOH). Currents were recorded at a constant holding potential of −50 mV in the absence and presence of nucleotides as indicated. Where included, free Mg^{2+} concentrations were maintained at 0.5 mm by supplementation of $MgCl_2$ as calculated using CaBuf (Katholieke Universiteit Leuven). Where stated, porcine brain PIP_2 (Avanti Polar Lipids) was applied at 5 µg/ml. Rapid solution exchange was attained using a Dynaflow Resolve perfusion chip (Cellectricon). Experiments were performed at 20–22 °C. K_{ATP} channel currents in solutions of varying nucleotide concentrations were normalized to the basal current in the absence of nucleotides, and dose-response data were fit with a four-parameter Hill fit according to **Equation 3**, using the Data Solver Function in Microsoft Excel,

$$\text{normalized current} = I_{\text{min}} + (I_{\text{max}} - I_{\text{min}})/(1 + ([X]/\text{IC}_{50})^H)$$

where the current in K_{INT} = I_{max} = 1; I_{min} is the normalized minimum current observed in ATP/MgATP/glibenclamide; [*X*] refers to the concentration of ATP/MgATP/glibenclamide; IC_{50} is the concentration of half-maximal inhibition; and *H* denotes the Hill coefficient.

Data were tested for statistical significance using the Mann Whitney *U* test, and presented as mean ± S.E. in dose-response plots, and as mean ± S.D. in scatter plots showing IC_{50} values from individual experiments.

2.2 RESULTS

2.2.1 Cantu syndrome mutations result in gain-of-function of K_{ATP} channel in intact cells

Y981S (human Y985S), G985E (G989E), and M1056I (M1060I) cluster together at the link between NBD1 and TMD2 (Figure 2.1). To determine the effect of mutations on K_{ATP} channel function, SUR2A constructs were co-expressed with Kir6.2 in Cosm6 cells, and channel activity was assessed using a radioactive $^{86}Rb^+$ flux assay. First, basal K_{ATP} activity under quasi-physiological regulation by intracellular nucleotides in intact cells was determined by measuring $^{86}Rb^+$ efflux from cells bathed in Ringer's solution. As shown in Figure 2.2A and 2.2B, the K_{ATP} -dependent $^{86}Rb^+$ efflux rate in these conditions was significantly increased by the G985E and M1056I substitutions, although a trend toward an increase was observed for Y981S. Efflux rates in basal conditions are a function of both channel activity and surface membrane expression. Efflux rates were measured in cells subjected to metabolic inhibition (MI) to decrease intracellular ATP synthesis and relieve channels of nucleotide regulation. Assuming that the single channel conductance is unaffected and that MI maximally activates available channels, the comparison of the MI efflux rate between constructs provides an estimation of the relative number of channels in the membrane. As shown in Figure 2.2C and 2.2D, there was a statistically insignificant decrease in Y981S efflux rate, implying that this mutation results in only a small decrease in channel number. Otherwise, the maximum flux under these conditions was not markedly different between constructs, suggesting that the number of active channels was similar.

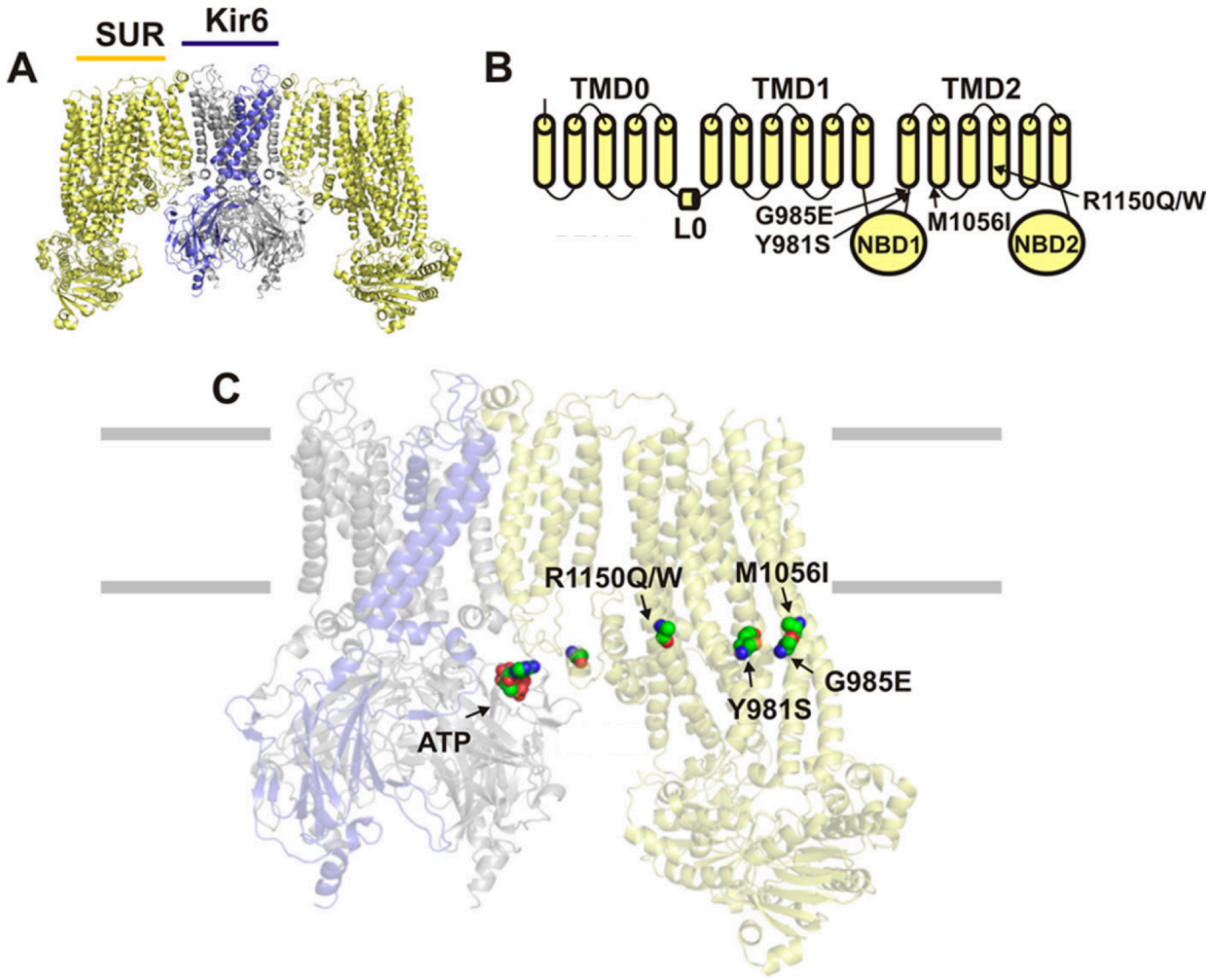

Figure 2.1: SUR2 CS mutations in K_{ATP} channel structure. (**A**) K_{ATP} channels form as hetero-octamers of four pore-forming Kir6.x subunits each associated with a SUR subunit (two SUR subunits omitted from figure). (**B**) Schematic representation of the position of Y981S, G985E, M1056I, and R1150Q/R1150W in the linear sequence of SUR2. (**C**) Expected positions of Y981S, G985E, M1056I, and R1150Q/R1150W mapped onto the K_{ATP} channel structure (Kir6.2/SUR1). The residues shown are the analogous positions in rat SUR1 (Tyr-1004, Ala-1008, Thr-1089, and Arg-1183, respectively; there is 70% sequence identity between hSUR1 and rSUR2A, and structural the domains are expected to be conserved). ATP is modeled in the Kir6.2-binding site.

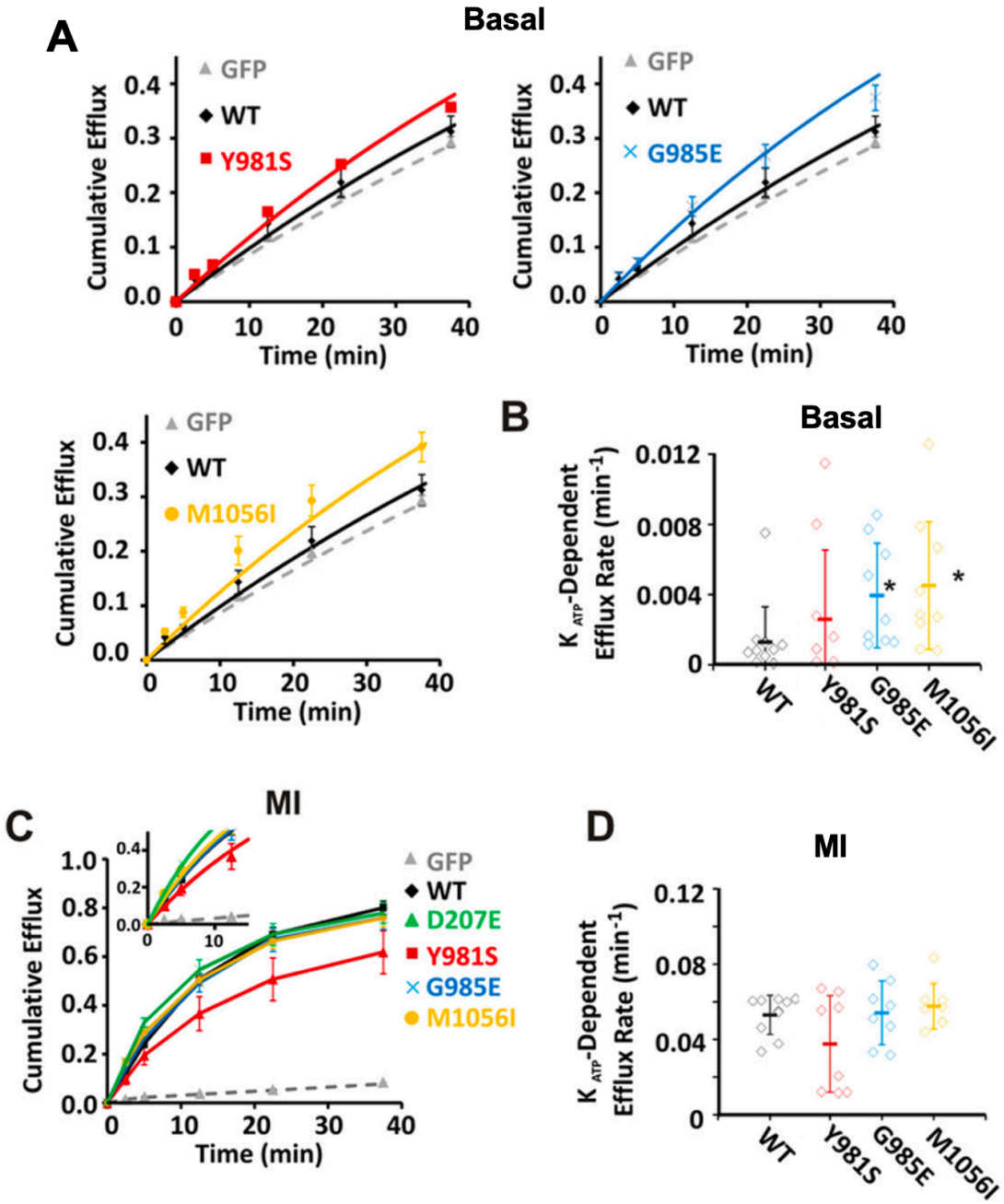

Figure 2.2: G985E and M1056I significantly increase basal K_{ATP} channel activity in intact cells. (**A**) Cumulative $^{86}Rb^{+}$ efflux was measured from Cosm6 cells transfected either with GFP alone or with Kir6.2 plus WT or mutant SUR2A. Efflux as a function of time was first recorded in basal conditions (cells incubated in Ringer's solution). (**B**) The K_{ATP}-dependent efflux rate was attained from exponential fits to efflux time data. (**C**) Efflux was measured from cells subjected to MI (induced by incubation in Ringer's solution with 2.5 mg/ml oligomycin and 1 mm 2-deoxy-d-glucose from 10 min prior to commencing the flux assay). (**D**) The rate constant for K_{ATP}-dependent efflux in MI conditions was calculated from exponential fits to the early time points (2.5, 5, and 12.5 min, inset in C). Efflux-time data are shown as mean ± S.E., and K_{ATP}-dependent efflux rate scatter plots show mean ± S.D. from 3 to 5 independent experiments. Statistical significance is denoted by *asterisk* and defined as $p < 0.05$ according to Mann-Whitney *U* test.

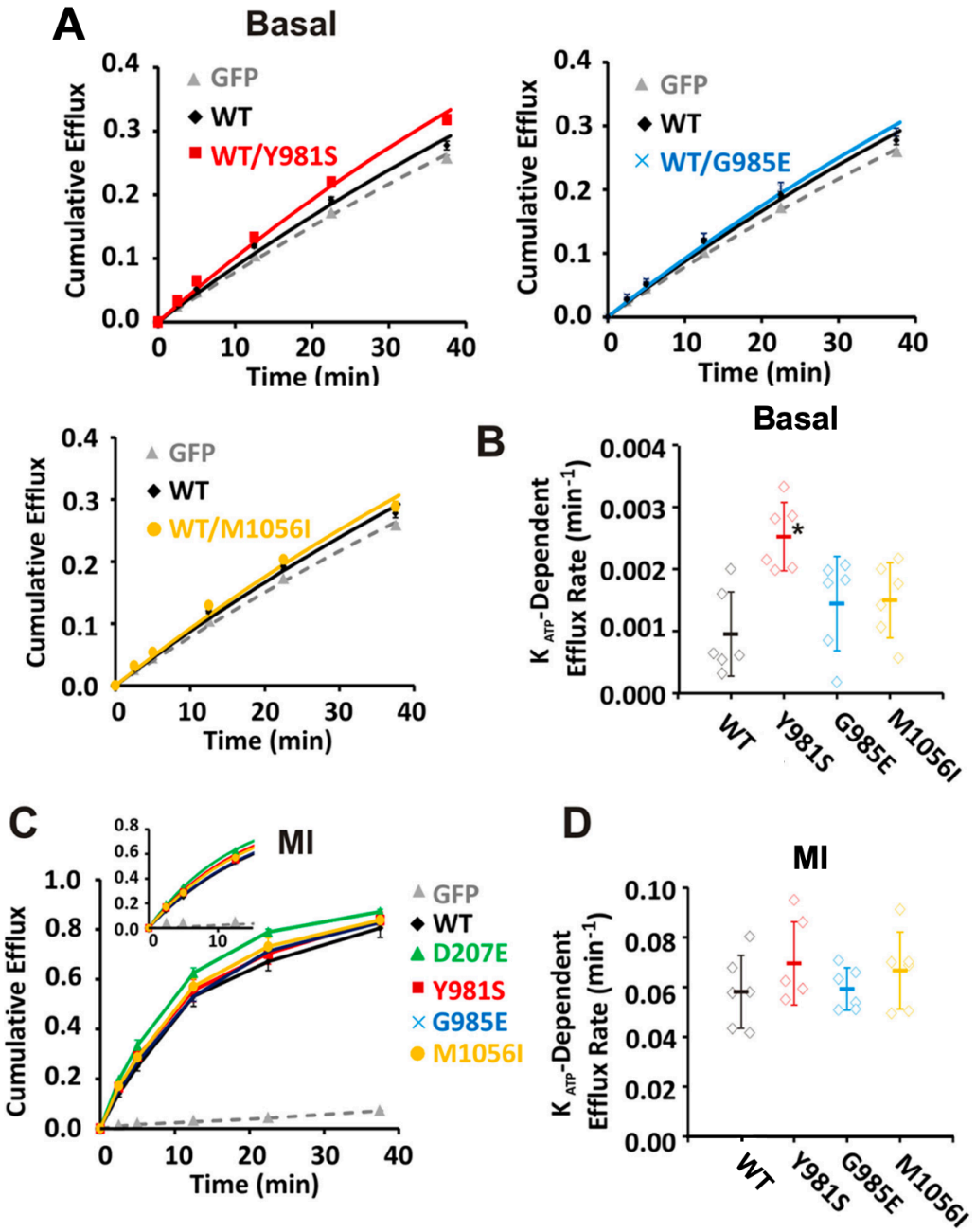

Figure 2.3: Y981S confers GoF when co-expressed with WT subunits in intact cells whereas only minor effects are observed for other mutations. (**A**) Cumulative $^{86}Rb^{+}$ efflux was measured from Cosm6 cells transfected either with GFP alone or with Kir6.2 alongside SUR2A-WT alone or SUR2A-WT with mutant SUR2A at a 1:1 ratio. Basal efflux shown as function of time. (**B**) The K_{ATP}-dependent efflux rate constants were calculated from exponential fits to efflux time data. (**C**) Efflux rate was measured in MI conditions (induced by incubation in Ringer's solution with 2.5 mg/ml oligomycin and 1 mm 2-deoxy-d-glucose from 10 min prior to commencing the flux assay). (**D**) Rate constants were calculated from early time points (2.5, 5, and 12.5 min, inset in C). Efflux-time data are shown as mean ± S.E., and K_{ATP}-dependent efflux rate scatter plots show mean ± S.D. from 3 to 5 independent experiments. Statistical significance is denoted by *asterisk* and defined as $p < 0.05$ according to Mann-Whitney *U* test.

Since all known CS patients are heterozygous, these conditions were modeled by co-expressing Kir6.2 together with WT SUR2A and mutant SUR2A subunits at a 1:1 ratio. The resultant channels were assayed by monitoring $^{86}Rb^{+}$ efflux. Only very minor increases in basal efflux rate were observed for G985E and M1056I, although a moderate, statistically significant increase was observed for Y981S channels (Figure 2.3). Taken together, these data demonstrate that whereas all tested mutations result in K_{ATP} GoF, the effect of heterozygous conditions is subtle under basal conditions.

2.2.2 Mutations within the Y981/G985/M1056 cluster increase Mg^{2+}-nucleotide activation

The disease-associated mutations Y981S, G985E, and M1056I are all clustered together on transmembrane helices 12 and 13 in TMD2 (Figure 2.1). In comparison with WT SUR2A, the IC_{50} for ATP inhibition in the presence of Mg^{2+} was significantly increased by each of these mutations; however, there was no effect on ATP sensitivity in the absence of Mg^{2+} (Figure 2.4). This is further demonstrated by the increase in IC_{50}[MgATP]/ IC_{50}[ATP] for all mutants (Figure 2.4G), indicating that the mutations in this cluster of residues linking NBD1 to TMD2 increase channel activity by enhancing Mg^{2+}-nucleotide activation.

2.2.3 R1150Q and R1150W in TMD2 enhance Mg2+-nucleotide activation

Having established that the TMD2 Y981S, G985E, and M1056I mutations enhance Mg^{2+}-nucleotide activation, I sought to test whether this mechanism was conserved for other TMD2 mutations, and the most common CS–associated mutations are R1150Q and R1150W. In agreement with a previous report (Harakalova et al., 2012), I found that R1150Q causes a large increase in MgATP IC_{50}, whereas R1150W has a more modest effect (Figure 2.5). In contrast, R1150Q and R1150W caused only slight increases in ATP IC_{50} (Figure 2.5), again reflected in increased IC_{50}[MgATP]/ IC_{50}[ATP] for R1150Q and R1150W (Figure 2.5F), and thus both R1150Q and R1150W cause gain-of-function predominantly by enhancing Mg^{2+}-nucleotide sensitivity.

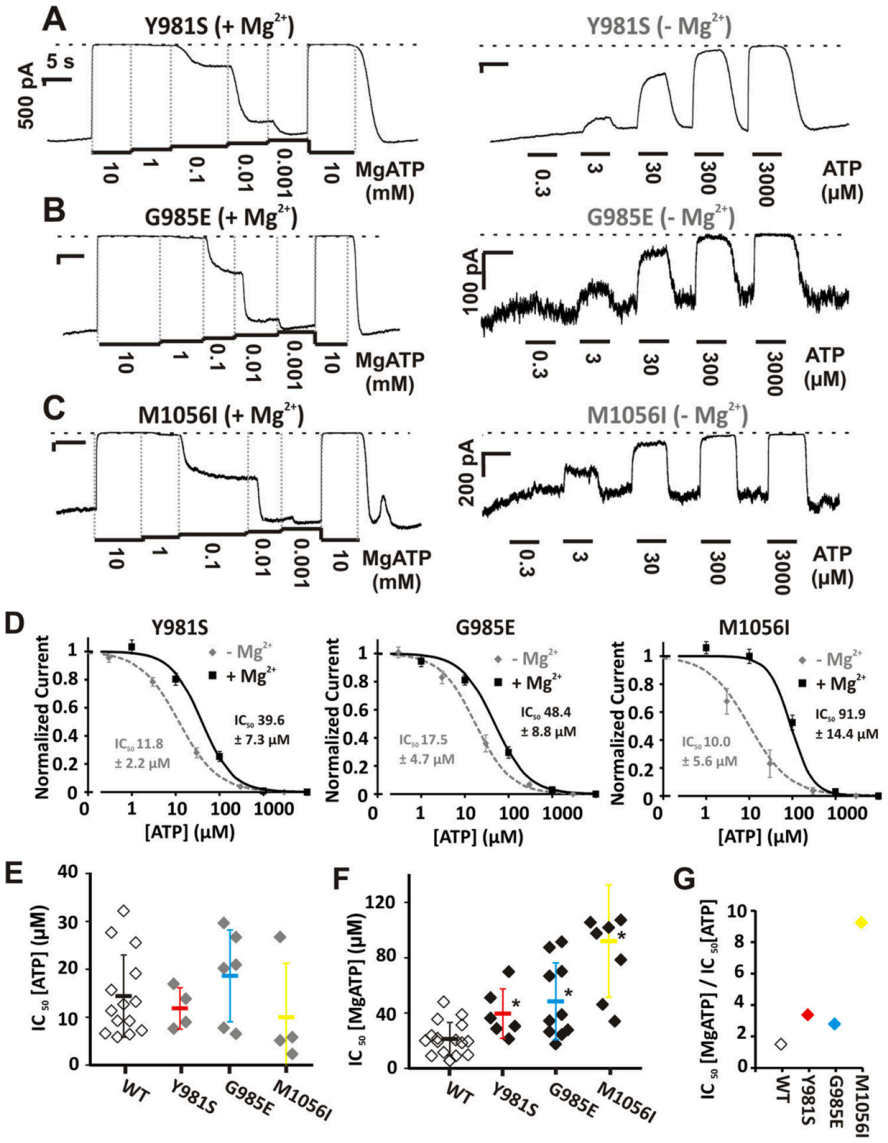

Figure 2.4: Y981S, G985E, and M1056I cause K_{ATP} GoF by enhancing Mg^{2+}-nucleotide activation. (**A**-**C**) Inside-out patch-clamp recordings were made from Cosm6 cells transfected with Kir6.2 alongside mutant SUR2A. The response to ATP in the presence (left) and absence (right) of Mg^{2+} was determined from voltage-clamped patches (−50 mV) of cells expressing either Y981S (A), G985E (B), or M1056I (C), as shown in representative traces (*scale bars* denote 500 pA/5 s unless otherwise stated). (**D**) Analysis of dose-response experiments showed that each mutation increased the IC_{50} for MgATP compared with WT (MgATP IC_{50} for Y981S was 39.6 ± 7.3 μm, Hill coefficient 1.2 ± 0.1, n = 6; MgATP IC_{50} for G985E was 48.4 ± 8.7 μm, Hill coefficient 1.1 ± 0.1, n = 11; MgATP IC_{50} for M1056I was 91.9 ± 14.4 μm, Hill coefficient 1.7 ± 0.2, n = 6), with little effect on ATP inhibition in the absence of Mg^{2+} (ATP IC_{50} for Y981S was 11.8 ± 2.2 μm, Hill coefficient 1.0 ± 0.1, n = 4; ATP IC_{50} for G985E was 17.5 ± 4.7 μm, Hill coefficient 1.1 ± 0.1, n = 6; ATP IC_{50} for M1056I was 10.0 ± 5.6 μm, Hill coefficient 0.9 ± 0.1, n = 3). (**E**-**F**) Scatter plots show data from individual experiments with mean IC_{50} ± S.D. (**G**) Decreased ATP inhibition in the presence of Mg^{2+} only is demonstrated by the ratio of the IC_{50} for ATP in the presence and absence of Mg^{2+}, which is markedly increased for Y981S, G985E, and M1056I. Statistical significance is denoted by *asterisk* and defined as $p < 0.05$ according to Mann Whitney *U* test.

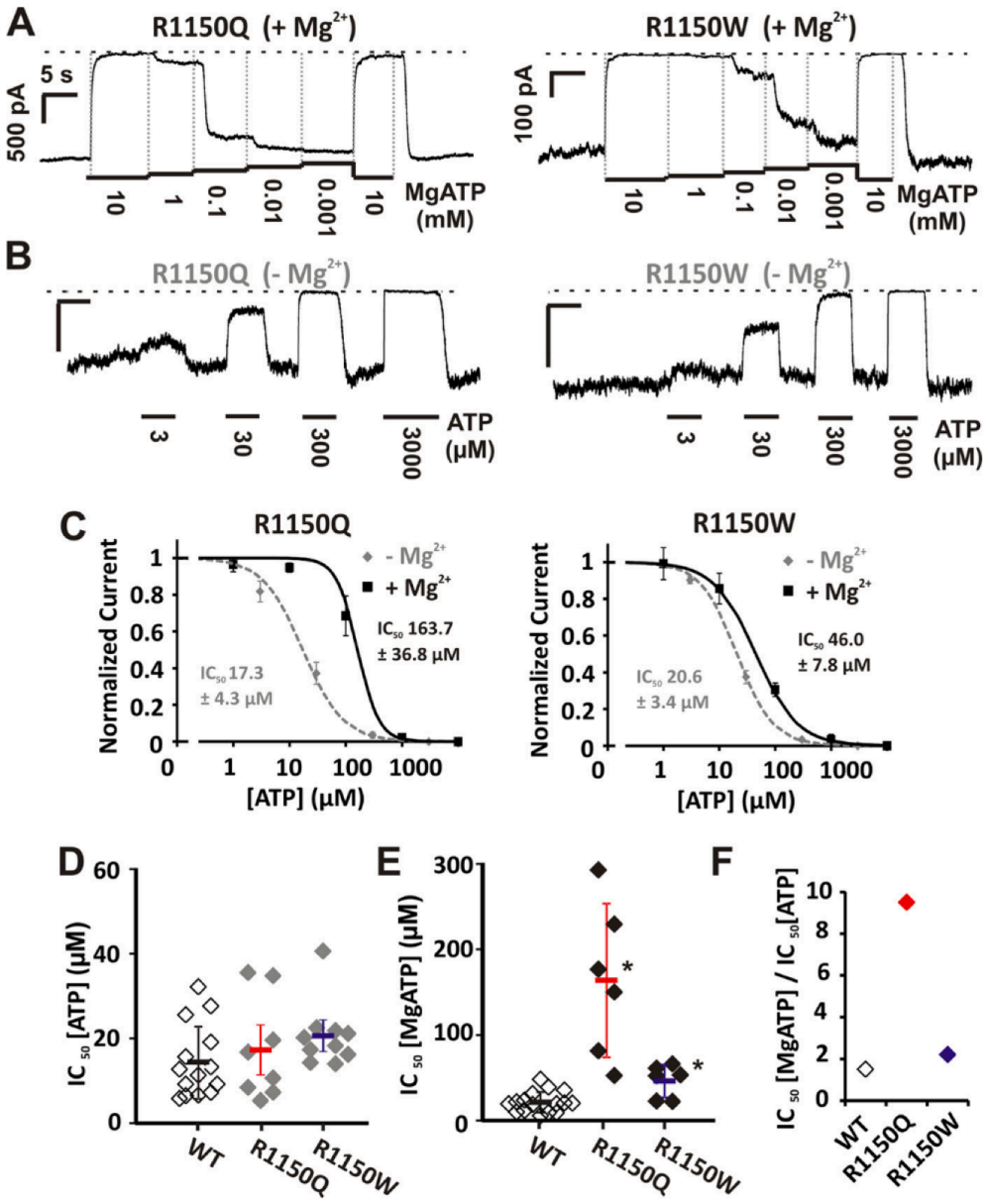

Figure 2.5: R1150Q and R1150W also cause K_{ATP} GoF by enhancing Mg^{2+}-nucleotide activation. (**A**-**B**) The response to ATP in the presence (*A*) and absence (*B*) of Mg^{2+} was determined for channels expressing Kir6.2 with R1150Q or R1150W, by inside-out patch-clamp recordings from Cosm6 cells as shown in representative traces (*scale bars* denote 500 pA/5 s unless otherwise stated). (**C**) Dose-response analysis demonstrated that both mutations markedly increased the IC_{50} for ATP in the presence of Mg^{2+}, compared with WT (MgATP IC_{50} for R1150Q was 163.7 ± 36.8 μm, Hill coefficient 2.3 ± 0.3, n = 6; MgATP IC_{50} for R1150W was 46.0 ± 7.8 μm, Hill coefficient 1.2 ± 0.2, n = 6). (**D**-**E**) The effect on ATP sensitivity in the absence of Mg^{2+} was more modest for both mutations (ATP IC_{50} for R1150Q was 17.3 ± 4.3 μm, Hill coefficient 1.2 ± 0.2, n = 8; ATP IC_{50} for R1150W was 20.6 ± 3.4 μm, Hill coefficient 1.3 ± 0.2, n = 10). Scatter plots show data from individual experiments with mean IC_{50} ± S.D. (**F**) An increase in the ratio of the IC_{50} for ATP in the presence over the IC_{50} for ATP in the absence of Mg^{2+} indicates that these mutations also predominantly confer GoF by augmentation of Mg^{2+}-nucleotide activation. Statistical significance is denoted by *asterisk* and defined as $p < 0.05$ according to Mann-Whitney *U* test.

2.2.4 Effect of CS GoF mutations on glibenclamide sensitivity

Glibenclamide (glyburide) inhibits K_{ATP} channels in a biphasic manner, with high-affinity inhibition arising from interaction with the SUR subunit occurring at nanomolar to micromolar concentrations and low-affinity inhibition due to interaction with the Kir6.x subunit (Gribble & Reimann, 2003). To specifically measure high-affinity inhibition, glibenclamide was applied up to 10 μm. Glibenclamide inhibited WT SUR2A K_{ATP} currents (in the absence of nucleotides), Y981S, G985E, and M1056I (Figure 2.6), with maximal inhibition of ~70% and IC_{50} values ranging from ~15 to 45 nm. In contrast, mutations at residue 1150, in particular R1150W, resulted in a significant decrease in glibenclamide potency (Figure 2.7).

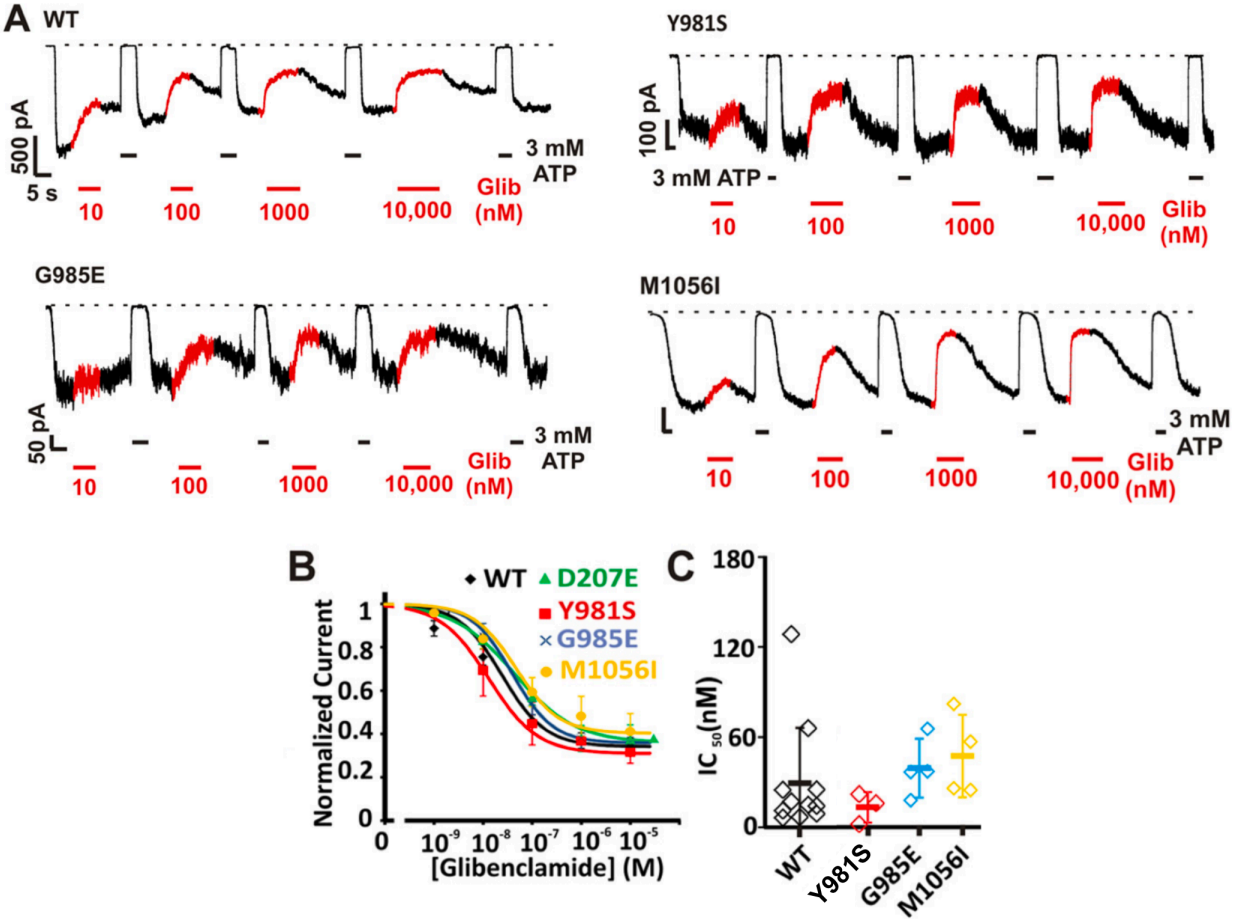

Figure 2.6: Y981S, G985E, and M1506I have no significant effect on glibenclamide sensitivity. (**A**) Inside-out patch-clamp recordings were made from Cosm6 cells transfected with Kir6.2 alongside WT or mutant SUR2A. Reversible inhibition was observed following administration of increasing glibenclamide concentrations, as shown in representative traces (*scale bars* denote 500 pA/5 s unless otherwise stated). (**B**) Dose-response analysis demonstrated that only minor, non-statistically significant variations in glibenclamide IC_{50} values were observed for these mutations (IC_{50} for SUR2A-WT was 29.5 ± 11.1 nm, Hill coefficient 1.0 ± 0.1, n = 11; IC_{50} for Y981S 13.1 ± 5.9 nm, Hill coefficient 0.9 ± 0.1, n = 3; IC_{50} for G985E 39.2 ± 9.8 nm, Hill coefficient 1.0 ± 0.2, n = 4; IC_{50} for M1056I 47.3 ± 13.8 nm, Hill coefficient 1.0 ± 0.4, n = 4). (**C**) Scatter plots show data from individual experiments with mean IC_{50} ± S.D. Statistical significance was determined using Mann-Whitney *U* test.

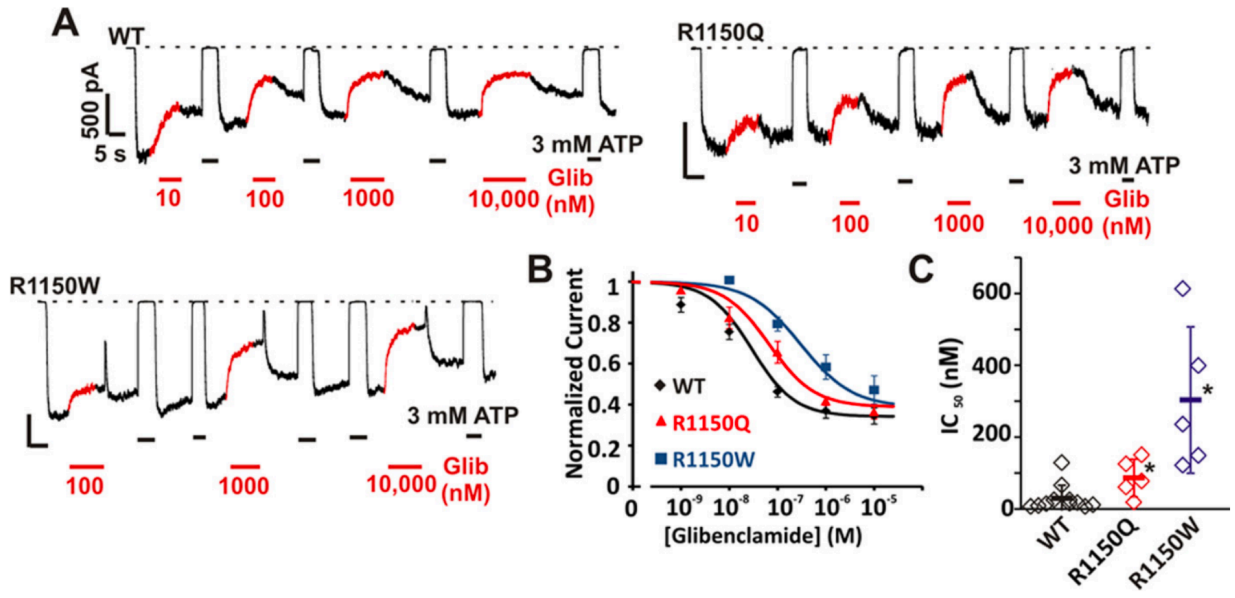

Figure 2.7: R1150Q and R1150W decrease glibenclamide sensitivity. (**A**) Glibenclamide sensitivity was measured from inside-out patch-clamp recordings from Cosm6 cells expressing Kir6.2 with either SUR2A-WT, R1150Q, or R1150W as shown in representative traces (*scale bars* denote 500 pA/5 s unless otherwise stated). (**B**) Dose-response analysis shows that both R1150Q and R1150W induce a statistically significant decrease in glibenclamide sensitivity (IC_{50} for R1150Q was 86.3 ± 23.4 nm, Hill coefficient 0.8 ± 0.3, n = 5; IC_{50} for R1150W was 303.5 ± 91.1 nm, Hill coefficient 0.8 ± 0.1, n = 5). (**C**) Scatter plots show data from individual experiments with mean IC_{50} ± S.D. Statistical significance is denoted by *asterisk* and defined as $p < 0.05$ according to Mann-Whitney *U* test.

Chapter 3: Complex consequences of CS SUR2 variant R1154Q in genetically modified mice

Adapted from Zhang, Hanson*, et al. "Complex consequences of Cantu syndrome SUR2 variant R1154Q in genetically modified mice", published 2021 in JCI Insight*
** authors contributed equally to this work*

At the outset of this project, two CRISPR/Cas9-generated CS murine models (i.e., SUR2[A478V] and Kir6.1[V65M]) had been generated, which closely recapitulated the known cardiovascular pathologies of human CS patients. However, several unexpected findings had been observed in the mouse model with the most common CS mutation (i.e., SUR2[R1150Q]), including an unexpectedly mild phenotype, novel *ABCC9* splicing, and an apparent isoform switch in cardiac K_{ATP} channels. Ultimately, the actual nature of these findings was defined, which is described in the following chapter. It was also unknown whether CS-dependent changes affected other (i.e., non-K_{ATP}) vascular ionic currents *in vivo*. This chapter includes the functional characterization of non-K_{ATP} vascular ionic conductances from a CS murine model with a severe phenotype.

Haixa Zhang and Colin Nichols originally conceived the study. Colin Nichols oversaw the generation of the mutant mice. I carried out all patch-clamp experiments characterizing cardiac K_{ATP} activity from the RQ mouse, and determined that dominant pharmacology does not result from isoform mixing in recombinant K_{ATP} channels. I designed and performed patch-clamp experiments demonstrating membrane potential hyperpolarization of RQ mouse VSMCs. I isolated RNA from all cardiac, vascular, and skeletal myocyte tissues, and quantified novel *ABCC9* splicing in each of these tissues. I discovered that functional *ABCC9* LoF was the basis for the initially hypothesized 'SUR1 switch' in RQ mouse cardiomyocytes. I designed and performed patch-clamp experiments characterizing the functional expression of non-K_{ATP} vascular ion channels. I carried out data analysis and designed figures for all aforementioned experiments.

Remaining experiments and associated analysis were performed by other authors. I helped Conor McClenaghan and Colin Nichols write the manuscript, which was edited by the other authors.

3.1 METHODS

3.1.1 CRISPR/Cas9 genome editing

Using CRISPR/Cas9-mediated genome engineering technology (Ran et al., 2013), knockin mice were engineered to carry a human GoF mutation in the *ABCC9* gene, which encodes the accessory SUR2 subunit of the K_{ATP} channel. Guide RNA (gRNA) target sequences predicted using the MIT CRISPR design tool (http://crispr.mit.edu) were cloned into plasmid pX330 (Addgene 42230). sgRNA activity was validated *in vitro* by transfection of N2A cells using Roche X-tremeGENE HP (MilliporeSigma), followed by T7E1 assay (New England BioLabs Inc.). The T7 sgRNA template and T7 Cas9 template were prepared by PCR amplification and gel purification, followed by RNA *in vitro* transcription with the MEGAshortscript T7 kit (gRNA) or the T7 mMessage mMachine Ultra kit (Cas9). After transcription, RNA was purified with the Megaclear kit (Life Technologies). 200 nt ssODN donor DNAs with the appropriate mutation centered within the oligonucleotide were synthesized by Integrated DNA Technologies as ultramer oligonucleotides.

B6CBA F1/J female mice (3–4 weeks old; The Jackson Laboratory) were superovulated and mated overnight with B6CBA F1/J male mice (>7 weeks old). Zygotes were harvested from the ampullae of superovulated females and placed in potassium-supplemented simplex optimized medium (KSOM; MR106D) before microinjection. Microinjection of the Cas9, sgRNA, and ssDNA template (at a final concentration of 50 ng/μL Cas9 WT RNA, 25 ng/μL gRNA, and 20 ng/μL ssODN DNA) was performed in flushing holding medium (FHM; EmbryoMax, MR-024-D, MilliporeSigma). After injection, zygotes were incubated at 5.5% CO_2 at 37°C for 2 hours, and surviving embryos were transferred to ICR recipient mice (The Jackson Laboratory) by oviduct transfer. Founders were identified using a QIAGEN pyrosequencer and Pyromark Q96 2.5.7 software.

Multiple viable and fertile positive founder mice were identified carrying the SUR2[R1151Q] mutation (equivalent to human SUR2[R1154Q]), which are referred to as SUR2[R1154Q] mice for direct comparison to the human CS equivalent. Successful mutation was verified in founder (F0) mice by Sanger sequencing of gDNA. Mutant mice were subsequently crossed with C57BL/6J mice (The Jackson Laboratory) to generate heterozygous F1 $SUR2^{WT/RQ}$ lines. PCR was used to generate amplicons of *ABCC9* spanning more than 5 kb on either side of the introduced mutation, from gDNA isolated from mouse tails, and resultant PCR products were sequenced to confirm the absence of additional, unintended mutations. After verification, 1 F1 animal from 1 line of each genotype was selected and subsequently bred with C57BL/6J mice for multiple (>6) generations to generate the hetero- and homogeneous R1154Q as well as WT littermates that were used in experiments.

3.1.2 RNA extraction and analysis

RNA was isolated from freshly dissecting cardiac apices or from iPSC-derived cardiomyocyte cultures using TRIzol (Thermo Fisher Scientific), and first-strand cDNA was synthesized using SuperScript III First-Strand Synthesis System (Thermo Fisher Scientific).

3.1.3 Protein analysis

3.1.3.1 Protein extraction from heart tissue

Snap-frozen tissue was thawed on ice and equilibrated with ice-cold homogenization buffer (protease inhibitors, 50 mM NaCl, 0.32 M sucrose, 2 mM EDTA, 20 mM HEPES pH 7.4). Atria were dissected from ventricles. The ventricular tissue was diced, resuspended in homogenization buffer, and homogenized via a Miccra D-1 homogenizer and subsequent strokes by a manual glass-Teflon Dounce homogenizer. The suspension was then centrifuged at 100,000g. The obtained membrane pellet was resuspended in homogenization buffer, aliquoted, and snap frozen with liquid nitrogen. Membranes were resuspended in solubilization buffer (1.5% Triton X-100, 0.75% sodium deoxycholate,

0.1% SDS, protease inhibitors in 10 mM NaCl, 5 mM EDTA, 2.5 mM EGTA, 50 mM Tris-HCl pH 7.35) and centrifuged at 50,000g at 4°C. Supernatant was subjected to TCA to a final concentration of 12.5 % and incubated for 30 minutes on ice. The pellet was acetone washed twice and air dried at 37°C; supplemented with 1× SDS sample buffer (50 mM Tris-HCl pH 6.8, 2% SDS, 0.1% bromophenol blue, 10% glycerol) containing 100 mM DTT; and resuspended for subsequent analysis by SDS-PAGE.

3.1.3.2 Protein analysis by Western blotting

For separating proteins via SDS-PAGE, 6% polyacrylamide gels were used for proteins greater than 100 kDa and 12% for other proteins. Electrophoresis was performed at constant current, limited to 15 mA per gel. Gels with separated proteins were put onto a nitrocellulose membrane and placed between 2 blotting papers, and electroblotted for 90 minutes in transfer buffer (25 mM Tris, 192 mM glycine, pH 8.3) at 4°C with a constant voltage of 60 V and the current limited to 1 A. Membranes were washed and blocked with blocking buffer (5% wt/vol milk powder, 25 mM Tris/HCl pH 7.4, 135 mM NaCl, 3 mM KCl, 0.02% IGEPAL).

As previously described, the anti-Kir6.2 antibody (raised in guinea pig and yielded as serum of the third bleeding; ref. 51) recognizes the last 36 amino acids of the protein and was characterized on native tissue against Kir6.2-knockout controls (Arakel et al., 2014). Information about antibodies against proteins other than Kir6.2 is shown in Table 1. Primary antibodies were diluted in blocking buffer and incubated overnight at 4°C. For antibodies against SUR proteins, a different blocking buffer (“SUR-blocking buffer”: 4% wt/vol milk powder, 25 mM Tris/HCl pH 7.4, 135 mM NaCl, 3 mM KCl, 0.1% Tween-20) was used. Subsequently, membranes were washed 3 times with their respective blocking buffer and incubated with IRDye LI-COR secondary antibodies (800CW) diluted in blocking buffer at 1:4000. Blots were incubated for 90 minutes at room temperature and washed with washing buffer (25 mM Tris/HCl pH 7.4, 135 mM NaCl, 3 mM KCl, 0.1% Tween-20 for SUR proteins, 5% wt/vol milk powder, 25 mM Tris/HCl pH 7.4, 135 mM

NaCl, 3 mM KCl, 0.02% IGEPAL for others), and antibody signals were subsequently visualized using an Odyssey Sa Infrared imaging system.

Table 3.1. Antibody List

Antigen	Clone/name	Species	Source	Catalog no.	Lot no.	Concentration	Dilution (Western blot)
Kir6.2	#3	Guinea pig	Produced in our laboratory	–	–	Serum	1:2000
Na^+,K^+-ATPase	C464.6	Mouse	Santa Cruz Biotechnology Inc.	sc-21712	C0713	200 µg/mL	1:2000
SUR1	N289/16	Mouse	Neuromab	75-267 73-267	4492AK44 #4375VA10	1.03 mg/mL 26.9 µg/mL	1:500 1:25
SUR2A	N319A/14	Mouse	Neuromab	73-296	4376VA13	22 µg/mL	1:15

3.1.4 Patch clamp electrophysiology

3.1.4.1 Isolated VSMCs

Mice were anesthetized with 2.5% avertin (10 mL/kg, i.p.; MilliporeSigma), and the ascending aorta was rapidly dissected and placed in ice-cold physiological saline solution (PSS) containing (in mM): NaCl 134, KCl 6, $CaCl_2$ 2, $MgCl_2$ 1, HEPES 10, and glucose 10, with pH adjusted to 7.4 with NaOH. Smooth muscle cells were enzymatically dissociated in dissociation solution containing (in mM): NaCl 55, sodium glutamate 80, KCl 5.6, $MgCl_2$ 2, HEPES 10, and glucose 10, pH 7.3 with NaOH, then placed into dissociation solution containing papain 12.5 µg/mL, DTT 1 mg/mL, and BSA 1 mg/mL for 25 minutes (at 37°C), before immediate transfer to dissociation solution containing collagenase (type H:F = 1:2) 1 mg/mL and BSA 1 mg/mL for 5 minutes (at 37°C). Cells were dispersed by gentle trituration using a Pasteur pipette, plated onto glass coverslips on ice and allowed to adhere for more than 1 hour before transfer to the recording chamber.

Whole-cell K_{ATP} currents were recorded using an Axopatch 200B amplifier and Digidata 1200 (Molecular Devices). Recordings were sampled at 3 kHz and filtered at 1 KHz. Currents were initially measured at a holding potential of –70mV in high-Na^+ bath

solution containing (in mM): NaCl 136, KCl 6, $CaCl_2$ 2, $MgCl_2$ 1, HEPES 10, and glucose 10, with pH adjusted to 7.4 with NaOH before switching to a high-K^+ bath solution (KCl 140, $CaCl_2$ 2, $MgCl_2$ 1, HEPES 10, and glucose 10, with pH adjusted to 7.4 with KOH) in the absence and presence of pinacidil and glibenclamide as indicated. The pipette solution contained (in mM) potassium aspartate 110, KCl 30, NaCl 10, $MgCl_2$ 1, HEPES 10, $CaCl_2$ 0.5, K_2HPO_4 4, and EGTA 5, with pH adjusted to 7.2 with KOH. Voltage-gated K^+ currents were measured in High Na^+ bath solution containing (in mM): NaCl 134, KCl 5.4, $CaCl_2$ 100 µM, $MgCl_2$ 1, HEPES 10, and glucose 10, with pH adjusted to 7.4 with NaOH. The pipette solution contained (in mM) KCl 140, $MgCl_2$ 1, HEPES 10, glucose 10, and EGTA 10, ATP 5, with pH adjusted to 7.2 with KOH. Voltage-gated LTCCs were measured in High Na^+ bath solution containing (in mM): choline chloride 124, BaCl2 20, $MgCl_2$ 1, HEPES 10, and glucose 5, with pH adjusted to 7.4 with NaOH. The pipette solution contained (in mM) CsCl 130, $MgCl_2$ 2, HEPES 10, glucose 10, and EGTA 10, Na_2ATP 3.5, with pH adjusted to 7.3 with KOH.

3.1.4.2 Isolated cardiac ventricular myocytes

Ventricular myocytes were isolated from adult mice, anesthetized using 2.5% Avertin (10 mL/kg), and the heart and ascending aorta were removed and immersed in ice-cold calcium free Wittenberg isolation medium (WIM; in mM): 116 NaCl, 5.4 KCl, 8 $MgCl_2$, 1 NaH_2PO_4, 1.5 KH2PO4, 4 $NaHCO_3$, 12 glucose, 21 HEPES, 2 glutamine plus essential vitamins (Gibco) and essential amino acids (Gibco) (pH 7.40). The heart was cannulated via the aorta and Langendorff perfused with WIM for 5 minutes at 37°C, followed by 20 minutes of perfusion with WIM supplemented with 270 U/ml collagenase type 2 (Worthington Biochemical Corp.) and 10 µM $CaCl_2$ at 37°C. The heart was then transferred to WIM containing 50 mg/mL BSA, 12.5 mg/mL taurine, and 150 µM $CaCl_2$; and ventricular tissue was manually dissociated using forceps before single-cell dissociation by trituration with a fire-polished Pasteur pipette.

Inside-out patch clamp recordings were made in symmetrical KINT solution which contained (in mM): 140 KCl, 10 HEPES, 1 EGTA (pH 7.4 with KOH). Varying MgATP

concentrations were applied using a Dynaflow Resolve perfusion chip (Cellectricon). $MgCl_2$ was added to each solution to achieve a free [Mg^{2+}] 0.5 mM according to calculations using CaBuf (Katholieke Universiteit Leuven). Membrane currents were sampled at 3 KHz and filtered at 1 KHz at a holding potential of –50 mV using an Axopatch 700B amplifier and Digidata 1200 (Molecular Devices). K_{ATP} channel currents in solutions of varying nucleotide concentrations were normalized to the basal current in the absence of nucleotides, and dose-response data were fit with a 4-parameter Hill fit according to the following equation: Normalized current = I + (Imax – Imin)/(1 + ([X]/IC_{50})H); where the current in Kint = Imax = 1, Imin is the normalized minimum current observed in MgATP, [X] refers to the concentration of MgATP, IC_{50} is the concentration of half-maximal inhibition, and H denotes the Hill coefficient.

3.1.5 Arterial compliance

After mice were euthanized under isoflurane anesthesia, the ascending aorta and left common carotid artery of 3-week-old mice were excised and placed in a PSS containing 130 mM NaCl, 4.7 mM KCl, 1.18 mM $MgSO_4$-7H2O, 1.17 mM KH2PO4, 14.8 mM $NaHCO_3$, 5.5 mM dextrose, and 0.026 mM EDTA (pH 7.4). The vessels were then cleaned from surrounding fat, mounted on a pressure arteriograph (Danish Myo Technology), and maintained in PSS at 37°C. Vessels were visualized with an inverted microscope connected to a charge-coupled device camera and a computerized system, which allowed continuous recording of vessel diameter. Intravascular pressure was increased from 0 to 175 mmHg by 25 mmHg increments, and the vessel outer diameter was recorded at each step (12 seconds per step). The average of 3 measurements at each pressure was reported.

3.1.6 Blood pressure measurement

3.1.6.1 In anesthetized mice

Mice were anesthetized with 1.5% inhaled isoflurane and restrained on a heating pad to maintain body temperature. A 2- to 3-mm incision was made in the midline of the neck;

the thymus and muscle were separated to expose the right carotid artery. A Millar pressure transducer (model SPR-671) was inserted into the right carotid artery and moved to the ascending aorta. Systolic BP (SBP), diastolic BP (DBP), and HR were recorded using the PowerLab data acquisition system (ADInstruments), and data were analyzed using LabChart 7 (ADInstruments). For blood pressure measurements in conscious mice, a radio-telemetry pressure transmitter (DSI) was surgically inserted into the left carotid artery and moved to the ascending aorta, where BPs during day and night were recorded by the DSI data acquisition system after mice recovered from surgery.

3.1.6.2 Telemetry probe implantation and telemetry recording

Mice (6–8 months old) were implanted with TA11PA-C10 (DSI) telemetric implants under anesthesia, with a gas concentration of 1.5%–2.5% isoflurane. The catheter was advanced into the ascending aorta via the left carotid artery, and the body of transmitter was slipped into the pocket subcutaneously in the right flank. Animals were housed in an isolated recording room and allowed at least 1 week of recovery before recordings were taken. Systolic (SBP), diastolic (DBP), mean arterial pressure (MBP = DBP + 1/3[SBP — DBP]), and HR were collected using the Dataquest ART system. Data were sampled by averaging 10 seconds of each 1-minute period. Values of day and night were averages of day time (6 am–6 pm) or night time (6 pm–6 am). After 3 days of baseline recording, the mice were injected with pinacidil (i.p. 0.01, 0.1, 1 mg) daily.

3.1.7 Heart weight measurement and histology

Mice were anesthetized with 2.5 % Avertin, and hearts were excised and rinsed with PBS, which contained (in mM): 137 NaCl, 2.7 KCl, 10 Na2HPO4, KH2PO4 (pH 7.4 with NaOH). The hearts were arrested in diastole with 10% KCl and blotted to remove excess liquid. Hearts were then weighed, and weight was normalized to tibia length. After weighing, the hearts were fixed in 10% buffered formalin for 24 hours and embedded in paraffin. Sections (3 μm) were cut and stained with H&E for the morphometric analysis.

3.1.8 Echocardiography

Short-axis left ventricular scans were obtained via M-mode echocardiography using an ATL 5000cv instrument (Phillips) with a 15-MHz compact linear array. The operator was blinded to genotype. Left ventricular end-diastolic dimension (LVEDD), LV end-systolic dimension (LVESD), end diastolic anterior wall thickness (AWT), end diastolic posterior wall thickness (PWT), R-R interval, and ejection time (ET) were recorded from 3 separate cardiac cycles for each mouse. Wall thickness divided by chamber radius was calculated at diastole. LV mass (LVM) was calculated using the Devereux equation. Fractional shortening (FS%) refers to (LVEDD – LVESD)/LVEDD as a percentage. Stroke volume (SV) refers to the amount of blood ejected by the left ventricle in one contraction, determined by subtracting LV end-systolic volume from LV end-diastolic volume (LVEDV – LVESV), assuming LVEDV and LVESV are simply cubed. The ejection fraction (EF%; SV/LVEDV) refers to the percentage of blood that is pumped out of the ventricles with each contraction.

3.1.9 Statistics

Unless otherwise noted, all data are presented as mean ± SEM and were tested for statistical significance using 1-way ANOVA, with post hoc Tukey's test or 2-tailed Student's t test as indicated. P values less than 0.05 were considered statistically significant.

3.1.10 Study Approval

Studies were performed in compliance with the standards for the care and use of animal subjects defined in the Guide for the Care and Use of Laboratory Animals (National Academies Press, 2011) and were reviewed and approved by the Washington University Institutional Animal Care and Use Committee. All human studies were approved by the Washington University Human Studies Committee and carried out with the full written consent of participating patients.

3.2 RESULTS

3.2.1 The human R1154Q substitution causes K_{ATP} GoF, but only a mild CS phenotype

CRISPR/Cas9 gene editing was used to introduce a single nucleotide mutation (*ABCC9*[c.3452G>A]; SUR2[p.R1151Q]) in the endogenous mouse *ABCC9* locus, resulting in protein substitution analogous to the most common human CS mutation, SUR2[R1154Q]. Both heterozygous ($SUR2^{WT/RQ}$) and homozygous ($SUR2^{RQ/RQ}$) mice were viable and fertile. Subsequently, cellular, organ, and whole animal phenotypes of these animals were analyzed, which are referred to here as SUR2[R1154Q] mice to distinguish it from human CS.

One of the most consistent features of patients with CS is pronounced cardiomegaly (Grange et al., 2019; Levin et al., 2016). Consistent with this, hearts were larger in heterozygous $SUR2^{WT/RQ}$ than WT mice, but not obviously more so in homozygous $SUR2^{RQ/RQ}$ mice (Figure 3.1, A and B). Therefore, R1154Q hearts displayed chamber dilation and cardiac enlargement similar to, although much less dramatic than, that seen previously in A478V or V65M CS mouse hearts (Y. Huang et al., 2018). Isolated aortic diameter was greater in $SUR2^{WT/RQ}$ than WT mice at all pressures (Figure 3.1C) although, again, there was no further increase in $SUR2^{RQ/RQ}$ mice, and carotid artery dimensions were not different between WT and R1154Q animals (Figure 3.1D). Slope compliance (reflecting noncontractile biomechanical properties) was not obviously different between genotypes (Figure 3.1C). As shown in Figure 3.2A, both $SUR2^{WT/RQ}$ and $SUR2^{RQ/RQ}$ mice maintained diurnal fluctuation in blood pressure, but unlike in SUR2[A478V]-expressing mice (Y. Huang et al., 2018), blood pressures were not significantly lower than control in either $SUR2^{WT/RQ}$ or $SUR2^{RQ/RQ}$ mice (Figure 3.2A). Moreover, while pinacidil had similar BP-lowering effect in control and Het $SUR2^{WT/RQ}$ mice, it had almost no effect on BP in $SUR2^{RQ/RQ}$ mice (Figure 3.2C). In contrast, pinacidil raised heart rates (HRs) similarly in all genotypes (Figure 3.2D).

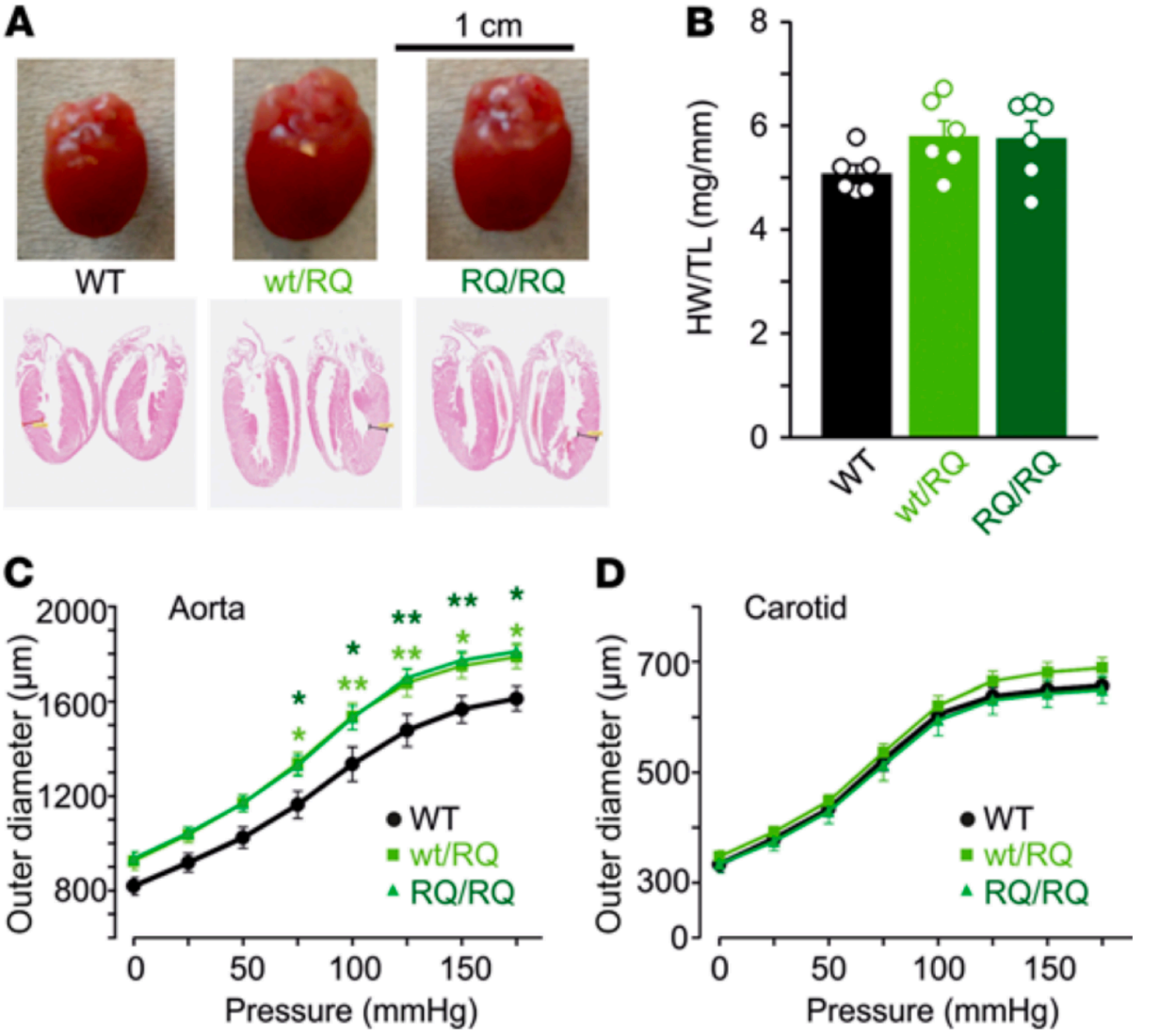

Figure 3.1: Cardiovascular phenotype of R1154Q mice. (**A**-**B**) Cardiomegaly in heterozygous $SUR2^{WT/RQ}$ (WT/RQ) and homozygous $SUR2^{RQ/RQ}$ (RQ/RQ) hearts. (**C**-**D**) Isolated ascending aortas of WT/RQ and RQ/RQ hearts show similar increases in diameter at all pressures relative to WT (**C**), but carotid artery mechanical properties are not different from those of WT (**D**) (n = 5 for WT, n = 7 for WT/RQ, n = 6 for RQ/RQ). Statistical significance was determined by 2-way ANOVA followed by post hoc Tukey's test correction for multiple comparisons; *$p < 0.05$, **$p < 0.01$ compared with WT. HW, heart weight; TL, tibia length.

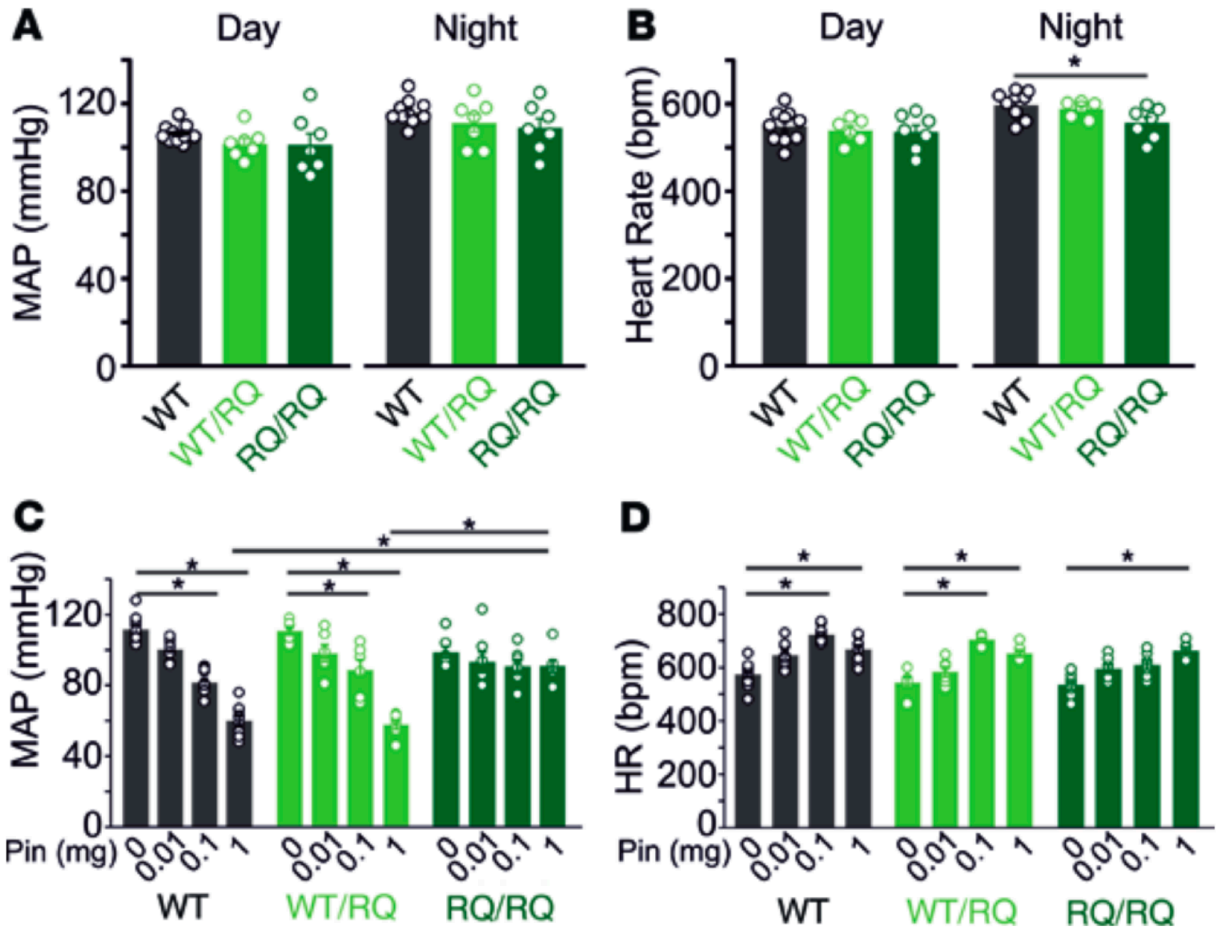

Figure 3.2: Cardiovascular function of R1154Q mice. (**A**-**B**) Mean arterial pressure (MAP) (**A**) and mean HR (**B**) in conscious WT, heterozygous SUR2$^{WT/RQ}$, and homozygous SUR2$^{RQ/RQ}$ mice during day and night. (**C**-**D**) MAP and HR in anesthetized mice showing blunted response to the K_{ATP} channel activator pinacidil (Pin) in SUR2$^{RQ/RQ}$ mice. Statistical significance was determined by 1-way ANOVA followed by Tukey's test for pairwise comparison; *asterisk* indicates significant difference ($p < 0.05$) within genotypes.

3.2.2 Unexpected K_{ATP} channel properties in R1154Q cardiac and vascular smooth muscle cells.

Mice expressing introduced SUR2[A478V] and Kir6.1[V65M] CS GoF mutations exhibit marked lowering of blood pressure and cardiac enlargement (Y. Huang et al., 2018). Since previous studies show that recombinant SUR2[R1154Q] causes a significant GoF — in both human SUR2 (Harakalova et al., 2012) and rat SUR2 with the identical DNA mutation (McClenaghan et al., 2018) — the above results (i.e., limited or no increase in vessel diameters and compliance, lack of effect on BP, and lack of pinacidil action in $SUR2^{RQ/RQ}$) are unexpected, and raise questions regarding the level and nature of K_{ATP} channels in these mutant tissues. I therefore examined the density of K_{ATP} channels, and sensitivity to the K_{ATP} channel openers pinacidil (acting primarily on SUR2) and diazoxide (acting primarily on SUR1) in excised membrane patches from ventricular myocytes (Figure 3.3A). Overall K_{ATP} channel density was much lower than WT in $SUR2^{WT/RQ}$ myocytes, and dramatically so in homozygous $SUR2^{RQ/RQ}$ myocytes (Figure 3.3B). Moreover, in striking contrast to the findings in recombinant R1154Q channels, pinacidil-mediated activation was essentially absent in homozygous $SUR2^{RQ/RQ}$ cardiomyocytes, while relative diazoxide-mediated activation was markedly enhanced (Figure 3.3C).

This unexpected lowering of channel density and apparent switch in pharmacological sensitivity from pinacidil to diazoxide suggests that levels of SUR2-dependent channel complexes are reduced in R1154Q hearts, almost completely in homozygous $SUR2^{RQ/RQ}$ hearts, and that the remaining functional sarcolemmal channels are predominantly SUR1 dependent. To test the latter suggestion directly, $SUR2^{RQ/RQ}$ mice on a SUR1–/– background (Shiota et al., 2002) were also generated; in this case, no K_{ATP} was detected (Figure 3.3B), indicating that channels in $SUR2^{RQ/RQ}$ animals are essentially SUR1 dependent. Underlying K_{ATP} subunit levels in isolated ventricular tissue were further examined by Western blot analysis (Figure 3.3D). This revealed a marked decrease in core- and complex-glycosylated SUR2A proteins in homozygous $SUR2^{RQ/RQ}$ hearts compared with littermate control hearts (Figure 3.3D). In contrast, levels of core-glycosylated SUR1 protein were increased in $SUR2^{RQ/RQ}$ hearts (Figure 3.3D).

The effects of the introduced mutation on K_{ATP} channel function were also examined in vascular smooth muscle cells (VSMCs). In contrast to the findings in A478V and V65M animals (Y. Huang et al., 2018), whole-cell patch clamp recordings using an intracellular pipette solution containing no ATP (see Methods) revealed no elevation of basal K_{ATP} conductance in acutely isolated aortic smooth muscle cells from $SUR2^{WT/RQ}$ compared with WT mice, and significantly lower conductance in $SUR2^{RQ/RQ}$ compared with WT cells (Figure 3.4A and 3.4B). Application of pinacidil provoked a significant increase in conductance in WT VSMCs, but there was less of an effect in $SUR2^{RQ/RQ}$ and very little effect in VSMCs from $SUR2^{RQ/RQ}$ mice (Figure 3.4, A and B). These results indicate that K_{ATP} density was also markedly reduced in R1154Q smooth muscle, although $SUR2^{RQ/RQ}$ VSMCs were hyperpolarized relative to WT VSMCs following break-in in current clamp mode (Figure 3.4, C and D), indicating at least some net K_{ATP} GoF under intact cell physiological conditions in $SUR2^{RQ/RQ}$ VSMCs.

Taken together, the data indicate that, while the expected molecular consequence of the SUR2[R1154Q] substitution is a significant GoF of SUR2-dependent K_{ATP} channels in blood vessels and the heart, there were minimal cardiovascular CS features. There was an unexpected downregulation of SUR2-dependent K_{ATP} channel density in heterozygous $SUR2^{WT/RQ}$ cardiac and vascular smooth muscle myocytes — dramatically so in homozygous $SUR2^{RQ/RQ}$ tissues — accompanied by an increase in SUR1 levels in the heart.

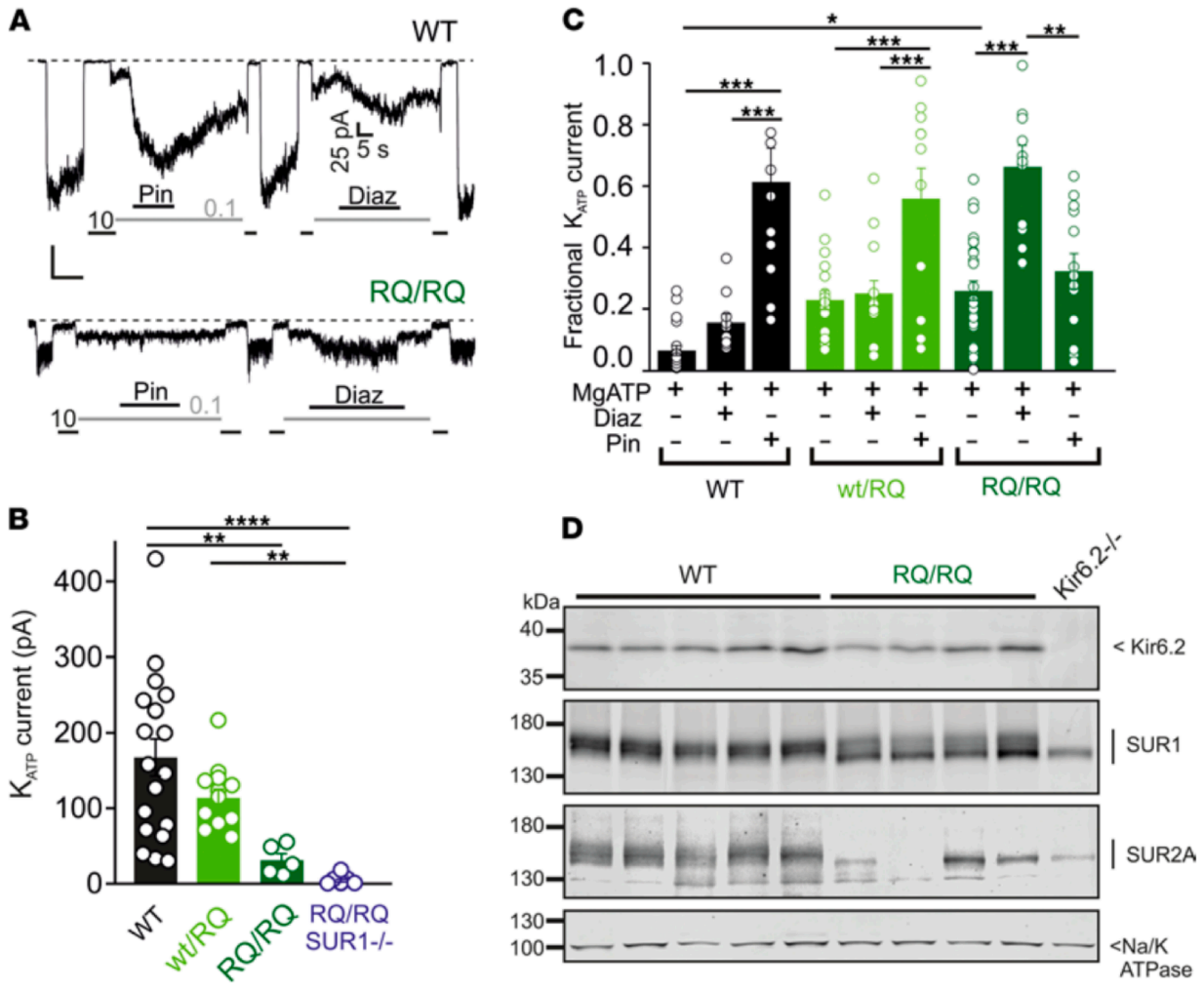

Figure 3.3: Decreased K_{ATP} channel density and switch to SUR1 dependence in SUR2A[R1154Q] hearts. (**A**) Representative inside-out patch clamp recordings of K_{ATP} channel activity from acutely dissociated ventricular myocytes from WT and $SUR2^{RQ/RQ}$ mice. Inhibition by 10 or 0.1 μM MgATP and the response to the K channel openers pinacidil and diazoxide (Diaz) at 100 μM, in the presence of MgATP (recording at –50 mV membrane potential), are shown. (**B**) Absolute K_{ATP} current level in zero ATP, from experiments as in **A**. (**C**) K_{ATP} current, as a fraction of current in zero ATP, from experiments as in **A**. (**D**) Western blot analysis of the membrane fraction from ventricular heart tissue of WT and $SUR2^{RQ/RQ}$ mice (4 biological replicates each) showing protein steady-state levels of K_{ATP} channel subunits and Na/K-ATPase α subunits. Since both SUR subunits are only core-glycosylated when the Kir6.2 subunit is missing (28), tissue from a single $Kir6.2^{-/-}$ mouse is also shown for reference. Statistical significance was determined by 1-way ANOVA followed by Tukey's test for pairwise comparison; * $p < 0.05$, ** $p < 0.01$, *** $p < 0.001$.

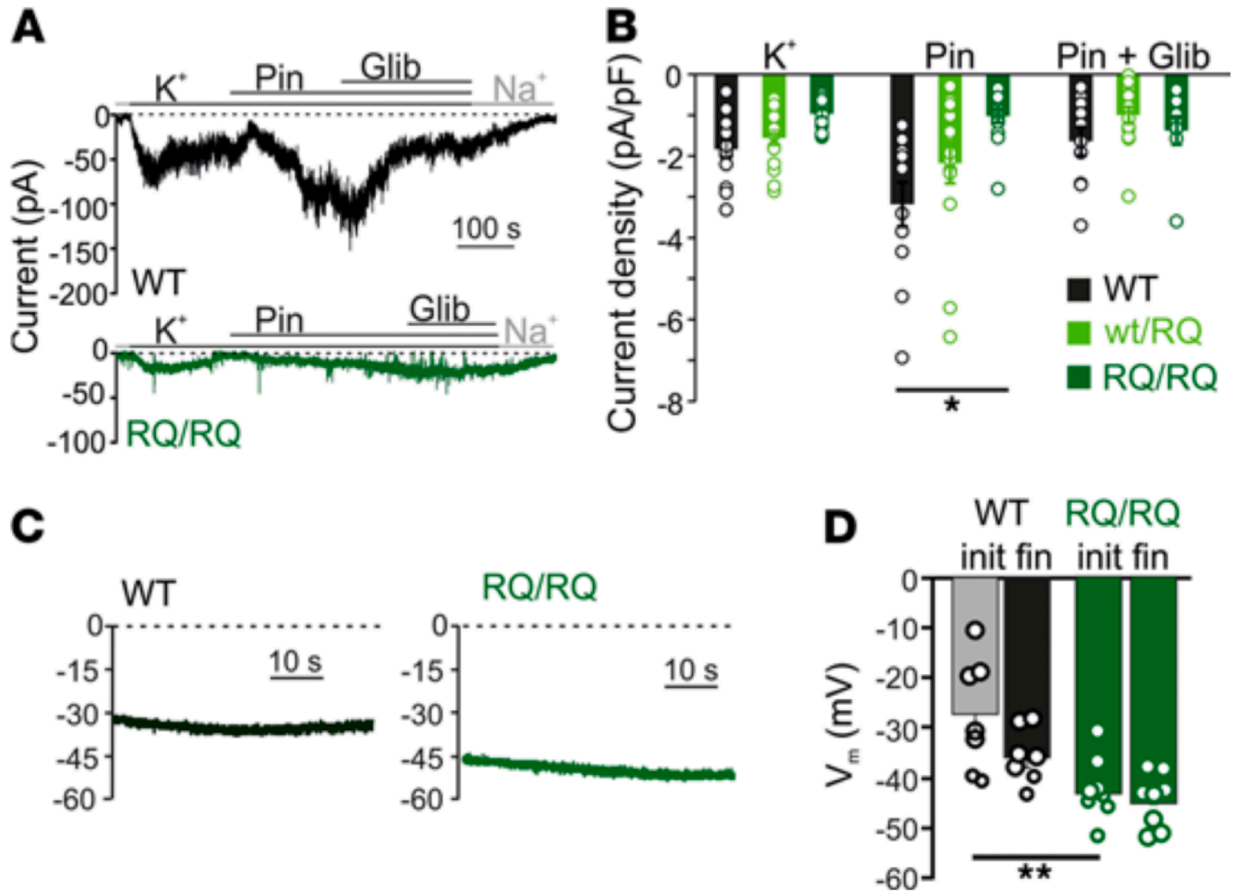

Figure 3.4: Loss of pinacidil-sensitive SUR2-dependent K_{ATP} channels in SUR2A[R1154Q] vascular smooth muscle. (**A**) Representative whole-cell voltage clamp recordings from acutely isolated aortic smooth muscle cells from WT and $SUR2^{RQ/RQ}$ mice. Cells were voltage clamped at –70 mV. Glib, glibenclamide. (**B**) Summary of whole-cell current densities from voltage clamp recordings as in **A**, showing significantly reduced pinacidil-activated K_{ATP} conductance in $SUR2^{RQ/RQ}$ cells. Statistical significance was determined by multi-way ANOVA, followed by 2-tailed *t* test pairwise comparison with Bonferroni's correction for multiple comparisons (adjusted $\alpha = 0.008$); $^*p < 0.008$. (**C**) Representative whole cell current-clamp recordings from acutely isolated aortic smooth muscle cells from WT and homozygous $SUR2^{RQ/RQ}$ mice using an intracellular pipette solution absent of nucleotides. (**D**) Summary of initial (init) and final (fin) membrane potentials from experiments as in **C**. Statistical significance was determined by 1-way ANOVA followed by Tukey's tests; $^{**}p < 0.01$.

3.2.3 Unanticipated alternate splicing of SUR2 exon 28 in R1154Q tissues

The above results led us to conclude that although the R1154Q mutation indeed causes a GoF in K_{ATP} channel properties (since smooth muscle is still relatively hyperpolarized), the expressivity of CS features is severely blunted in these animals by the unexpected reduction in SUR2-dependent K_{ATP} density that is not seen in other (A478V, V65M) CS mice (Y. Huang et al., 2018). In homozygous $SUR2^{RQ/RQ}$ mice there was almost complete disappearance of SUR2-dependent K_{ATP} channels in both heart and blood vessels, and a consequent reduction in disease severity, as reflected by lack of obvious effects on BP and reduced effects on heart size (Figures 3.1 and 3.2). The possibility was considered that CRISPR-generated mistakes may have led to additional mutations that resulted in defective protein, but sequencing of gDNA more than 5000 bp on either side of the introduced mutation failed to detect any additional mutations (data not shown). It has long been recognized that there are multiply spliced forms of the SUR2 protein (Chutkow et al., 1999; Pu et al., 2008; Shi, Ye, & Makielski, 2005; Yamada et al., 1997), the best characterized being the SUR2A and SUR2B isoforms, which result from alternate splicing of the terminal exon 38A/B. The R1154Q and R1154W mutations are in exon 27, and while there is to our knowledge no evidence in the literature for alternate splicing of this region of the gene, the specific location of the underlying mutations (13 and 14 bases, respectively, before the end of exon 27; Figure 3.5, A–C) places them in a potential exon splicing enhancer (ESE) region that may influence exon splicing (Pozzoli & Sironi, 2005). mRNA was isolated from WT and R1154Q mouse hearts, generated cDNA corresponding to SUR2A and SUR2B, and sequenced the entire coding region. The introduced c.3452G>A mutation was present in fewer than 50% of heterozygous $SUR2^{WT/RQ}$ and close to 100% of homozygous $SUR2^{RQ/RQ}$ transcripts, but, strikingly, heterozygous cDNA reads became doubled sequences immediately following the last nucleotide of exon 27 (Figure 3.5B). Close inspection revealed that this corresponds to approximately half of the reads in heterozygous $SUR2^{WT/RQ}$, and essentially all reads in homozygous $SUR2^{RQ/RQ}$, transcripts, reflecting an exact in-frame deletion of the 93 bases in the following exon, exon 28 (Figure 3.5B).

It might be hypothesized that this exon 28 splicing of SUR2 mRNA could be a cellular regulatory mechanism to moderate abnormally increased K_{ATP} channel function activity. However, this does not seem likely, since no alternative splicing of exon 28 was detected in heterozygous or homozygous SUR2[A478V] or Kir6.1[V65M] hearts (data not shown), or in WT hearts (Figure 3.5B). Instead, the tight dependence of splicing on the presence of the c.3452G>A mutation indicates that the nucleotide change itself is directly responsible for the splicing event.

To assess the effect of deleting exon 28 on K_{ATP} channel activity, SUR2A cDNA was engineered with exon 28 deleted. When coexpressed with WT Kir6.2, SUR2A[R1154Q,Δexon28] failed to generate significant K_{ATP} channel activity in heterologous expression (Figure 3.6, A and B). In subunit mixing experiments, with equal transfection of WT SUR2A and SUR2A[R1154Q,Δexon28] cDNA, there was no evidence for dominant-negative suppression of heterologously expressed K_{ATP} channels by exon-deleted subunits (Figure 3.6C). The data were best fit under the assumption that even 1 full-length WT subunit would be sufficient to rescue function (Figure 3.6C), consistent with truncated subunits being rapidly degraded and not incorporated into K_{ATP} complexes.

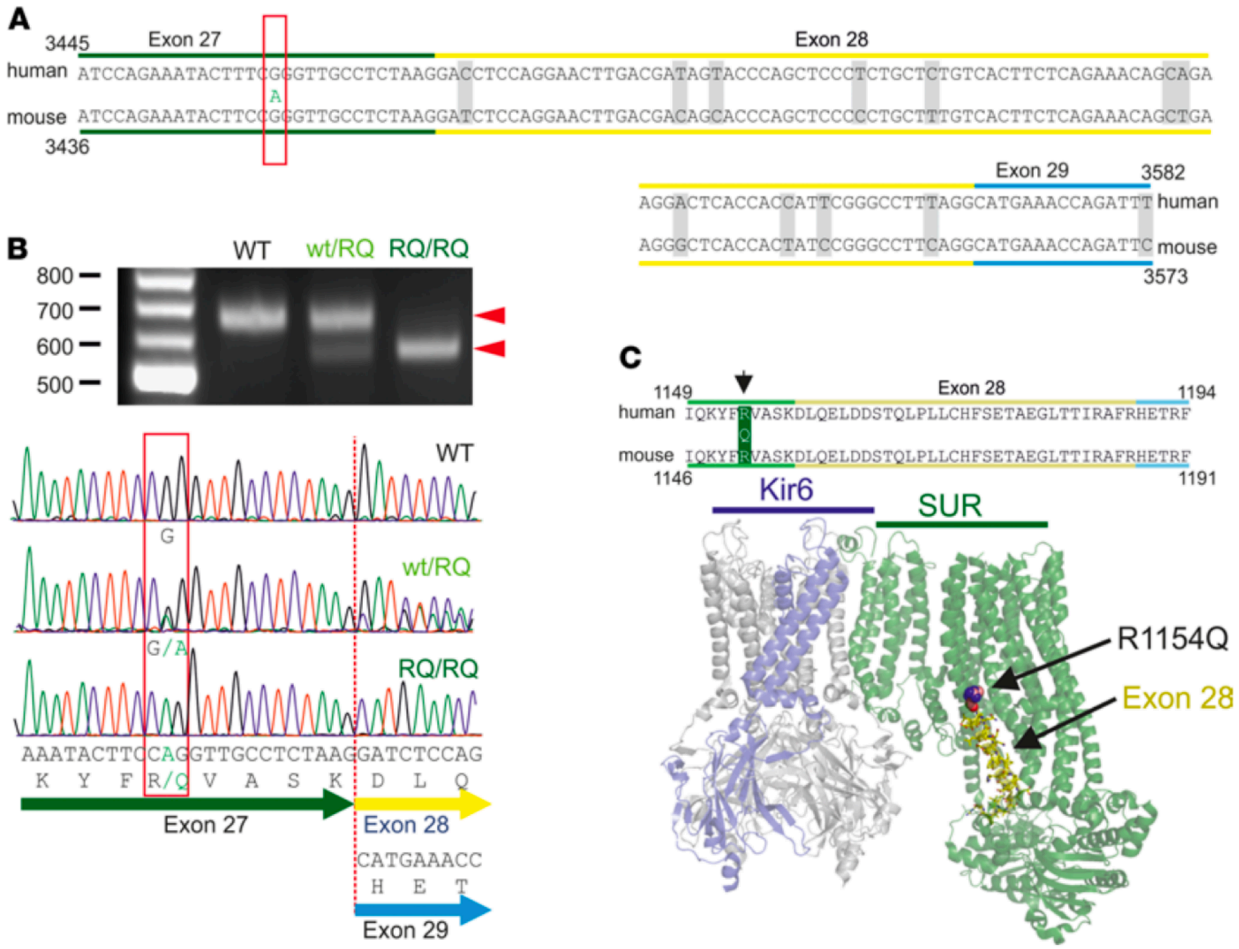

Figure 3.5: Abnormal splicing in SUR2A[R1154Q] mRNA. (**A**) Canonical cDNA sequence for human and mouse SUR2 over the exon 27–29 region (non-identities indicated by gray). Human nucleotide c.3461 (mouse c.3452) G>A mutation generating p.R1154Q is indicated by the red box. (**B**) Analysis of cDNA PCR product by gel electrophoresis and by direct sequencing of the selected bands reveals an exact deletion corresponding to the 93 nucleotides of exon 28 in approximately half of heterozygous WT/RQ and almost all homozygous RQ/RQ mouse transcripts (red arrowheads). (**C**) Top: Amino acid sequence of residues 1149–1194 (human) is identical in human and mouse SUR2. Bottom: Model of the Kir6/SUR complex (Protein Data Bank 5WUA) indicates the predicted location of the R1154Q mutation and amino acids encoded by exon 28.

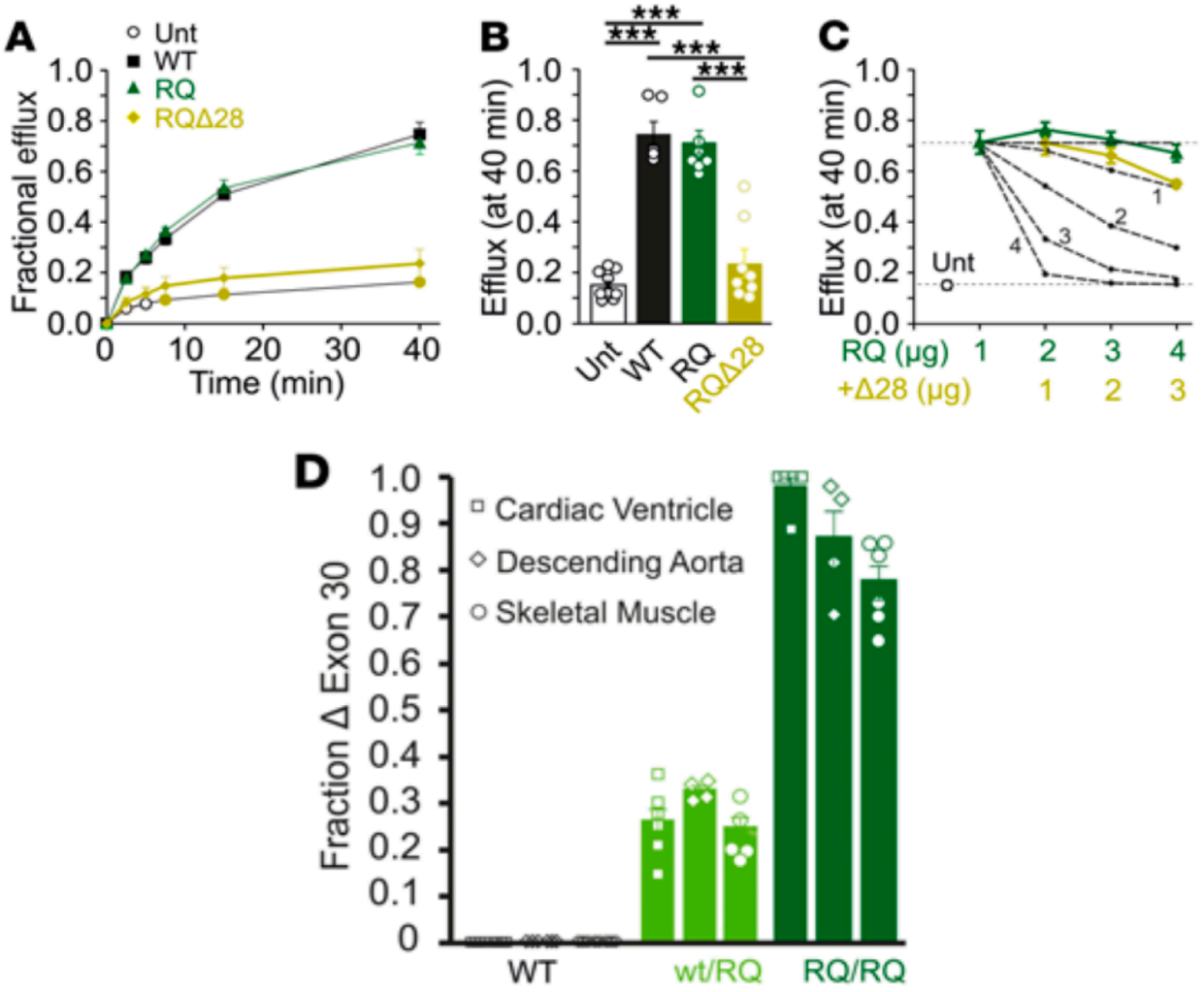

Figure 3.6: Functional consequence of SUR2[R1154Q] mRNA splicing. (**A**) Representative $^{86}Rb^{+}$ efflux experiments from untransfected Cosm6 cells (Unt) and cells transfected with WT, R1154Q (RQ), and R1154Q[Δexon28] SUR2A, plus Kir6.2. (**B**) Fractional efflux at 40 minutes, from experiments as in **A**. Statistical significance was determined by 1-way ANOVA followed by Tukey's tests; ***$p < 0.001$. (**C**) Fractional efflux at 40 minutes, from experiments similar to those in **A**, in cells transfected with SUR2[R1154Q,Δexon28] subunits in addition to SUR2[R1154Q] (plus Kir6.2) subunits. Dashed lines are predicted levels of efflux assuming that 1, 2, 3, or 4 WT subunits in a randomly assembling complex are necessary to restore function. (**D**) cDNA PCR product analyzed by gel electrophoresis reveals similar levels of splicing in R1154Q ventricle, smooth muscle, and skeletal muscles, suggesting that SUR2 function will be significantly reduced in all tissues.

3.2.4 Non-K_{ATP} ionic currents that govern vascular excitability are unaltered in the pathophysiological context of CS vasculopathy

VSMC excitability depends on the concerted activity of multiple ion conductances, in particular voltage-gated K^+ (K_v) channels and L-Type Ca^{2+} currents (LTCCs). To provide a benchmark of these currents in native wild type VSMCs, whole-cell voltage-clamp was first used to assess functional activity of K_v channels in acutely dissociated WT mouse aortic VSMCs (Figure 3.7). The voltage protocol was designed to inclusively measure the ensemble of expressed vascular K_v channels, and high (5mM) ATP was included in the internal solution to exclude K_{ATP} currents. Very small, linear, K^+ conductance was detected below ~-25mV, but additional K^+ conductance with apparently instantaneous and time-dependent components were increasingly activated at more positive voltages (Figure 3.7A). Additionally, more positive voltage steps revealed observable single-channel activity consistent with large-conductance calcium-activated potassium (BK_{Ca}) channels (Figure 3.7A). K_v currents were also assessed in aortic VSMCs acutely dissociated from mice carrying the Kir6.1[V65M] (VM) mutation, a CS-associated variant that causes marked K_{ATP} GoF and severe CS vasculopathy (Cooper et al., 2017; Y. Huang et al., 2018). K_v currents in VM VSMCs were very similar to WT (Figure 3.7), and summarized I-V curves show that overall K_v current amplitudes were indistinguishable between WT and VM VSMCs (Figure 3.7A). To separate K_v and BK_{Ca} currents, and to assess K_v current kinetics, a monoexponential function representing 'idealized' K_v currents was fit directly to each recording at the three most positive voltage steps (i.e., +25mV, +35mV, and +45mV), as shown in Figure 3.7B. This allowed separation of instantaneous K_v amplitudes, time-dependent K_v amplitudes, and assessment of K_v time constant (Tau). BK_{Ca} channel activity (NP_o) was separately estimated for each record at +25mV, +35mV, and +45mV by subtracting the idealized K_v current from each raw recording. Instantaneous and time-dependent Kv amplitudes, as well as K_v kinetics, and BK_{Ca} activity, were all statistically unaltered in the setting of CS vasculopathy (Figure 3.7B).

Next, whole-cell voltage-clamp was used to assess functional activity of voltage-sensitive LTCC. Ba^{2+} was used as a charge carrier, and included in the bath was BayK8644 (1μM), a potentiator of vascular LTCCs. K^+ currents were minimized by inclusion of Cs^+ (130mM) in the internal solution, as well as 3.5mM ATP to exclude K_{ATP} currents. LTCCs were undetectable in acutely isolated WT mouse aortic VSMCs (*n* = 8 recordings from three animals). However, characteristic LTCCs that were fully inhibited by nifedipine (10μM) were present in VSMCs acutely dissociated from first- through fourth-order mesenteric arteries, which are resistance vessels (Figure 3.8A). Again, LTCCs recorded from mesenteric VSMCs acutely dissociated from VM mice were essentially identical to WT (Figure 3.8B).

Together, the above experiments indicate that, despite marked changes in K_{ATP} currents in VSMCs from Cantu mice (Y. Huang et al., 2018), there are no accompanying compensatory or downstream changes in vascular K^+ currents or LTCCs.

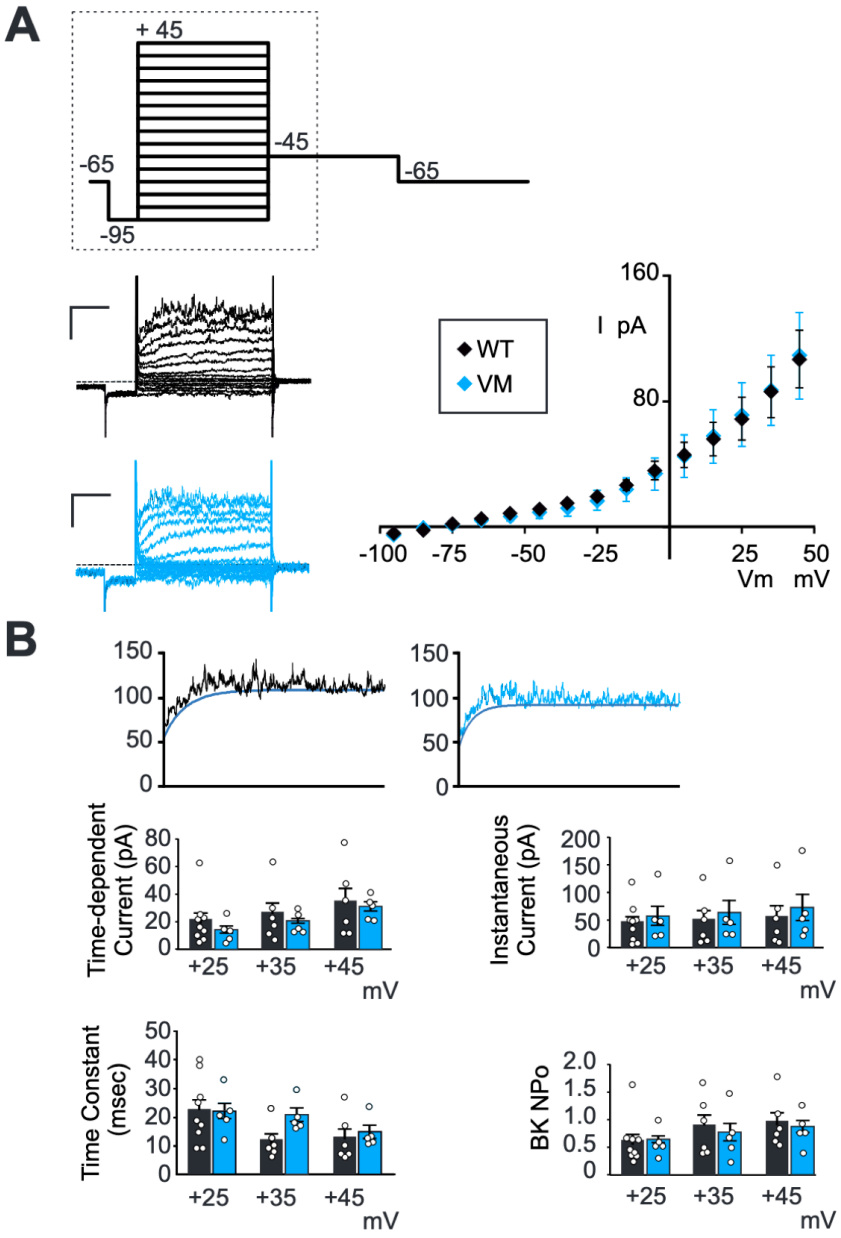

Figure 3.7: Voltage-gated K^+ currents in mouse CS and WT VSMCs. (**A**) (*left)* Representative whole-cell voltage-clamp recordings show K_v currents from acutely isolated aortic VSMCs from a WT (black) and VM (blue) mouse (*scale bars* = 50 pA, 100 ms). Voltage was stepped from holding potential of -65 mV to pre-pulse at -95 mV, then stepped more positive in 10 mV increments. Hashed box demarcates the portion depicted in the representative patch-clamp traces. (*right*) I-V relationships show mean ± standard error (s.e.m.), for *n* = 9 (WT) and *n* = 5 (VM) cells in each case. (**B**) Representative traces following step to +45 mV from WT (black) and VM (blue) VSMCs, fit with monoexponential functions to the minimal currents as a function of time, assumed to reflect K_v currents without the contaminating fluctuating, presumably BK_{Ca} current. From such traces, K_v amplitudes and kinetics, as well as BK_{Ca} currents, were calculated, as shown to the right (*n* as above). Statistical significance was determined by Mann-Whitney *U* test (α = 0.05, no significant differences detected).

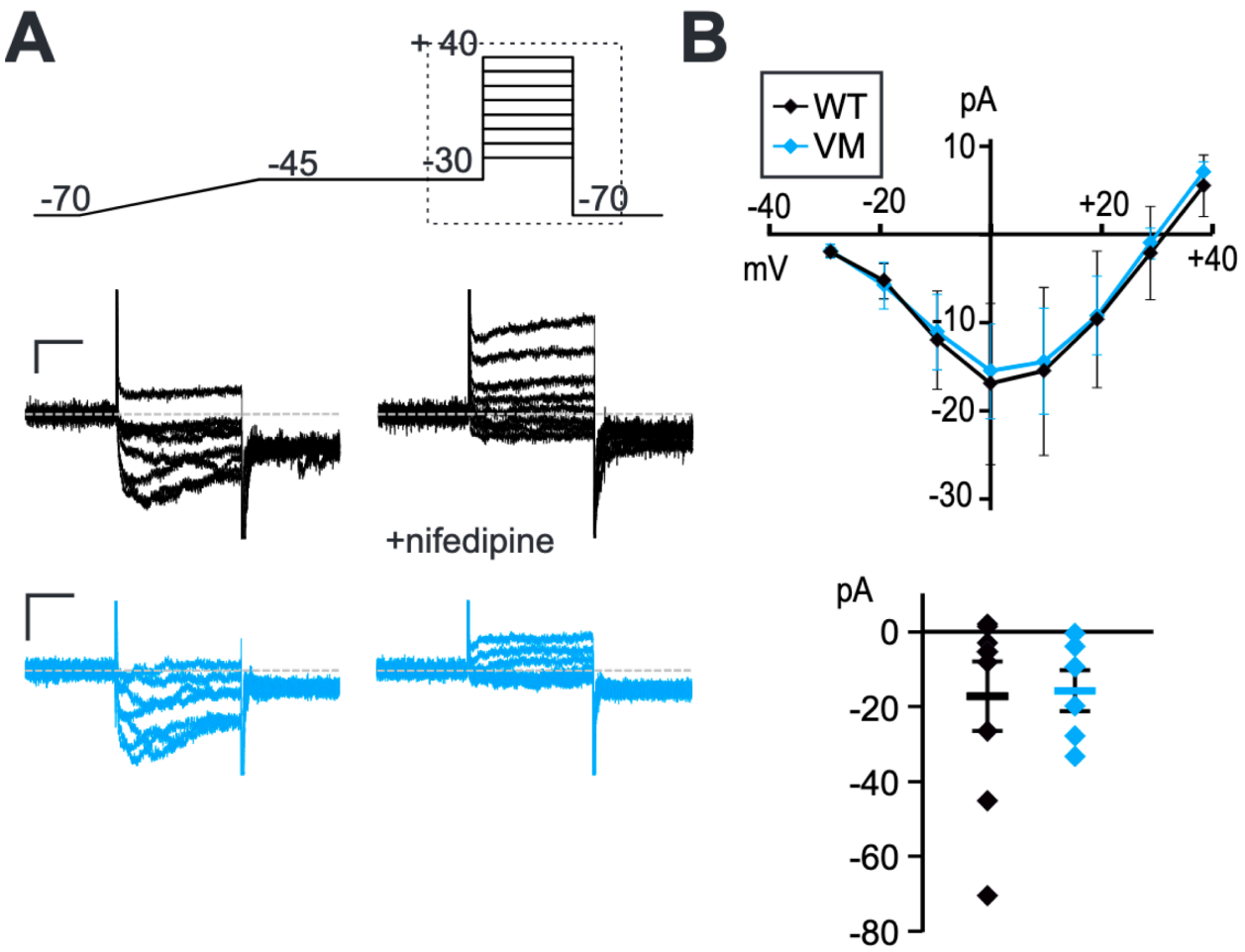

Figure 3.8: L-type Ca^{2+} currents (LTCCs) in mouse CS and WT VSMCs. (**A**) (*left)* Representative whole-cell voltage-clamp recordings of LTCCs were obtained from acutely isolated mesenteric VSMCs from WT (black) and VM (blue) mouse (*scale bars* = 10 pA, 75 ms). Voltage was ramped from -70 mV to -45 mV over 400 msecs to inactivate any high voltage activated currents, then stepped to voltages between -30 and +40 mV in 10 mV steps. Hashed box demarcates the portion depicted in the representative patch-clamp traces. Recordings were obtained in the presence of 1μM Bay K8644 (*left*), and conductance by LTCC was confirmed by >95% inhibition with 10μM nifedipine (*right*). (**B**) (*above*) Peak I-V relationships on Bay K8644 are summarized, with (*below*) peak current at 0 mV for individual traces. Error bars show mean + s.e.m. (*n* = 8 WT and *n* = 6 VM cells in each case). Statistical significance was determined by Mann-Whitney *U* test (α = 0.05, no significant differences detected).

Chapter 4: Electrophysiology of human iPSC-derived vascular smooth muscle cells and cell autonomous consequences of CS mutations

Adapted from Hanson, et al. "Electrophysiology of human iPSC-derived vascular smooth muscle cells and cell autonomous consequences of Cantu Syndrome mutations", submitted 2022 to Cell Stem Cell

Prior to this project, there was no published electrophysiological characterization of hiPSC-derived VSMCs. This chapter describes the first such study. Prior to this project, despite prevailing evidence that vascular K_{ATP} GoF is the etiology of the diverse cardiovascular changes in CS, the molecular effect had never been demonstrated in human vascular cells with CS mutations. This chapter describes the electrical consequences of CS mutations on K_{ATP} channel activity and membrane potential in CS patient-derived hiPSC-VSMCs, explaining the hypomyotonic component of CS vasculopathy. Finally, although the CS phenotype is indicative of hyperelastic changes to the vasculature, increased vascular elastogenesis had never previously been demonstrated in any cells with CS mutations. This chapter describes cell-autonomous hyperelastogenic consequences of CS mutations in patient-derived hiPSC-VSMCs and CS murine models, explaining the hyperelastogenic basis of CS vasculopathy.

I conceived of this study, with the help of Conor McClenaghan and Colin Nichols. I procured hiPSC lines, and acquired R1154Q patient-derived primary cells, developed the novel hiPSC-cardiomyocyte model for CS, carried out all patch-clamp experiments on these cells, and performed RNA analysis on these cells. I gained IRB approval for acquisition of primary tissues surgically removed from the human RQ patient, and I carried out all RNA analysis on these tissues. I adapted a published VSMC differentiation protocol to generate control hiPSC-VSMCs, and generated the novel hiPSC-VSMC

models for CS. I carried out immunofluorescent staining of these cells, as well as RNA isolation and *ABCC9* transcript analysis. I designed and carried out all patch-clamp electrophysiology experiments, and performed all associated analyses. Carmen Halabi carried out vessel compliance measurements and q-PCR experiments. I wrote the manuscript with input and edits by Colin Nichols, and other contributing authors helped review the manuscript.

4.1 METHODS

4.1.1 Study approval

Animal studies were performed in compliance with the standards for the care and use of animal subjects defined in the NIH Guide for the Care and Use of Laboratory Animals (Jahangir & Terzic, 2005) and were reviewed and approved by the Washington University Institutional Animal Care and Use Committee. Human studies were approved by the Washington University Human Studies Committee and carried out with the full consent of participating patients.

4.1.2 Human iPSC generation and differentiation to cardiomyocytes and VSMCs

Patient-derived human induced pluripotent stem cells (hiPSCs), heterozygous for the RQ and RW variants were generated, respectively, from peripheral blood mononuclear cells and renal epithelial cells, which were generously provided by CS patients who had been genetically confirmed to carry these variants. Human R1154W patient renal epithelial cells (RECs) were reprogrammed to hiPSCs by the WUSM Genome Engineering and iPSC Core (GEiC) using Sendai Virus-based reprogramming vectors. After four unsuccessful attempts to reprogram human R1154Q patient RECs, peripheral blood mononuclear cells were provided by the patient, and were successfully reprogrammed by the GEiC using the Sendai Virus-based reprogramming cocktail. hiPSCs were maintained on a 4-day passaging cycle. Two subclonal hiPSC lines were generated for each patient sample, and DNA sequencing analysis confirmed the expected gene variant in each line. Two control

lines, C2a (gift of Dr. Gordana Vunjak-Novakovic, Columbia University), and AN-1.1 (gift of Amber Neilson) were used as controls.

Differentiation to cardiomyocytes was carried out in entirely chemically defined conditions via temporal modulation of canonical Wnt signaling (Lian et al., 2012). hiPSCs were differentiated to hiPSC-VSMCs by adapting the chemically-defined protocol published by Patsch et al. (Patsch et al., 2015), which involves initially 'priming' hiPSCs into lateral plate mesodermal progenitors through Wnt activation and hBMP4 treatment, with subsequent induction to VSMC fate though co-treatment with PDGF-BB and ActivinA. The original protocol was followed exactly, except that differentiation was carried out in 12-well plates, rather than in T175 flasks. Immunohistochemical (IHC) staining for smooth muscle actin was carried out using anti alpha-Smooth Muscle-Cy3 monoclonal antibody C6198 (Sigma-Aldrich Co.).

4.1.3 RNA analysis in native VSMCs and hiPSC-VSMCs

RNA was isolated from WT and RQ hiPSC-VSMCs, and analyzed by RT-PCR for *ABCC9* or elastin transcripts using TRIzol (Thermo Fisher) and first strand cDNA was synthesized using SuperScript™ III First-Strand Synthesis System (Thermo Fisher).

4.1.4 Patch clamp electrophysiology

Mice were anesthetized with 2.5% avertin (10ml/kg, intraperitoneal Sigma-Aldrich) and the descending aorta or mesenteric arteries were rapidly dissected and placed in ice-cold Physiological Saline Solution (PSS) containing (in mM): NaCl 134, KCl 6, $CaCl_2$ 2, $MgCl_2$ 1, HEPES 10, and glucose 10, with pH adjusted to 7.4 with NaOH. Smooth muscle cells were enzymatically dissociated in dissociation solution containing (in mM): NaCl 55, sodium glutamate 80, KCl 5.6, $MgCl_2$ 2, HEPES 10, and glucose 10, pH 7.3 with NaOH, then placed into dissociation solution containing papain 12.5 µg/mL, dithioerythreitol 1 mg/mL, and BSA 1 mg/mL for 25 minutes (at 37°C), before transfer to dissociation solution containing collagenase (type H:F=1:2) 1 mg/mL, and BSA 1 mg/mL for 5 minutes (at 37°C). Cells were dispersed by gentle trituration using a Pasteur pipette, plated onto

glass coverslips on ice and allowed to adhere for >1 h before transferal to the recording chamber.

Whole-cell ion currents were recorded using an Axopatch 200B amplifier and Digidata 1200 (Molecular Devices). Recordings were sampled at 3 kHz and filtered at 1 KHz. Voltage-gated K^+ currents were measured in High Na^+ bath solution containing (in mM): NaCl 134, KCl 5.4, $CaCl_2$ 100 µM, $MgCl_2$ 1, HEPES 10, and glucose 10, with pH adjusted to 7.4 with NaOH. The pipette solution contained (in mM) KCl 140, $MgCl_2$ 1, HEPES 10, glucose 10, and EGTA 10, ATP 5, with pH adjusted to 7.2 with KOH. Voltage-gated LTCCs were measured in High Na^+ bath solution containing (in mM): choline chloride 124, BaCl2 20, $MgCl_2$ 1, HEPES 10, and glucose 5, with pH adjusted to 7.4 with NaOH. The pipette solution contained (in mM) CsCl 130, $MgCl_2$ 2, HEPES 10, glucose 10, and EGTA 10, Na_2ATP 3.5, with pH adjusted to 7.3 with KOH. To assess K_{ATP} conductances, currents were initially measured at a holding potential of -70mV in High Na^+ bath solution containing (in mM): NaCl 136, KCl 6, $CaCl_2$ 2, $MgCl_2$ 1, HEPES 10, and glucose 10, with pH adjusted to 7.4 with NaOH before switching to a High-K^+ bath solution (KCl 140, $CaCl_2$ 2, $MgCl_2$ 1, HEPES 10, and glucose 10, with pH adjusted to 7.4 with KOH) in the absence and presence of pinacidil and glibenclamide as indicated. The pipette solution contained (in mM) potassium aspartate 110, KCl 30, NaCl 10, $MgCl_2$ 1, HEPES 10, $CaCl_2$ 0.5, K_2HPO_4 4, and EGTA 5, with pH adjusted to 7.2 with KOH.

4.1.5 Arterial compliance

After mice were euthanized under isoflurane anesthesia, the aortae of 3 week-old mice were excised and placed in a physiologic saline solution (PSS) containing (mM) 130 NaCl, 4.7 KCl, 1.18 $MgSO_4^-$, 1.17 KH2PO4, 14.8 $NaHCO_3$, 5.5 dextrose, and 0.026 EDTA (pH 7.4). The vessels were then cleaned from surrounding fat, mounted on a pressure arteriograph (Danish Myo Technology) and maintained in PSS at 37°C. Vessels were visualized with an inverted microscope connected to a charged-coupled device camera and a computerized system, which allows continuous recording of vessel diameter. Intravascular pressure was increased from 0 to 175 mmHg by 25-mmHg increments and

the vessel outer diameter was recorded at each step (12 seconds per step). The average of three measurements at each pressure was reported.

4.1.6 Data Analysis

Unless otherwise noted, data are presented as mean ± S.E.M. The Real Statistics add-in package was used to run statistical analysis in Microsoft Excel. All data were tested for statistical significance using Mann Whitney *U* test, or Kruskal-Wallis test with post hoc Dunn's test.

4.2 RESULTS

4.2.1 Differentiation of human iPSCs to vascular smooth muscle cells

To examine the electrophysiology of hiPSC-VSMCs, and to gain further insight to vascular consequences of CS variants, two genetically unrelated control human iPSC lines (C2a and AN-1.1, from individuals with no known disease-associated variants) were first differentiated to vascular smooth muscle cells. hiPSC-VSMCs were differentiated using the protocol developed by Patsch et al. (Patsch et al., 2015), which allows rapid and efficient differentiation to VSMCs that resemble native VSMCs based on expression of key marker genes, global transcriptomic and metabolomic signatures, and key functional characteristics including contractility and extracellular fibronectin deposition mediated by TGF-ß signaling (Patsch et al., 2015). This protocol is completely chemically defined and, in our hands, is reproducible under the published conditions. hiPSCs begin as relatively small, round, gray cells with dark nuclei (Figure 4.1A). For four days, the cells are induced to become lateral mesodermal progenitors, which appear slightly enlarged but morphologically similar to hiPSCs. At this stage, the cells form a confluent monolayer, and patches of dead cells begin to accrue near the end of the 4-day lateral mesoderm induction. Finally, the cells are committed to a VSMC fate via exposure to PDGF-BB and Activin A. Once fully differentiated and cultured on a collagen-coated surface, the hiPSC-VSMCs possess a tapered, spindle-shaped morphology, and tend to align with one another, forming networks of multicellular whorls (Figure 4.1A). I verified that the

differentiation was effective by fixing the cells and staining for the VSMC marker, alpha-SMA (smooth muscle actin). Figure 4.1B shows a composite fluorescent image of C2a hiPSC-VSMCs, with DAPI nucleic stain (blue) and alpha-SMA expression revealed by a Cy3-conjugated antibody (red).

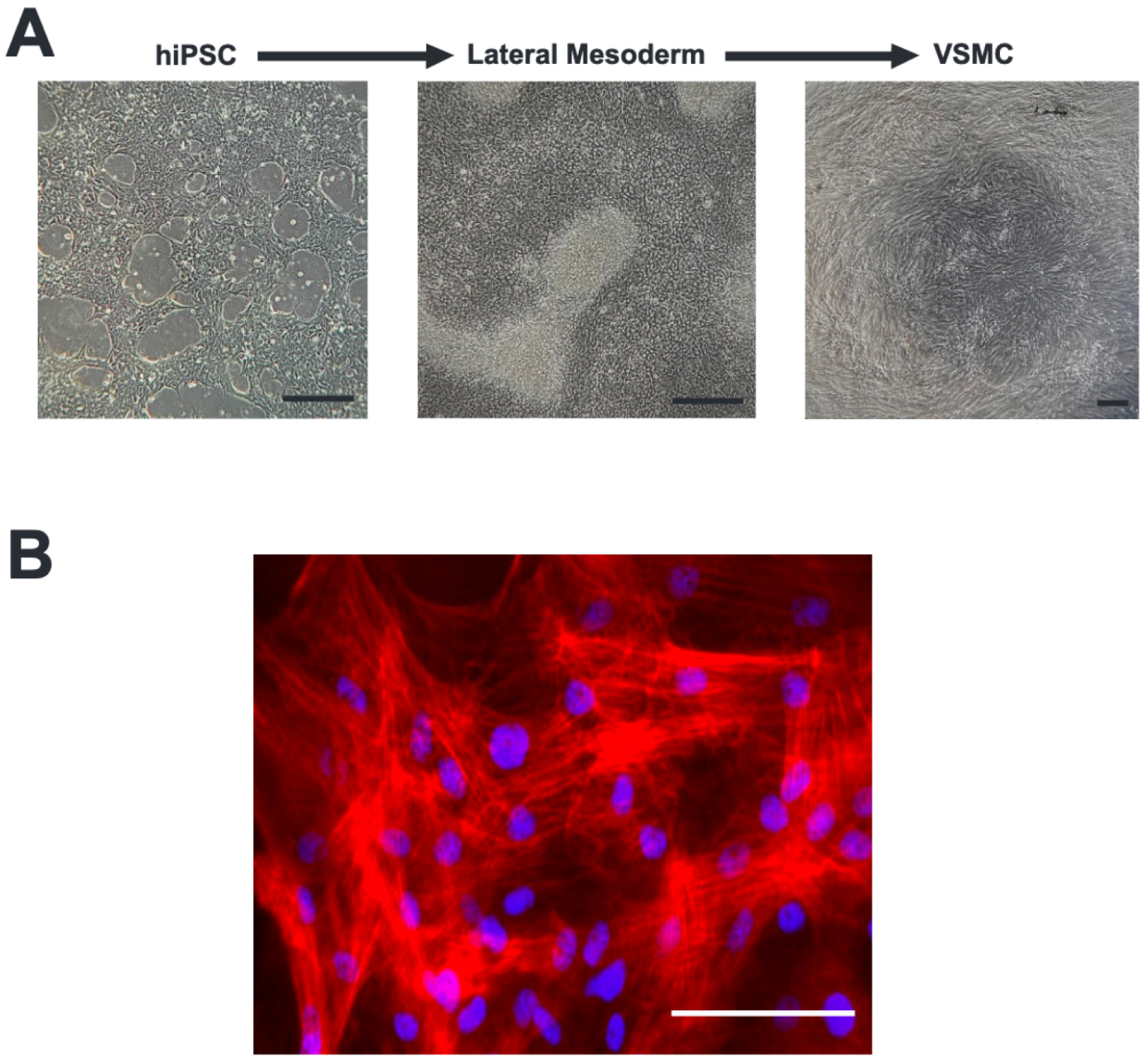

Figure 4.1: Differentiation of hiPSCs to VSMCs. (**A**) Images of (*left*) hiPSCs prior to differentiation, (*center*) after initial differentiation to lateral mesodermal progenitors, and (*right*) after full differentiation to hiPSC-VSMCs cultured on a collagen-coated surface (*scale bars* = 200 μm). (**B**) Composite fluorescent image of hiPSC-VSMCs with DAPI nuclear stain (blue) and Cy3-conjugated alpha-SMA stain (red), showing a dense network of discrete, co-aligned filaments expressed by hiPSC-VSMCs (*scale bar* = 50 μm).

4.2.2 hiPSC-VSMCs express very similar ion channels to those in native mouse arterial VSMCs

To assess the vascular ensemble of K_v currents functionally expressed in hiPSC-VSMCs, recordings were obtained in these cells with the same protocols and solutions as above, in mouse VSMCs (Figure 4.2). Consistently, I observed vascular K_v currents that were very similar to those measured in native VSMCs, with nearly identical similar current amplitudes and time-dependence (Figure 4.2A). BK_{Ca} currents were also evident in some recordings, although less consistently than in mouse VSMCs, and were not characterized. I also detected nifedipine-sensitive LTCCs with essentially identical time dependence and current density to those in native mesenteric VSMCs (Figure 4.2B).

These experiments provide a key first demonstration of hiPSC-VSMC electrophysiology, which shows similarity with native vascular ionic currents, essential for any future studies using these cells for assessing vascular function in general, and particularly in response to electrically active agents.

4.2.3 Pinacidil-sensitive K_{ATP} channels are present in hiPSC-VSMCs

Pinacidil-sensitive K_{ATP} channels, formed by Kir6.1 and SUR2 subunits, are key determinants of VSMC membrane voltage and excitability (Flagg, Enkvetchakul, Koster, & Nichols, 2010). In previous studies, vascular K_{ATP} activity and pharmacology in mouse aortic VSMCs was characterized using an intracellular pipette solution containing no ATP (Y. Huang et al., 2018). Using identical experimental conditions, I obtained whole-cell voltage-clamp recordings of basal K^+ conductance in hiPSC-VSMCs (Figure 4.2C). K^+ current increased substantially when the SUR2-selective activator pinacidil (100μM) was applied, and current decreased following the addition of the K_{ATP} inhibitor glibenclamide (10μM) in the continued presence of pinacidil (Figure 4.2C), reflecting activation of very similar K_{ATP} currents to those recorded in WT mouse VSMCs (Y. Huang et al., 2018). Pinacidil responsivity indicates that hiPSC-VSMC K_{ATP} channels comprise the same vascular-type SUR2 isoform that is expressed in native VSMCs. Reduction of pinacidil-activated currents to essentially basal levels by glibenclamide further confirms that these

currents are conducted by K_{ATP}, with glibenclamide efficacy closely resembling that previously measured in native VSMCs (Y. Huang et al., 2018). Given these observations, hiPSC-VSMCs constitute a promising approach for the study of molecular and cellular consequences of CS variants.

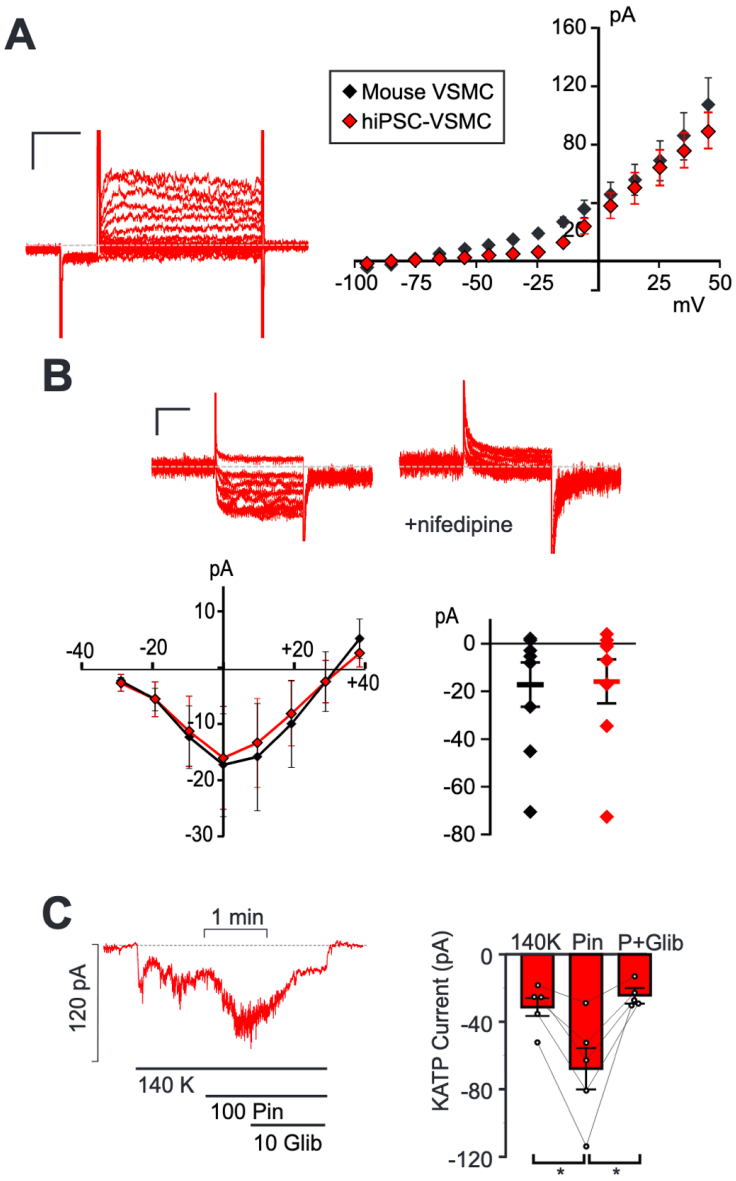

Figure 4.2: Electrophysiological characterization of hiPSC-VSMCs. (**A**) (*left)* Representative whole-cell voltage-clamp recordings show K_v currents from a hiPSC-VSMC (*scale bars* = 50 pA, 100 ms). Voltage-clamp protocol was as in Figure 1. (*right*) I-V relationship shows mean ± s.e.m, for *n* = 9 cells, as well as the WT mouse I-V from Figure 3.7. (**B**) (*top)* Representative whole-cell voltage-clamp recordings of LTCCs were obtained from a hiPSC-VSMC (*scale bars* = 10 pA, 75 ms). Voltage-clamp protocol as in Figure 2. Recordings were obtained in the presence of 1μM Bay K8644 (*left*), and conductance by LTCC was confirmed by >95% inhibition with 10μM nifedipine (*right*). (*bottom*) Peak I-V relationships in Bay K8644 are summarized (together with data from WT mouse VSMCs from Figure 3.8), with peak current at 0 mV displayed right for individual traces. Error bars show mean + s.e.m. (*n* = 8 WT and *n* = 6 VM cells in each case). (**C**) (*left*) Representative whole-cell voltage-clamp recordings of K_{ATP} channel conductance from control C2a hiPSC-VSMC using an intracellular pipette solution containing no nucleotides. Cells were voltage-clamped at -70 mV. (*right*) Summary of mean currents in basal conditions, in 100μM pinacidil, and in 100μM pinacidil plus 10μM glibeclamide (mean + s.e.m., *n* = 5 cells). Statistical significance was

determined by pairwise *t*-test with Bonferroni correction for multiple comparisons. * $p < 0.05$, ** $p < 0.01$, *** $p < 0.001$.

4.2.4 Increased basal K_{ATP} activity, and decreased sensitivity to glibenclamide, in CS patient-derived hiPSC-VSMCs

I next developed human iPSC-derived vascular myocyte models for Cantú Syndrome using two patient-derived iPSC lines, which had been generated using Sendai virus–based reprogramming vectors on PBMCs and renal epithelial cells. These cells were obtained from CS patients carrying the R1154Q (RQ) and R1154W (RW) mutations, respectively, which are the first- and second-most common CS-associated variants (Grange et al., 2019). Two subclonal hiPSC lines were produced for each mutation, and DNA sequencing analysis confirmed the expected mutation in each. Expression of human pluripotency-associated genes and a normal karyotype were confirmed for all hiPSCs prior to subsequent experiments, and CS hiPSC-VSMCs were differentiated as described above. Differentiation was highly efficient for all lines, with alpha-SMA consistently expressed in control, RQ, and RW hiPSC-VSMCs (>99% positive for each cell line, Figure 4.3A).

To assess the molecular consequences of CS mutations in human iPSC-VSMCs, whole-cell voltage-clamp was used to measure K_{ATP} currents in RQ and RW hiPSC-VSMCs, as well as control C2a hiPSC-VSMCs (Figure 4.3B). Experimental conditions were similar to those described above, but the pipette solution contained 100μM MgATP and 500μM MgADP (see Methods), to determine channel behaviors under nucleotide regulation. As shown in Figure 4.3B, basal K^+ conductances were significantly elevated in each of the CS patient-derived hiPSC-VSMCs compared to control cells (>4-fold in RQ cells and >2-fold in RW cells, note logarithmic scale). Pinacidil-activated currents were ~2.5x basal in WT (Figure 4.3B) and ~5.5x in RQ hiPSC-VSMCs (Fig 4.3B), but only ~1.9x in RW hiPSC-VSMCs (Figure 4.3B).

In control hiPSC-VSMCs, glibenclamide inhibited almost 100% of the pinacidil-activated current, but glibenclamide action was reduced in mutant cells, inhibiting only ~80% and ~55% of pinacidil-activated current in RQ and RW, respectively (Figure 4.3B).

Increased basal currents in the CS variant cells are consistent with elevated basal K_{ATP} activity due to the known molecular consequences of the mutations (Harakalova et al., 2012). However, since glibenclamide fails to reduce these currents to basal levels, I could not rule out the possibility that increased basal K^+ currents are non-K_{ATP} mediated. To test this possibility, whole-cell voltage-clamp was used, as described above, to characterize the vascular ensemble of functional K_v currents with high (5mM) ATP in the pipette (Figure 4.3C). I-V relationships revealed no significant basal K^+ conductances, nor differences in K_v currents between control, RQ, and RW hiPSC-VSMCs, confirming that elevated basal currents in Figure 4.3B are indeed K_{ATP} -mediated, and further demonstrating that there are no secondary, cell-autonomous changes in K_v currents associated with CS K_{ATP} GoF.

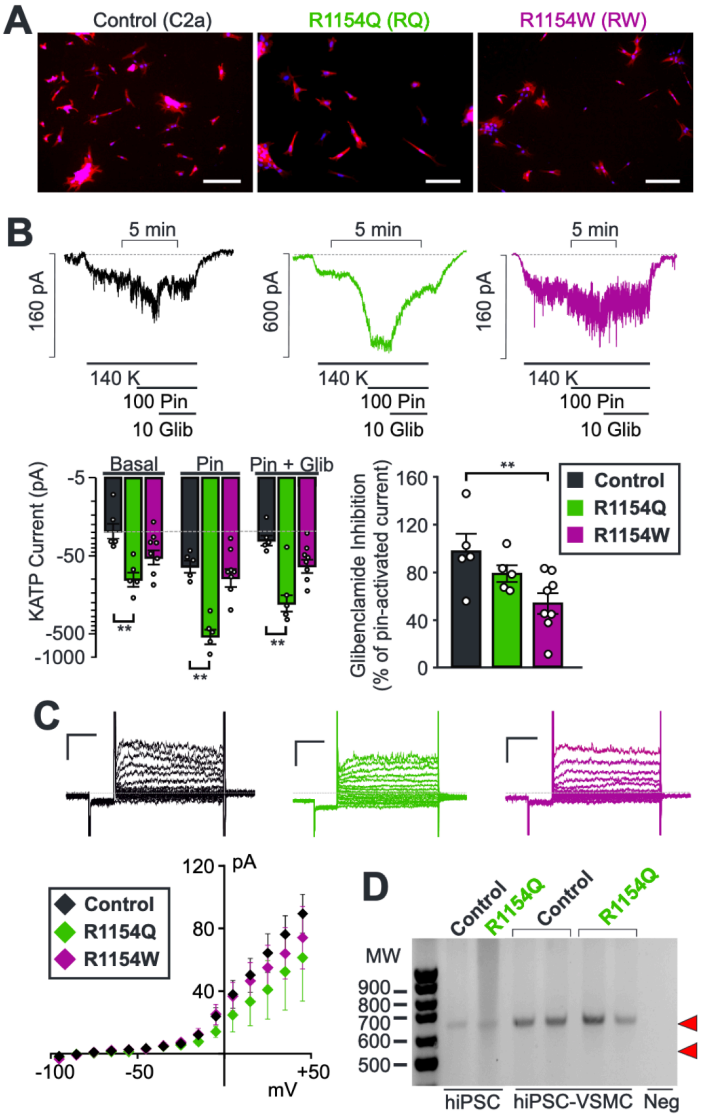

Figure 4.3: Electrophysiological characterization of CS hiPSC-VSMCs. (**A**) Composite fluorescent image of sparsely plated control C2a, R1154Q and R1154W hiPSC-VSMCs with DAPI nuclear stain (blue) and Cy3-conjugated alpha-SMA stain (red) (*scale bar* = 200 μm). (**B**) Representative whole-cell voltage-clamp recordings from control hiPSC-VSMCs (*left*), RQ hiPSC-VSMCs (*middle*), and RW hiPSC-VSMCs (*right*) using an intracellular pipette solution containing 100μM MgATP and 500μM MgADP. Cells were voltage-clamped at -70 mV. (*below*) Summary of mean currents in basal conditions, in 100μM pinacidil, and in 100μM pinacidil plus 10μM glibeclamide (mean + s.e.m., n = 5 cells in each case), as well as fraction of current inhibited by glibenclamide (*right*). (**C**) (*left)* Representative whole-cell voltage-clamp recordings show K_v currents from control, RQ and RW hiPSC-VSMCs (*scale bars* = 50 pA, 100 ms), voltage-clamp protocol as in Figure 3.7. (*below*) I-V relationships show mean ± s.e.m. in each case, for n = 9 (control), n = 5 (RQ) and n = 5 (RW) cells. (**D**) cDNA PCR product from control and RQ hiPSCs reveals only a single band corresponding to a 642 bp fragment from full-length SUR2 cDNA (predicted site indicated by upper red arrowhead) and no band corresponding to the predicted 549 bp from exon 28-excluded cDNA (predicted site indicated by lower red arrowhead). For hiPSC-VSMCs, two control samples and two RQ samples are shown, generated from two separate differentiations. Statistical significance was determined by Mann-Whitney *U* test (α = 0.05). * $p < 0.05$, ** $p < 0.01$, *** $p < 0.001$.

4.2.5 Lack of alternate *ABCC9* splicing in human R1154Q patient tissues and RQ patient-derived hiPSC-CMs

The introduced mutation thus results in alternate splicing and consequent loss of SUR2 protein in CS mice. In turn, this leads to significantly blunted phenotype severity, despite the R1154Q mutation showing a marked molecular GoF (McClenaghan et al., 2018). If the same splicing is similarly present in humans, it would tend to mitigate the effects of the mutation. In addition, variable SUR2 splicing between individuals could potentially account for the quite variable expressivity in CS individuals with the R1154Q mutation (Grange et al., 2019). I further examined the tissue dependence of exon 28 skipping in cDNAs generated from mRNA isolated from multiple R1154Q mouse tissues. As shown in Figure 3.6D, the apparent fraction of spliced transcripts was similar in skeletal, smooth, and cardiac muscle, being approximately 25%–35% in heterozygous, $SUR2^{WT/RQ}$ and approximately 75%–100% in homozygous, $SUR2^{RQ/RQ}$ animals. This further indicates that alternate SUR2 splicing is driven by the nucleotide change via a cell-autonomous mechanism, independent of tissue type. The less-than-stoichiometric ratio of spliced to unspliced transcript in the heterozygous case further suggests slower transcription or reduced stability of the mutant mRNA. I obtained a skin and skeletal muscle biopsy sample from a single R1154Q patient and successfully isolated *ABCC9* mRNA. However, PCR from both samples revealed only single product bands corresponding to full-length SUR2A cDNA and no band corresponding to exon 28–deleted cDNA (Figure 4.4A).

I also obtained PBMCs from a patient with the R1154Q mutation, and renal epithelial cells (RECs) were obtained from a patient with the R1154W mutation. Human induced pluripotent stem cells (hiPSCs) were generated from these primary cells using Sendai virus–based reprogramming vectors. Two subclonal hiPSC lines were produced for each mutation, and DNA sequencing analysis confirmed the expected mutation in each CS hiPSC line. A GCaMP6-expressing hiPSC line from an unaffected individual was used as a control. Expression of human pluripotency-associated genes and a normal karyotype were confirmed for all hiPSCs prior to subsequent experiments. WT and CS

hiPSCs were differentiated into cardiomyocytes as previously described (Lian et al., 2012). When I used this approach, hiPSC-derived cardiomyocytes exhibiting robust rhythmic contractile behavior were present by days 7–9. Subsequently, a 10-day lactate purification step was used to metabolically select for cells (Figure 4.4B) with cardiomyocyte-specific biochemical properties enabling survival exclusively via lactate metabolism, as previously described (Tohyama et al., 2013). For unknown reasons, I was unable to detect K_{ATP} channels in these myocytes (data not shown). However, RT-PCR analysis of RNA isolated from WT, R1154Q, and R1154W hiPSC–derived cardiomyocytes on day 45 revealed full-length SUR2A transcripts in each genotype, with no evidence of detectable alternate splicing (Figure 4.4B). Although the amino acid sequence in this region of SUR2 is identical in mice and humans (Figure 3.5C), there are slight variations in codon usage between the 2 species (Figure 3.5A) that could affect *ABCC9* mRNA splicing. Nevertheless, the lack of detectable alternate splicing in human R1154Q and R1154W iPSC–derived cardiomyocytes suggests that the disease mutation may not lead to alternate splicing in native human tissues.

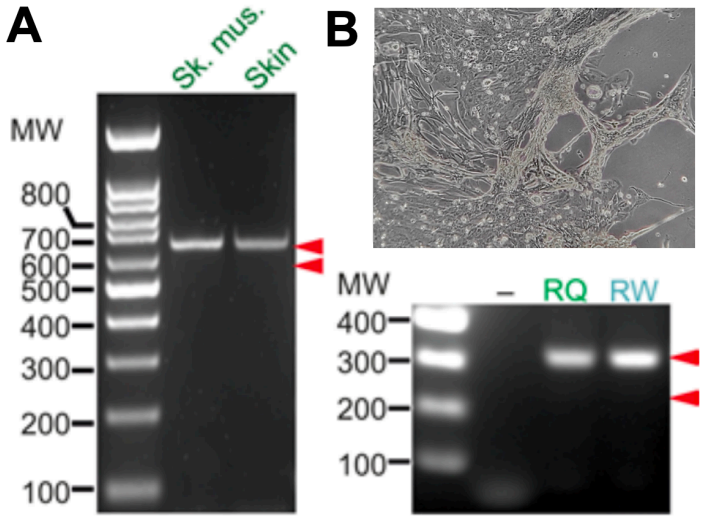

Figure 4.4: Alternate *ABCC9* splicing is not observed in human R1154Q patient tissues and RQ patient-derived hiPSC-CMs. (**A**) cDNA PCR product from human R1154Q patient skeletal muscle and skin analyzed by gel electrophoresis reveals only a single band corresponding to a 642 bp fragment from full-length SUR2A cDNA and no band corresponding to the predicted 549 bp from exon 28–deleted cDNA (red arrowheads). (**B**) Image of R1154Q patient iPSC–derived cardiomyocytes (*scale bar*: 50 μm). cDNA PCR product from R1154Q or R1154W patient iPSC–derived cardiomyocytes analyzed by gel electrophoresis reveals only a single band corresponding to the 325 bp fragment from full-length SUR2A

cDNA and no band corresponding to the predicted 232 bp fragment from exon 28–deleted cDNA (red arrowheads) (representative result from *n*= 3 repeats).

4.2.6 Cell-autonomous consequences of genetic K_{ATP} overactivity underlie both hypomyotonic and hyperelastic components of CS vasculopathy

A third CS mouse model was previously generated in which the SUR2[R1154Q] was knocked-in to the endogenous locus (H. Zhang et al., 2021). In contrast to the mice carrying the SUR2[A478V] or Kir6.1[V65M] CS-associated variants, SUR2-dependent K_{ATP} currents and the resultant CS phenotype were both minimal in R1154Q mice. This was a result of alternate splicing leading to excision of exon 28, 3' of the introduced variant, which led to non-functional SUR2 (H. Zhang et al., 2021). If occurring in human patients with this variant, such splice excision could significantly ameliorate the CS features resulting from the molecular GoF itself. However, RT-PCR analysis of cDNA amplified from RNA isolated from control and RQ hiPSC-VSMCs (Figure 4.3D) revealed no evidence of exon 28 exclusion, in agreement with observations from primary human tissues samples, discussed below (H. Zhang et al., 2021). This finding is consistent with the RQ hiPSC-VSMC patch-clamp recordings (Figure 4.3B), which revealed a striking increase in K_{ATP} activity, in contrast to native RQ mouse aortic VSMCs.

To understand how K_{ATP} GoF impacts VSMC excitability under physiological conditions, whole-cell current-clamp (I=0) was used to measure membrane voltage (V_m) immediately (<2s) upon break-in. In the two genetically unrelated control C2a and AN-1.1 hiPSC-VSMC lines, I observed identical mean V_m values (-44 mV), consistent with reports of native VSMC resting V_m, which lies in the range of -35 to -45mV (Loutzenhiser et al., 1997; Welsh et al., 1998; Welsh et al., 2000). Consistent with enhanced basal K_{ATP} conductance (Figure 4.3B), both RQ and RW hiPSC-VSMCs were markedly hyperpolarized by 10-15mV relative to both controls (Figure 4.5A).

Finally, joint hyperelasticity (Czeschik et al., 2013; Grange et al., 2019), tracheomalacia (Grange et al., 2019), and tortuous, dilated blood vessels (Brownstein et al., 2013; Kisilevsky et al., 2019; Leon Guerrero et al., 2016) are major features of CS, all potentially related to excess elastin production, which has also been reported in response to treatment of blood vessels and cultured VSMCs with the K_{ATP} activator minoxidil

(Hayashi et al., 1994; Knutsen et al., 2018; Tajima et al., 1995). As shown in Figure 4.5B, compliance was increased in aortae from both A478V and V65M mice at P21, the effect being dependent on the molecular severity (from WT < Het < Hom in each case). The increased compliance was paralleled in each case by increased elastin mRNA expression in vessels at 3 months. I also measured mRNA expression from control (C2a), RQ and RW hiPSC-VSMCs. There was a marked increase in elastin expression in both of the CS lines relative to control (Figure 4.5C), a clear demonstration that increased vascular elastogenesis is a cell-autonomous response to K_{ATP} GoF.

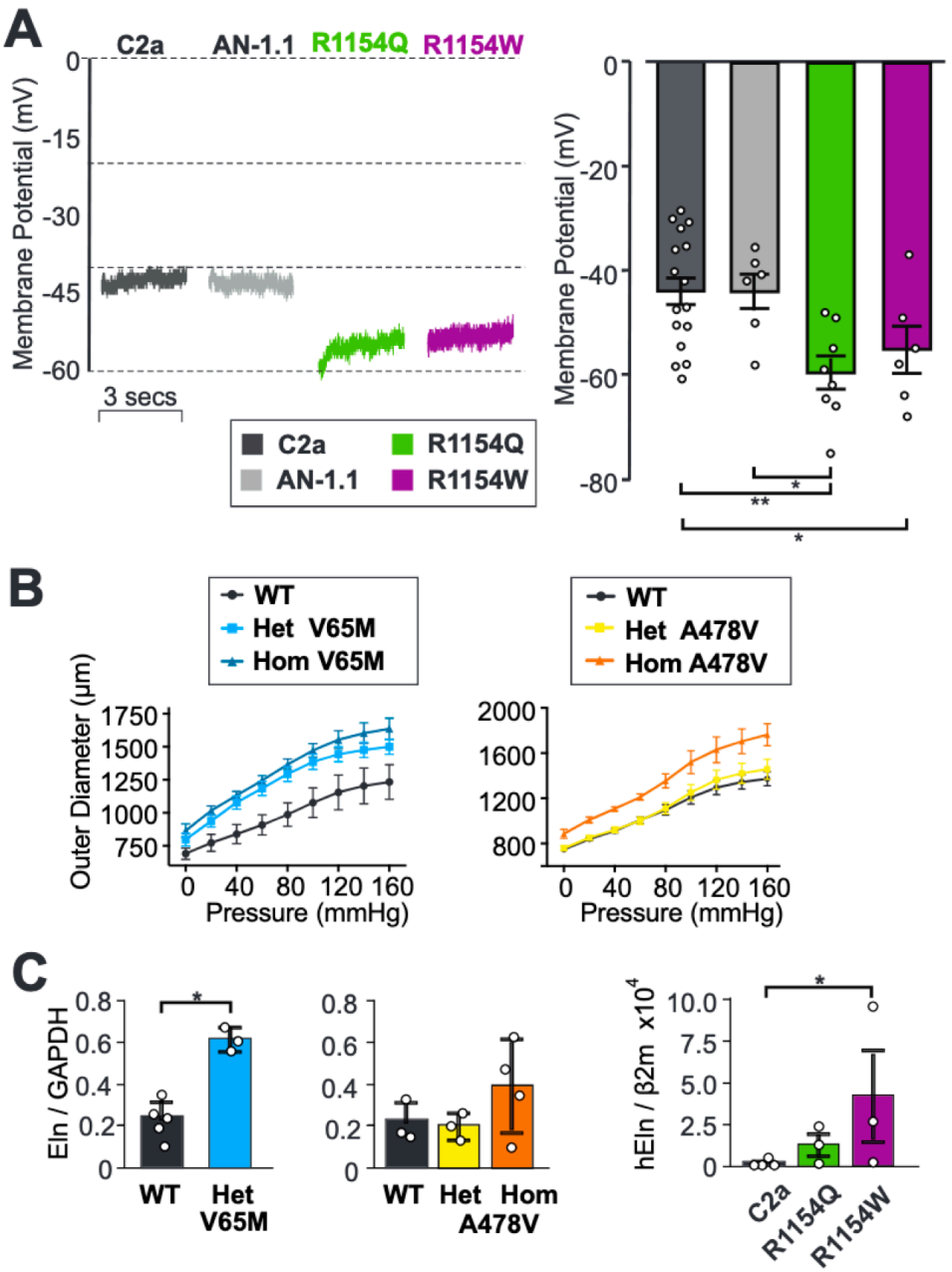

<u>Figure 4.5:</u> Cell-autonomous consequences of CS mutations on human iPSC-VSMC excitability and elastogenesis. (**A**) (*above*) Representative whole-cell current-clamp (*I*=0) recordings from two control hiPSC-VSMC lines (*left*; C2a, AN-1.1) and two CS variant hiPSC-VSMC lines (*right*; RQ, RW) using an intracellular pipette solution absent of nucleotides. (*below*) Individual and mean (± s.e.m., *n* = 6-16 cells) initial V_m immediately following break-in from experiments as above. (**B**) Vessel compliance in pressurized aortae of p21 WT, heterozygous and homozygous Kir6.1[V65M] mice (*left*), and WT, heterozygous and homozygous SUR2[A478V] (*right*) mice. Data shows mean + s.e.m., *n* = 4-5 animals in each case. (**C**) Elastin mRNA expression (normalized to GAPDH expression) in aortae from WT and V65M or A478V CS mice (left 2 panels), and from C2a control or R1154W and R1154Q hiPSC-VSMCs, normalized to β-2 microglobulin (right panel). Statistical significance was determined by Mann-Whitney *U* test (α = 0.05). * $p < 0.05$, ** $p < 0.01$, *** $p < 0.001$.

Chapter 5: Thesis Discussion

5.1 Molecular consequences of Cantú Syndrome-associated mutations in recombinant K_{ATP} channels

5.1.1 A cluster of novel Cantú Syndrome–associated *ABCC9* mutations cause K_{ATP} GoF

Prior to this project, the few characterized CS-associated mutations in *ABCC9* (SUR2) had been shown to result in GoF in recombinant K_{ATP} channels in the presence of Mg^{2+}-nucleotides, which can arise either from decreased sensitivity to inhibitory ATP, or augmented activation by Mg^{2+}-nucleotides (Cooper et al., 2015; Harakalova et al., 2012). In this study, I identified three novel (i.e., previously uncharacterized) polymorphisms from suspected CS patients that appear to cluster together in the TMD2 domain of SUR2: Y981S (human Y985S), G985E (G989E), and M1056I (M1060I). When electrical recordings were obtained from recombinant K_{ATP} channels in which these novel-variant constructs were heterologously expressed, I observed increased K_{ATP} channel activity in the presence of regulatory nucleotides via diverse molecular mechanisms. As in previous reports, I used Kir6.2/SUR2A channels for analysis due to the difficulty of recording Kir6.1/SUR2 currents, although it is expected that the mechanism of SUR2 mutations will be conserved irrespective of the pore-forming subunit. In addition, although the dependence of channel activity on intracellular nucleotides differs quantitatively between the two major SUR2 splice variants (SUR2A and SUR2B, which differ only in their C-terminal exon) (Matsuoka et al., 2000; Reimann et al., 2000), it is anticipated that, qualitatively, the changes observed for mutant SUR2A-containing channels will be common for SUR2B-containing channels.

5.1.2 A conserved molecular mechanism of GoF between the cluster of novel mutations and the two most common CS-associated mutations

Here, I compared the sensitivity of WT and mutant channels to ATP in the absence and presence of Mg^{2+} to dissect the Mg^{2+}-independent inhibitory effect of ATP from the activating effect of MgATP. This analysis reveals that the molecular mechanism by which the three clustered mutations (Y981S/G985E/M1056I) caused K_{ATP} GoF is through increased sensitivity to activatory MgATP signaling (Figure 2.4). These residues are all predicted to lie in close proximity to each other in a cluster within TMD2; Tyr-981 and Gly-985 are found at the N-terminal end of TM12, immediately following the NBD1-TMD2 linker, whereas M1056I is situated on the opposing TM13 (Figure 2.1). The location of the Tyr-981/Gly-985/Met-1056 cluster, at the link between the NBDs and the TM domains (Figure 2.1), is appropriate for transduction of movements between the intracellular and transmembrane domains of SUR2. Biochemical analyses of SUR and related ABC proteins indicate that MgADP or MgATP binding to the NBDs of SUR may act to stabilize dimerization of NBD1 and NBD2 (C. G. Nichols et al., 1996; Ueda, Komine, Matsuo, Seino, & Amachi, 1999; Zingman et al., 2001). However, how binding or NBD dimerization is coupled to gating of the channel pore remains poorly understood.

Notably, the GoF induced by each novel mutation is quite subtle when mutant and WT SUR2A subunits are co-expressed to mimic the clinically relevant heterozygosity (Figure 2.2). Recent reports of GoF mutations in Kir6.2 and SUR1 that underlie neonatal diabetes demonstrate that even very subtle biophysical effects can result in disease (Vedovato et al., 2016), suggesting that dramatic changes may not be necessary. Additionally, because SUR2B appears to be the more pathologically relevant splice variant, and nucleotide-dependent channel activity differs quantitatively between SUR2A and SUR2B (Matsuoka et al., 2000; Reimann et al., 2000), it is possible that these mutations will have a greater effect on channels containing SUR2B. Furthermore, the channel activity measured in $^{86}Rb^{+}$ experiments under basal conditions may not fully recapitulate the metabolic and physiological context for K_{ATP} channels in myocytes, and so I cannot rule out a more significant activating effect under other conditions.

I also characterized the molecular mechanism of the previously reported CS mutations R1150Q and R1150W (human residue R1154, located in TM15 of TMD2), which are the first- and second-most common known CS-associated mutations, respectively (Grange et al., 2019). As with the novel cluster described above, the RQ and RW mutations enhance MgATP activation, with a particularly dramatic effect observed in the RQ channels (Figure 2.5). There was also a trend toward diminished ATP sensitivity for the RW channels, although this effect did not reach statistical significance. Taken together with the molecular effects of the novel cluster, above, these findings demonstrate that multiple transmembrane regions of TMD2 are involved in the conformational changes associated with Mg^{2+}-nucleotide activation.

The concentration of free Mg^{2+} varies in different cell types (Swaminathan, 2003); in cardiomyocytes (which express Kir6.2/SUR2A), free Mg^{2+} is reported to be ~0.5 mm, the concentration used in this study (Quamme & Rabkin, 1990). As free Mg^{2+} levels are tightly regulated in most cells, the physiological effect of CS mutations that alter Mg^{2+}-nucleotide sensitivity will reflect altered response to nucleotide concentrations (in the presence of Mg^{2+}), not to changing Mg^{2+} concentrations (Foster & Coetzee, 2016a).

5.1.3 Consequences for sulfonylurea sensitivity

Previous studies have demonstrated that second generation sulfonylureas, such as glibenclamide, inhibit SUR2-containing K_{ATP} channels, albeit with lower potency than for SUR1-containing channels (Gribble, Tucker, Seino, & Ashcroft, 1998). As such, glibenclamide (or other sulfonylureas) represents a potential pharmacotherapy for CS. However, the CS–associated mutation Kir6.1[V65M] profoundly reduces glibenclamide inhibition of recombinant channels (Cooper et al., 2017), and there are multiple reports of neonatal diabetes mutations in the Kir6.2/SUR1 K_{ATP} subunits that reduce sulfonylurea sensitivity (Koster, Remedi, Dao, & Nichols, 2005; Proks, 2013). Therefore, it is important to assess whether CS mutations in SUR2 affect inhibitor sensitivity. It was determined that the cluster of Y981S, G985E, and M1056I mutations do not obviously affect glibenclamide sensitivity (Figure 2.6). It has been reported that sulfonylurea inhibition of

SUR2-containing channels is affected by nucleotide regulation (Hambrock, Loffler-Walz, & Quast, 2002; Proks, de Wet, & Ashcroft, 2014), and so it is possible that these mutations may alter pharmacological sensitivity under more complex physiological regulation, but this remains to be established.

A decrease in glibenclamide potency was observed in both the RQ and RW mutations, particularly for the latter (Figure 2.7). Interestingly, Arg-1150 lies in TM15 (Figure 2.1), and previous studies have demonstrated that TMs 14–16 are critical for high-affinity sulfonylurea binding to SUR subunits (Ashfield et al., 1999; Hambrock et al., 2001). Indeed, serine to tyrosine substitution of a single residue in TM16 (predicted to lie within ~15 Å of Arg-1150 on the cytoplasmic extensions of the TM helix) is sufficient to confer SUR2-like sulfonylurea sensitivity to SUR1, and vice versa (Ashfield et al., 1999; Hambrock et al., 2001). This raises the possibility that the Arg-1150 mutations may directly decrease glibenclamide sensitivity via disruption of the drug-binding site. The RW mutation exhibited a more pronounced effect than the glutamine mutation at the same site, perhaps due to a greater steric effect of the bulky tryptophan side chain. Regarding the relevance to treatability of disease, it is important to note that glibenclamide sensitivity was evaluated in a “homozygous” context where all SUR2 subunits were mutated, but all CS patients identified so far are heterozygous. The data suggest that most mutations may have relatively minor effects on drug sensitivity, but the two most common mutations arising in the Arg-1150 residue may reduce sulfonylurea sensitivity in CS patients. Studies of native channels in hiPSC-derived cardiovascular cells may allow more accurate assessment of the potential impact of CS mutations on the pharmacological response.

Collectively, these results provided further evidence for K_{ATP} GoF consequences of CS mutations arising in the SUR2 protein. The results illustrate a common molecular mechanism of enhanced MgATP activation for several mutations clustered in TM12–13, as well as the two most common mutations occurring in TM15. The cluster of mutations did not markedly affect sulfonylurea sensitivity, whereas the RQ and RW mutations led to considerably reduced glibenclamide response, particularly in the case of RW. The results provide novel insights to the function of K_{ATP} channel complexes, which will be useful for

linking CS genotype to phenotype in this complex disorder, and will inform the consideration of therapeutic approaches to CS.

5.2 Consequences of CS mutations in CRISPR/Cas9-generated murine models

5.2.1 Complex cardiovascular consequences of CS-associated K_{ATP} mutations: Additional outcome twists with R1154Q

The present study demonstrates that the most common CS-associated mutation, SUR2[R1154Q], when introduced into the analogous locus of the mouse genome, resulted in qualitatively the same cardiovascular features as the SUR2[A478V] and Kir6.1[V65M] mutations (Y. Huang et al., 2018), providing further confirmation of the common cardiovascular outcome of vascular dilation and cardiac enlargement resulting from SUR2- or Kir6.1-dependent K_{ATP} GoF in CS. However, in RQ animals, the disease was quantitatively much less severe than naively predicted based on the relative molecular severity of the mutation. The reason for the reduced severity of outcome was shown to be a reduction in overall K_{ATP} density in both vascular smooth muscle and heart, particularly in the case of homozygous RQ mice. This in turn was shown to be a result of the genomic c.3452G>A mutation causing altered pre-mRNA splicing, with deletion of the following exon 28 and generation of nonfunctional SUR2 proteins, and downregulation of overall K_{ATP} density. SUR2A levels were profoundly reduced in homozygous RQ mice, with the remaining SUR2A protein showing lower complex glycosylation, indicative of ER localization, as seen in Kir6.2-knockout animals (Arakel et al., 2014).

In general, genetic or pharmacological manipulations that alter the levels of any K_{ATP} subunits, even complete knockout of any given subunit, have not been shown to result in marked compensatory changes in other subunits, in any tissues (Flagg et al., 2008; Koster et al., 2001; Miki & Seino, 2005). In the present case, there was a small increase in absolute levels of cardiac diazoxide-sensitive current, and of mature, glycosylated SUR1 protein in the heart. Previous studies have suggested that SUR1, while present in the heart, is outcompeted by SUR2A for association with Kir6 subunits, resulting in low levels of fully mature, glycosylated SUR1 being present in K_{ATP} channels

at the membrane surface (Arakel et al., 2014). I speculate this may be because SUR2A-containing channels normally leave the secretory pathway more efficiently, so that when mutant SUR2A protein is depleted, SUR1 accesses Kir6.2, which explains the higher levels of core-glycosylated SUR1 and diazoxide-sensitive current in R1154Q hearts.

Cardiac hypertrophy and enhanced cardiac output are a consistent finding in CS patients (Levin et al., 2016) and in both Kir6.1[V65M] and SUR2[A478V] mutant mice (Y. Huang et al., 2018). It has been shown in these mice that cardiac hypertrophy arises independently of ventricular K_{ATP} activity, as a secondary consequence of enhanced vascular K_{ATP} activity, resulting in vasodilation-mediated reduced vascular resistance, and, in response, enhancement of renin-angiotensin signaling, adrenergic signaling, or other vasoresponsive pathways (Y. Huang et al., 2018; McClenaghan, Huang, Matkovich, et al., 2020). Cardiac enlargement was also observed in SUR2[R1154Q] mutant mice, but this was less marked than in V65M or A478V mice, consistent with reduced overall expression of SUR2-dependent K_{ATP} channel levels in the vasculature (as well as the heart). Cardiac β-adrenergic receptor (β-AR) activation promotes cardiac hypertrophy (Scheuer, 1999) and, as the Nichols group has also shown, maximal pharmacological β-AR stimulation can facilitate forward-trafficking of SUR1-K_{ATP} channels to the myocardial plasma membrane (Arakel et al., 2014). This in turn could contribute to the modest elevation in functional expression of SUR1-containing channels in R1154Q hearts.

5.2.2 Variable disease-causing/modifying consequences of alternate splicing in *ABCC* genes

Strikingly, the SUR2[R1154Q] (*ABCC9* c.3461G>A) mutation induced alternate splicing of *ABCC9* mRNA, generating a truncated SUR2 protein with an in-frame deletion of the 31 amino acids that comprise exon 28. When heterologously expressed together with Kir6.2 in recombinant channels, the SUR2[R1154Q,Δexon28] construct failed to generate active K_{ATP} channels. In mixed expression with full-length SUR2A cDNA, there was no evidence for a dominant-negative effect of the SUR2[R1154Q,Δexon28] construct; the data were best fit by assuming that even one full-length subunit was sufficient to fully

rescue function. This can explain the observed reduction in overall channel density yet persistence of vascular hyperpolarization and cardiac enlargement in R1154Q animals; in the case of heterozygous mice, the disease features were less marked than seen in heterozygous SUR2[A478V] animals (Y. Huang et al., 2018; McClenaghan, Huang, Matkovich, et al., 2020), even though the molecular consequence of the mutation itself was more severe, as discussed above in studies on the RQ mutation in recombinant channels (Harakalova et al., 2012; McClenaghan et al., 2018). In contrast to SUR2[A478V] animals, the disease features of homozygous RQ animals were no more dramatic than those of the heterozygous animals, and myocyte K_{ATP} channel activity was more markedly decreased, particularly in smooth muscle — explained by the enhanced degree of splicing.

In many genes, exon inclusion/skipping is increasingly being recognized as a more common consequence of disease mutations than previously assumed (Anna & Monika, 2018; Dufner-Almeida, do Carmo, Masotti, & Haddad, 2019; Houdayer et al., 2012). Multiple intra-intronic and intra-exonic mutations in CFTR (*ABCC7*), a gene closely related to *ABCC8*, have been associated with nonfunctional protein and cystic fibrosis (CF) disease (Pagani, Buratti, Stuani, & Baralle, 2003). In one systematic study correlating *in silico* predictions with functional analyses of exon skipping in recombinant minigenes (Aissat et al., 2013), 9 of 19 disease-associated CFTR mutations induced exon skipping in a fraction of transcripts, but did not abolish WT expression completely, potentially underlying variably milder phenotypes. Mutations occurring at conserved intron–exon boundaries (i.e., splicing junctions at the −1, −2, −3, and +1, +2, +3 positions) are predicted to affect splicing of the immediately adjacent exons. The consequence of such mutations – for example, c.1117-1G>A and c.1209+1G>A in *ABCC7* – are generally considered to be severe, whereas mutations occurring at more distant positions – for example, +5, +6, or −5 and −6 – are mild, typically associated with only mild CF disease (Tsui & Dorfman, 2013).

Alternate splicing is well recognized as a component of *ABCC9* regulation; the canonical finding is that cardiomyocytes express SUR2A, a variant containing exon 38A,

whereas VSMCs typically express SUR2B, containing the alternate C-terminal exon 38B. Previous studies in mice have also identified multiple additional potential spliced SUR2 variants (Chutkow et al., 1999; Chutkow et al., 1996; Davis-Taber et al., 2000), including short forms of only 28 and 68 kDa (Pu et al., 2008), in addition to the full-length (~150 kDa) form in the WT cardiac sarcolemmal membrane. Some small exon deletions modulate channel ATP sensitivity (Chutkow et al., 1999), whereas coimmunoprecipitation of short forms lacking NBD1 but containing NBD2 with Kir6.1 or Kir6.2 suggests that abnormal channel properties could be generated (Pu et al., 2008). Other studies identified an additional 55 kDa form of the protein lacking exons 5–28 in mitochondria (termed mitoSUR2) generated by a nonconventional intraexonic splicing (IES) event within the 4th and 29th exons of SUR2 mRNA (Ye et al., 2009). Specific deletion of exon 5 of *ABCC9*, to ablate expression of both plasma membrane and the mitoSUR2 short form, resulted in neonatal cardiomyopathy, potentially due to failure of the heart to transition normally from fetal to mature myocardial metabolism (Fahrenbach et al., 2014). Conversely, mice overexpressing the 55 kDa short-form protein exhibited improved recovery from ischemia/reperfusion injury relative to WT hearts (Ramratnam et al., 2018).

Such studies indicate that exon splicing could result in distinct forms of the protein that are expressed in different cellular compartments, with profoundly different effects on cell function. The present data raise the possibility that R1154Q (and/or R1154W, and perhaps other) CS mutations might result not only in a functional K_{ATP} GoF, but also exon skipping, resulting in a truncated protein and hence an effective mixed loss/GoF phenotype, potentially explaining the variable expressivity of disease features in human CS (Grange et al., 2019). This finding illustrates the principle that SUR2 GoF mutations can also be associated with counteracting LoF resulting from variable splicing that leads to a reduction in functional protein levels, such that the net effect could be either GoF or LoF in different tissues, potentially dependent on individual genomic background dictating pre-mRNA processing. This may potentially underlie the highly variable expressivity in disease severity that is seen in CS patients, even for a given variant within the same family (Grange et al., 2019). Moreover, the Nichols group has demonstrated that isolated

SUR2 LoF results in a very distinct constellation of features in *ABCC9*-related intellectual myopathy syndrome (AIMS) (Smeland et al., 2019). Hence, dual GoF/LoF consequences of CS mutations could result in not just quantitatively, but qualitatively variable outcomes and marked variability of CS pathologies.

5.2.3 The lack of electrical compensation for K_{ATP} GoF in CS

Blood pressure depends on vascular tone, which in turn is bidirectionally responsive to homeostatic needs, increasing or decreasing in response to even modest membrane depolarization or hyperpolarization from a potential (V_m) that is typically close to the activation threshold for LTCCs (Brayden, 2002; Loutzenhiser et al., 1997; Welsh et al., 1998; Welsh et al., 2000). In this voltage range, subtle changes in the activity of K_{ATP} or other channels, whether genetic or in response to neurohumoral signaling, will change vascular excitability and tone, unless compensated for by changes in another current (Brayden, 2002; Loutzenhiser et al., 1997; Welsh et al., 1998; Welsh et al., 2000). CS vasculopathy leads to enhanced renin-angiotensin and baroreceptor-mediated adrenergic signaling, which in turn drive broader CV pathologies (Y. Huang et al., 2018; McClenaghan, Huang, Yan, et al., 2020). These signaling pathways are known to produce extensive changes in cardiovascular cells, including alterations to electrophysiology (Arakel et al., 2014; Briones et al., 2009). However, it remains unexplored whether the functional activity of vascular ion channels is altered by the complex pathophysiological signaling cascades at play *in vivo* in CS. Any such consequences in VSMC electrophysiology, whether additive or protective, would be directly relevant to the fundamental etiology of CS, as a vascular electrical disease.

VSMC excitability depends on the concerted activity of multiple ion conductances, in particular voltage-gated K^+ (K_v) channels and LTCCs. Using patch-clamp protocols and recording solutions that I designed to inclusively measure the vascular ensemble of K_v currents and LTCCs, I found no difference in the functional expression of these vascular electrical currents in native aortic and mesenteric VSMCs isolated from WT and Kir6.1[V65M] mice. Thus, despite marked changes in K_{ATP} currents in VSMCs from Cantú

mice (Y. Huang et al., 2018), there are no accompanying compensatory or downstream changes in vascular K_v currents or LTCCs. The observation that vascular K_{ATP} GoF is uncompensated is consistent with my finding, discussed above, that VSMCs from RQ mice are basally hyperpolarized (H. Zhang et al., 2021), as are GI SMCs (York et al., 2020). This is also consistent with previous findings in cardiac muscle, which show no compensation for K_{ATP} subunit knockout by other K_{ATP} subunits, nor changes in K_v currents in response to K_{ATP} GoF in other K_{ATP} channel subunits (Flagg et al., 2004; Koster et al., 2001). More broadly, genetic knockout of background Kir2.1 channels in vascular or cardiac myocytes are also not compensated for by changes in K_v or LTCCs (Zaritsky, Eckman, Wellman, Nelson, & Schwarz, 2000; Zaritsky, Redell, Tempel, & Schwarz, 2001).

Thus, while I cannot completely rule out changes in all vascular ion channels, no changes in the major K_v currents and LTCCs that govern vascular excitability appear to contribute to, or compensate for, CS vasculopathy. Lack of compensation by other currents helps to explain why, despite the homeostatic imperative, manipulation of VSMC K_{ATP} conductance leads to marked changes in blood pressure in experimental animals, from a mean blood pressure of ~115 mM Hg in Kir6.1-/- animals to ~85 mmHg in smooth muscle-specific K_{ATP} GoF transgenic animals (A. Li et al., 2013). Interestingly, the results contrast with the finding that cardiac LTCCs are actually increased with cardiac K_{ATP} GoF (Flagg et al., 2004; Levin et al., 2016), a potentially compensatory consequence in response to enhanced adrenergic signaling (Levin et al., 2016).

5.3 Consequences of CS mutations in human CS patient-derived cells

5.3.1 Implications from R1154Q CS patient-derived human iPSC-cardiomyocytes and primary tissues

In cardiomyocytes I differentiated from R1154Q and R1154W CS patient-derived hiPSCs, I failed to detect any exon 28 exclusion, in contrast to my findings in myocytes from the RQ mouse model. Upon gaining IRB approval, I also obtained primary skin and skeletal muscle tissue biopsies from a human CS patient with the RQ mutation, which were being

removed from a during a medically indicated surgical procedure in which the acquired tissues would have otherwise been discarded. I isolated RNA from these tissues and similarly found no detectable alternate *ABCC9* splicing (Figure 4.4), consistent with my findings from RQ/W hiPSC-CMs. The amino acid sequence in the region of R1154 is identical in mouse and human, but there is some variation in codon usage between the 2 species, and, although *in silico* splicing prediction algorithms suggest that the human mutation and the CRISPR-introduced mouse mutation should alter exon splicing similarly, it is possible that the mouse sequence is more susceptible. Nevertheless, the finding that R1154Q induces such splicing in any genome illustrates the principle that CS-associated SUR2 mutations can also be associated with LoF resulting from alternate splicing that leads to counteracting reduction in functional protein levels.

Despite having observed *ABCC9* message in RQ/W hiPSC-CMs, patch-clamp recordings I obtained from ~50 cells did not reveal measurable functional K_{ATP} activity (not shown). K_{ATP} channel activity had not been previously reported in hiPSC-CMs (Karakikes et al., 2015), and the lack of detectable K_{ATP} activity highlights a clear shortcoming of these cells, since K_{ATP} is the most densely expressed ion channel in native cardiomyocytes (Foster & Coetzee, 2016b). It is well-established in the field of hiPSC-CM biology that, in spite of the tremendous strides made in recent years, these cells fall far short of fully recapitulating human adult native cardiomyocytes (Kolanowski et al., 2017), and this finding exemplifies the need for further technological advances in *in vitro* cardiac differentiation approaches for generating hiPSC-CMs that electrically resemble their native counterparts.

5.3.2 Human iPSC-derived VSMCs recapitulate native VSMC electrophysiology, resembling VSMCs from resistance vessels

A major goal of disease modeling in animals is to translate the findings to the human condition, and it is critical that the animal model be biologically comparable. Native human VSMCs are not readily accessible, and even when available they only provide an avenue for observational, rather than interventional study, given the obvious ethical implications

that preclude exploratory gene editing and pharmacological testing. Moreover, electrophysiology of native human VSMCs has received relatively little attention (Akbarali, Wyse, & Giles, 1992; Hu, Lin, Liu, & Liao, 2008; Smirnov & Aaronson, 1992). Human iPSC-derived VSMCs therefore offer a potentially very profitable model in which to explore human VSMC biology in general, including electrophysiology (Ayoubi et al., 2017; Dash et al., 2015; Shen et al., 2021). Although characterization of cellular electrophysiology is essential for use of these cells to model disease processes, there has been no such study to date.

I used an established protocol consisting of fully chemically defined conditions to differentiate hiPSCs into alpha-SMA-positive hiPSC-VSMCs via lateral mesodermal lineage. Subsequently, whole-cell patch-clamp electrophysiology was used to characterize functional expression of key channels underlying vascular excitability in identical conditions to those used for native mouse VSMCs discussed above. The ensemble of K_v currents in human iPSC-VSMCs closely resembles that in native mouse VSMCs, confirming that hiPSC-VSMCs recapitulate a key component of native vascular electrophysiology. Moreover, the non-inactivating time-dependent delayed rectifier K^+ currents, as well as noisy, non-inactivating currents, which I ascribe to large-conductance Ca^{2+}-activated (BK_{Ca}) channels, are quite similar to those originally reported in human mesenteric arterial myocytes (Smirnov & Aaronson, 1992).

In addition, LTCCs are detected at similar levels, and with identical voltage-dependence to those in mouse mesenteric myocytes, and quite similar to those reported in human mesenteric arterial myocytes (P. Y. Li et al., 2013). Having not detected LTCC in native aortic VSMCs, I provided evidence that increased functional LTCC expression may represent an electrical ‘signature’ of contractile VSMCs, and that hiPSC-VSMCs differentiated under the conditions used may more closely resemble VSMCs from resistance vessels than from elastic vessels. In their original report, Patsch et al. (Patsch et al., 2015) mentioned two potential options for hydrogel substrate: collagen, for promotion of a ‘contractile’ phenotype, and gelatin, for promotion of a ‘synthetic’

phenotype. In the present study, I cultured cells on collagen-coated surface, consistent with the presence of LTCCs, as in contractile myocytes.

I also found that K_{ATP} channels are expressed in hiPSC-VSMCs at very similar levels to those in murine VSMCs (Y. Huang et al., 2018). Importantly, pharmacological sensitivity to the SUR2-selective drug pinacidil shows that these K_{ATP} channels comprise the appropriate 'vascular-type' architecture.

In addition, I found that two genetically distinct hiPSC-VSMC lines exhibit a membrane potential that is very consistent with past reports in native VSMCs (Loutzenhiser et al., 1997; Welsh et al., 1998; Welsh et al., 2000) – relatively depolarized compared to that of non-vascular myocytes, and near the activation range for LTCCs. Furthermore, my observation of essentially identical mean membrane potential in these two genetically-unrelated hiPSC-VSMC lines suggests phenotypic consistency of hiPSC-VSMCs generated through this differentiation approach, regardless of genomic background or genetic origin.

5.3.3 CS patient-derived hiPSC-VSMCs exhibit markedly elevated K_{ATP} activity, decreased glibenclamide sensitivity, and hyperpolarized membrane voltage

R1154Q and R1154W are the most common CS-associated variants in SUR2 (Grange et al., 2019). Upon generating RQ and RW patient-derived hiPSC-VSMCs, I measured K_{ATP} conductances that were markedly elevated under basal conditions, especially so in the RQ myocytes. This is consistent with my findings from recombinant RQ/W K_{ATP} channels, discussed above, in which I observed enhanced Mg^{2+}-nucleotide activation of recombinant K_{ATP} channels, particularly for RQ (McClenaghan et al., 2018). While both mutations also increased the pinacidil-activated current in hiPSC-VSMCs, this effect was much more prominent in RQ cells. Since pinacidil acts to stabilize Mg^{2+}-nucleotide activated channels, the striking pinacidil effect is also consistent with the much greater MgATP-activating effect in R1154Q versus R1154W channels (McClenaghan et al., 2018). Finally, the relative inhibitory effect of glibenclamide was lower for the CS hiPSC-

VSMCs, in this case particularly for RW – again consistent with findings from the recombinant channels (McClenaghan et al., 2018).

The striking K_{ATP} channel GoF I observed in R1154Q hiPSC-VSMCs diverges considerably from the molecular effect observed in the CRISPR/Cas9-engineered RQ mouse (H. Zhang et al., 2021). As discussed above, the phenotype of this murine model was unexpectedly mild compared to mice carrying the CS-associated SUR2[A478V] or Kir6.1[V65M] mutations (Y. Huang et al., 2018), which was mediated by spliceosomal exclusion of exon 28, leading to non-functional channels. However, I failed to detect any detectable *ABCC9* exon 28 exclusion in RQ hiPSC-VSMCs, consistent my observations from RQ/W patient-derived hiPSC-CMs and primary tissue samples from an RQ patient patient (Figure 4.4). This explains the basis for the much greater K_{ATP} GoF in human iPSC-VSMCs carrying the RQ mutation, compared to the RQ mouse. The marked GoF in RQ hiPSC-VSMCs is more consistent with my findings from recombinant K_{ATP} channels with these mutations, in which the RQ and RW mutations caused very marked molecular GoF, as discussed above (Harakalova et al., 2012; McClenaghan et al., 2018). However, in contrast to my studies on recombinant K_{ATP} channels, which were heterologously expressed and characterized in homozygous RQ/RQ channels, the CS patient-derived hiPSC-VSMCs were heterozygous for the RQ/W mutations, as are all known CS patients. Thus, the increased basal K_{ATP} conductances I observed in RQ/W hiPSC-VSMCs are likely a more accurate reflection of the molecular effect of these mutations in human vascular cells.

Consistent with K_{ATP} currents not only being major determinants of the VSMC membrane potential, but also major modulators of it and hence vascular excitability (Quayle, Nelson, & Standen, 1997), the resting membrane potential was markedly more negative in both CS lines, and – again consistent with the relative molecular effect on the K_{ATP} channel – even more so in RQ than RW. This can explain why VSMC hypomyotonia specifically, and vascular smooth muscle cell function more generally, is a major driver of CS pathology (Grange et al., 2019; McClenaghan, Huang, Matkovich, et al., 2020; C. G. Nichols et al., 2013; York et al., 2020).

5.3.4 Cell-autonomous effects on CS vascular pathogenesis

CS vasculopathy includes not only the hypomyotonic component mentioned above, but also a hyperelastic component, which is characterized by increased vessel compliance, vessel tortuosity, and aortic root dilation associated with aortic insufficiency and aortic aneurysms (Brownstein et al., 2013; Hiraki et al., 2014; Kisilevsky et al., 2019; Leon Guerrero et al., 2016; Parrott et al., 2020). These latter phenomena are not trivially explained by an effect of K_{ATP} activation, but are consistent with multiple previous *in vitro* and *in vivo* studies, which have shown increased elastogenesis in cultured cells and blood vessels exposed to the pharmacological K_{ATP} activator, minoxidil (Fhayli et al., 2019; Hayashi et al., 1994; Knutsen et al., 2018; Tajima et al., 1995). Evidence of functional hyperelastogenesis in the mouse (Figure 4.5) provide novel demonstration that elastogenic changes are indeed driven by genetic K_{ATP} GoF, and this effect was also observed in CS variant hiPSC-VSMCs *in vitro*, demonstrating that these K_{ATP}-mediated hyperelastogenic changes is a cell-autonomous consequence of K_{ATP} GoF in VSMCs, and is independent of any systemic signaling. Pharmacological K_{ATP}-mediated elastogenesis has been shown to cause increased transcription as well as enhanced post-transcriptional stability of elastin RNA (Slove et al., 2013). Moreover, many independent studies have established that elastin RNA levels closely correlate to functional elastic fiber production (Davidson, 2002; Davidson, LuValle, Zoia, Quaglino, & Giro, 1997; Duca, Floquet, Alix, Haye, & Debelle, 2004; Eoh et al., 2017; Hew, Grzelczak, Lau, & Keeley, 1999; James, Rich, Trinkaus-Randall, Rosenbloom, & Foster, 1998; Johnson, Robson, Hew, & Keeley, 1995; Kucich, Rosenbloom, Abrams, Bashir, & Rosenbloom, 1997; Kähäri et al., 1992; Lescan et al., 2018; McGowan, Jackson, Olson, Parekh, & Gold, 1997; Mecham et al., 1987; Parks, 1997; M. C. Zhang, Giro, Quaglino, & Davidson, 1995). The precise underlying molecular mechanisms by which K_{ATP} activity drives elastogenesis remain unexplained, but presumably, like the hypomyotonic component, it is driven by effects of membrane potential on cellular calcium levels. In addition to revealing cell-autonomous mechanisms underlying CS vasculopathy,

hyperelastogenesis in CS hiPSC-VSMCs has broader implications for cardiovascular disease modeling. Deficient *in vitro* elastin expression persists as a key obstacle hampering he use of hiPSC-VSMCs to study cardiovascular biology and disease (Ellis, Luo, & Qyang, 2019). The finding of increased elastogenesis in CS hiPSC-VSMCs suggests that K_{ATP} activation may be a viable approach to overcome this limitation, and address a key barrier in the field of hiPSC-VSMC disease modeling and 3D tissue engineering.

5.3.5 Implications for hiPSC-VSMCs in the search for vascular therapeutics

In demonstrating that hiPSC-VSMCs recapitulate typical electrophysiology of native VSMCs, our data validate the use of such cells for the study of vascular biology and vasculopathies in general. More specifically, CS includes both hypomyotonic and hyperelastic components, and while there is evidence that the former can be treated with sulfonylurea inhibitors *in vivo* (McClenaghan, Huang, Yan, et al., 2020), there is so far no evidence that the latter can be corrected or reversed. Our findings from hiPSC-VSMCs help to shed light on the cell-autonomous nature of both, and to provide a human cell model suitable both for detailed study of the earliest mechanisms of wide-ranging CS cardiovascular pathologies, as well as for identification of new pharmacotherapeutic candidates for the disease.

5.4 Conclusions of this Thesis

Cantú Syndrome was first described as a distinct disease 40 years ago. Recent studies have defined the genetic basis of CS as GoF in cardiovascular K_{ATP} channel genes, and have further characterized the fundamental mechanistic bases of several CS mutations. The most common human CS mutations, SUR2[R1154Q] and [R1154W], are present in approximately one-third of patients with CS. Moreover, prior to this project, multiple novel variants had been reported in patients suspected to have CS. In this project, I identified a predicted cluster of several such novel SUR2 variants, which gave rise to GoF in heterologously-expressed recombinant K_{ATP} channels via a shared molecular mechanism

of increased sensitivity to Mg^{2+}-nucleotide activation. At the time, the RQ and RW mutations had recently been reported to cause K_{ATP} GoF. I performed a more in-depth functional characterization of these mutations, demonstrating that RQ/W have a similar molecular mechanistic basis of elevated activatory sensitivity to MgATP, with the RQ mutation causing a particularly severe molecular effect. I also showed that RQ and especially RW channels exhibit markedly reduced pharmacological sensitivity to glibenclamide, the leading pharmacotherapeutic candidate for CS, which has implications for personalized treatment plans for the two most common CS mutations.

When the RQ mutation was introduced into the equivalent murine locus, it produced canonical features of CS, but also the unanticipated consequence of alternate *ABCC9* mRNA splicing in cardiac, vascular, and skeletal myocytes, which resulted in a decrease in functional SUR2 protein levels. This effectively confers concomitant LoF that counteracts the molecular GoF. However, by demonstrating membrane hyperpolarization of RQ mouse VSMCs, I demonstrated that the net effect is a mitigated GoF, which underlies the blunted CS phenotypic severity. I then generated RQ and RW patient-derived human iPSC-cardiomyocyte and hiPSC-VSMC models for CS. I analyzed the RNA from these cells, revealing undetectable levels of alternately spliced *ABCC9*, indicating that this phenomenon was not conserved in the human-specific models. This was consistent with my analysis of primary tissues surgically removed from a human RQ patient, which showed only full-length *ABCC9* transcripts. However, the possibility remains that other CS mutations may result in a counteracting loss of functional protein levels by a similar mechanism, which may underlie the striking variability of phenotypic expressivity in CS, even among patients affected by an identical genetic variant.

In spite of the complex pathophysiological signaling cascades at play in CS, which are known to induce myriad phenotypic changes in cardiovascular cell function, the functional expression of other (i.e., non-K_{ATP}) key vascular ion channels does not appear to be markedly affected by genetic K_{ATP} overactivity *in vivo*. Taken together with my observations of significantly hyperpolarized membrane potential in native and hiPSC-

derived VSMCs with CS mutations, this indicates that the electrophysiology of CS vascular cells reflects uncompensated K_{ATP} GoF.

Despite the presence of *ABCC9* mRNA in hiPSC-CMs, I failed to detect measurable K_{ATP} channel activity in these cells, highlighting a considerable electrical shortcoming of these cells for human disease modeling. In contrast, I found that hiPSC-VSMCs show remarkable electrical consistency with their native counterparts, including K_v currents, BK_{ca} channels, LTCCs, K_{ATP}, and overall membrane potential. This represented a critical advance for the use of these cells to model human biology and disease, as no studies had yet characterized hiPSC-VSMC electrophysiology, which is fundamental to their cellular function.

I then showed that functional K_{ATP} activity was markedly increased, and glibenclamide sensitivity decreased, in RQ and RW hiPSC-VSMCs, with relative severity of both effects consistent with my prior characterization of these mutations in recombinant channels. However, given that these recordings were obtained from human-specific, vascular-type K_{ATP} channels derived from CS patients with heterozygous mutations (all of which in contrast to recordings from heterologously expressed channels), the electrical effect observed in these cells is a more reliable reflection of that in human CS patients. I then demonstrated membrane potential hyperpolarization in hiPSC-VSMCs with the RQ and RW mutations – again, with comparative severity consistent with that of the molecular effects previously observed. This underpins the hypomyotonic component of CS vasculopathy, and clarifies that it results from cell-autonomous electrical mechanisms. There was also a hypothesized hyperelastic component of CS vasculopathy, based on biomechanical and gross morphological changes in CS. However, increased elastogenesis had not been directly demonstrated. I found that elastin levels were increased in native and hiPSC-derived VSMCs harboring CS mutations. This not only confirmed the molecular basis for hyperelastic changes in CS vasculopathy, but also revealed that these effects were mediated by cell-autonomous mechanisms, independent of systemic signaling *in vivo*. In addition to shedding light on the fundamental etiology of CS, this observation points to a potential approach for addressing deficient elastogenesis

in hiPSC-VSMCs, which has substantial implications for the field of hiPSC-VSMC disease modeling.

References

Aguilar-Bryan, L., Nichols, C. G., Wechsler, S. W., Clement, J. P. t., Boyd, A. E. r., Gonzalez, G., . . . Nelson, D. A. (1995). Cloning of the beta cell high-affinity sulfonylurea receptor: a regulator of insulin secretion. *Science, 268*(5209), 423-426.

Aissat, A., de Becdelièvre, A., Golmard, L., Vasseur, C., Costa, C., Chaoui, A., . . . Hinzpeter, A. (2013). Combined computational-experimental analyses of CFTR exon strength uncover predictability of exon-skipping level. *Hum Mutat, 34*(6), 873-881. doi:10.1002/humu.22300

Akbarali, H. I., Wyse, D. G., & Giles, W. R. (1992). Ionic currents in single cells from human cystic artery. *Circ Res, 70*(3), 536-545. doi:10.1161/01.res.70.3.536

Anna, A., & Monika, G. (2018). Splicing mutations in human genetic disorders: examples, detection, and confirmation. *Journal of applied genetics, 59*(3), 253-268. doi:10.1007/s13353-018-0444-7

Arakel, E. C., Brandenburg, S., Uchida, K., Zhang, H., Lin, Y. W., Kohl, T., . . . Schwappach, B. (2014). Tuning the electrical properties of the heart by differential trafficking of KATP ion channel complexes. *Journal of Cell Science, 127*(Pt 9), 2106-2119. doi:10.1242/jcs.141440

Ashcroft, F. M., Harrison, D. E., & Ashcroft, S. J. (1984). Glucose induces closure of single potassium channels in isolated rat pancreatic beta-cells. *Nature, 312*(5993), 446-448.

Ashfield, R., Gribble, F. M., Ashcroft, S. J., & Ashcroft, F. M. (1999). Identification of the high-affinity tolbutamide site on the SUR1 subunit of the K(ATP) channel. *Diabetes, 48*(6), 1341-1347.

Ashford, M. L., Sturgess, N. C., Trout, N. J., Gardner, N. J., & Hales, C. N. (1988). Adenosine-5'-triphosphate-sensitive ion channels in neonatal rat cultured central neurones. *Pflugers Archiv European Journal of Physiology, 412*(3), 297-304.

Ayoubi, S., Sheikh, S. P., & Eskildsen, T. V. (2017). Human induced pluripotent stem cell-derived vascular smooth muscle cells: differentiation and therapeutic potential. *Cardiovasc Res, 113*(11), 1282-1293. doi:10.1093/cvr/cvx125

Aziz, Q., Thomas, A. M., Gomes, J., Ang, R., Sones, W. R., Li, Y., . . . Tinker, A. (2014). The ATP-sensitive potassium channel subunit, Kir6.1, in vascular smooth muscle plays a major role in blood pressure control. *Hypertension, 64*(3), 523-529. doi:10.1161/HYPERTENSIONAHA.114.03116

Babenko, A. P., & Bryan, J. (2001). A conserved inhibitory and differential stimulatory action of nucleotides on K(IR)6.0/SUR complexes is essential for excitation-metabolism coupling by K(ATP) channels. *Journal of Biological Chemistry, 276*(52), 49083-49092.

Babenko, A. P., Gonzalez, G., & Bryan, J. (2000). Pharmaco-topology of sulfonylurea receptors. Separate domains of the regulatory subunits of K(ATP) channel isoforms are required for selective interaction with K(+) channel openers. *J Biol Chem, 275*(2), 717-720.

Ban, K., Wile, B., Kim, S., Park, H. J., Byun, J., Cho, K. W., . . . Yoon, Y. S. (2013). Purification of cardiomyocytes from differentiating pluripotent stem cells using molecular beacons that target cardiomyocyte-specific mRNA. *Circulation, 128*(17), 1897-1909. doi:10.1161/CIRCULATIONAHA.113.004228

Bari, F., Louis, T. M., & Busija, D. W. (1998). Effects of ischemia on cerebral arteriolar dilation to arterial hypoxia in piglets. *Stroke, 29*(1), 222-227; discussion 227-228. doi:10.1161/01.str.29.1.222

Baukrowitz, T., Schulte, U., Oliver, D., Herlitze, S., Krauter, T., Tucker, S. J., . . . Fakler, B. (1998). PIP2 and PIP as determinants for ATP inhibition of KATP channels. *Science, 282*(5391), 1141-1144.

Beech, D. J., Zhang, H., Nakao, K., & Bolton, T. B. (1993). K channel activation by nucleotide diphosphates and its inhibition by glibenclamide in vascular smooth muscle cells. *British Journal of Pharmacology, 110*(2), 573-582.

Beguin, P., Nagashima, K., Nishimura, M., Gonoi, T., & Seino, S. (1999). PKA-mediated phosphorylation of the human K(ATP) channel: separate roles of Kir6.2 and SUR1 subunit phosphorylation. *EMBO Journal, 18*(17), 4722-4732.

Berlin, J. R., Cannell, M. B., & Lederer, W. J. (1989). Cellular origins of the transient inward current in cardiac myocytes. Role of fluctuations and waves of elevated intracellular calcium. *Circulation Research, 65*(1), 115-126.

Bienengraeber, M., Alekseev, A. E., Abraham, M. R., Carrasco, A. J., Moreau, C., Vivaudou, M., . . . Terzic, A. (2000). ATPase activity of the sulfonylurea receptor: a catalytic function for the KATP channel complex [In Process Citation]. *Faseb J, 14*(13), 1943-1952.

Bonev, A. D., & Nelson, M. T. (1993). ATP-sensitive potassium channels in smooth muscle cells from guinea pig urinary bladder. *American Journal of Physiology, 264*(5 Pt 1), C1190-1200.

Bradley, A., Evans, M., Kaufman, M. H., & Robertson, E. (1984). Formation of germ-line chimaeras from embryo-derived teratocarcinoma cell lines. *Nature, 309*(5965), 255-256. doi:10.1038/309255a0

Brayden, J. E. (2002). Functional roles of KATP channels in vascular smooth muscle. *Clinical & Experimental Pharmacology & Physiology, 29*(4), 312-316.

Briones, A. M., Rodriguez-Criado, N., Hernanz, R., Garcia-Redondo, A. B., Rodrigues-Diez, R. R., Alonso, M. J., . . . Salaices, M. (2009). Atorvastatin prevents angiotensin II-induced vascular remodeling and oxidative stress. *Hypertension, 54*(1), 142-149. doi:10.1161/HYPERTENSIONAHA.109.133710

Brownstein, C. A., Towne, M. C., Luquette, L. J., Harris, D. J., Marinakis, N. S., Meinecke, P., . . . Beggs, A. H. (2013). Mutation of KCNJ8 in a patient with Cantu syndrome with unique vascular abnormalities - support for the role of K(ATP) channels in this condition. *European journal of medical genetics, 56*(12), 678-682. doi:10.1016/j.ejmg.2013.09.009

Bryan, J., Vila-Carriles, W. H., Zhao, G., Babenko, A. P., & Aguilar-Bryan, L. (2004). Toward linking structure with function in ATP-sensitive K+ channels. *Diabetes, 53 Suppl 3*, S104-112.

Burridge, P. W., Keller, G., Gold, J. D., & Wu, J. C. (2012). Production of de novo cardiomyocytes: human pluripotent stem cell differentiation and direct reprogramming. *Cell Stem Cell, 10*(1), 16-28. doi:10.1016/j.stem.2011.12.013

Burridge, P. W., Matsa, E., Shukla, P., Lin, Z. C., Churko, J. M., Ebert, A. D., . . . Wu, J. C. (2014). Chemically defined generation of human cardiomyocytes. *Nat Methods, 11*(8), 855-860. doi:10.1038/nmeth.2999

Cantu, J. M., Garcia-Cruz, D., Sanchez-Corona, J., Hernandez, A., & Nazara, Z. (1982). A distinct osteochondrodysplasia with hypertrichosis- Individualization of a probable autosomal recessive entity. *Hum Genet, 60*(1), 36-41.

Chutkow, W. A., Makielski, J. C., Nelson, D. J., Burant, C. F., & Fan, Z. (1999). Alternative splicing of sur2 Exon 17 regulates nucleotide sensitivity of the ATP-sensitive potassium channel. *Journal of Biological Chemistry, 274*(19), 13656-13665.

Chutkow, W. A., Simon, M. C., Le Beau, M. M., & Burant, C. F. (1996). Cloning, tissue expression, and chromosomal localization of SUR2, the putative drug-binding subunit of cardiac, skeletal muscle, and vascular KATP channels. *Diabetes, 45*(10), 1439-1445.

Cole, W. C., McPherson, C. D., & Sontag, D. (1991). ATP-regulated K+ channels protect the myocardium against ischemia/reperfusion damage. *Circ Res, 69*(3), 571-581.

Collins, F. S., & Varmus, H. (2015). A new initiative on precision medicine. *N Engl J Med, 372*(9), 793-795. doi:10.1056/NEJMp1500523

Concolino, D., Formicola, S., Camera, G., & Strisciuglio, P. (2000). Congenital hypertrichosis, cardiomegaly, and osteochondrodysplasia (Cant√∫ syndrome): a new case with unusual radiological findings. *American journal of medical genetics, 92*(3), 191-194. doi:papers2://publication/uuid/7FEE7ED8-034A-40D7-B005-E26FE0562B78

Cooper, P. E., McClenaghan, C., Chen, X., Stary-Weinzinger, A., & Nichols, C. G. (2017). Conserved functional consequences of disease-associated mutations in the slide helix of Kir6.1 and Kir6.2 subunits of the ATP-sensitive potassium channel. *The Journal of biological chemistry, 292*(42), 17387-17398. doi:10.1074/jbc.M117.804971

Cooper, P. E., Reutter, H., Woelfle, J., Engels, H., Grange, D. K., van Haaften, G., . . . Nichols, C. G. (2014). Cantu syndrome resulting from activating mutation in the KCNJ8 gene. *Hum Mutat, 35*(7), 809-813. doi:10.1002/humu.22555

Cooper, P. E., Sala-Rabanal, M., Lee, S. J., & Nichols, C. G. (2015). Differential mechanisms of Cantu syndrome-associated gain of function mutations in the ABCC9 (SUR2) subunit of the KATP channel. *J Gen Physiol, 146*(6), 527-540. doi:10.1085/jgp.201511495

Cowan, C. A., Atienza, J., Melton, D. A., & Eggan, K. (2005). Nuclear reprogramming of somatic cells after fusion with human embryonic stem cells. *Science, 309*(5739), 1369-1373. doi:10.1126/science.1116447

Cui, N., Li, L., Wang, X., Shi, Y., Shi, W., & Jiang, C. (2006). Elimination of allosteric modulation of myocardial KATP channels by ATP and protons in two Kir6.2 polymorphisms found in sudden cardiac death. *Physiol Genomics, 25*(1), 105-115. doi:10.1152/physiolgenomics.00106.2005

Cui, Y., Tran, S., Tinker, A., & Clapp, L. H. (2002). The molecular composition of K(ATP) channels in human pulmonary artery smooth muscle cells and their modulation by growth. *Am J Respir Cell Mol Biol, 26*(1), 135-143. doi:10.1165/ajrcmb.26.1.4622

Czeschik, J. C., Voigt, C., Goecke, T. O., Ludecke, H. J., Wagner, N., Kuechler, A., & Wieczorek, D. (2013). Wide clinical variability in conditions with coarse facial features and hypertrichosis caused by mutations in ABCC9. *American journal of medical genetics. Part A, 161A*(2), 295-300. doi:10.1002/ajmg.a.35735

Dabertrand, F., Kroigaard, C., Bonev, A. D., Cognat, E., Dalsgaard, T., Domenga-Denier, V., . . . Nelson, M. T. (2015). Potassium channelopathy-like defect underlies early-stage cerebrovascular dysfunction in a genetic model of small vessel disease. *Proc Natl Acad Sci U S A, 112*(7), E796-805. doi:10.1073/pnas.1420765112

Dash, B. C., Jiang, Z., Suh, C., & Qyang, Y. (2015). Induced pluripotent stem cell-derived vascular smooth muscle cells: methods and application. *Biochem J, 465*(2), 185-194. doi:10.1042/BJ20141078

Daut-J. Maier-Rudolph-W. von Beckerath-N. Mehrke-G. Gunther-K. Goedel-Meinen-L. IN Physiologisches Institut der Technischen Universitat Munchen, B., Federal Republic of Germany. (1990). Hypoxic dilation of coronary arteries is mediated by ATP-sensitive potassium channels. In *Science. 1990 Mar 16. 247(4948). P 1341-4. JT SCIENCE. LG EN. IS 0036-8075*.

Davidson, J. M. (2002). Smad about elastin regulation. *Am J Respir Cell Mol Biol, 26*(2), 164-166. doi:10.1165/ajrcmb.26.2.f228

Davidson, J. M., LuValle, P. A., Zoia, O., Quaglino, D., & Giro, M. (1997). Ascorbate differentially regulates elastin and collagen biosynthesis in vascular smooth muscle cells and skin fibroblasts by pretranslational mechanisms. *J Biol Chem, 272*(1), 345-352. doi:10.1074/jbc.272.1.345

Davies, N. W. (1990). Modulation of ATP-sensitive K+ channels in skeletal muscle by intracellular protons. *Nature, 343*(6256), 375-377.

Davies, N. W., Standen, N. B., & Stanfield, P. R. (1992). The effect of intracellular pH on ATP-dependent potassium channels of frog skeletal muscle. *Journal of Physiology, 445*, 549-568.

Davis, R. P., Casini, S., van den Berg, C. W., Hoekstra, M., Remme, C. A., Dambrot, C., . . . Mummery, C. L. (2012). Cardiomyocytes derived from pluripotent stem cells recapitulate electrophysiological characteristics of an overlap syndrome of cardiac sodium channel disease. *Circulation, 125*(25), 3079-3091. doi:10.1161/CIRCULATIONAHA.111.066092

Davis-Taber, R., Choi, W., Feng, J., Hoogenboom, L., McNally, T., Kroeger, P., . . . Scott, V. E. (2000). Molecular characterization of human SUR2-containing K(ATP) channels. *Gene, 256*(1-2), 261-270.

de Wet, H., Mikhailov, M. V., Fotinou, C., Dreger, M., Craig, T. J., Venien-Bryan, C., & Ashcroft, F. M. (2007). Studies of the ATPase activity of the ABC protein SUR1. *FEBS J, 274*(14), 3532-3544. doi:EJB5879 [pii]
10.1111/j.1742-4658.2007.05879.x

Doetschman, T., Gregg, R. G., Maeda, N., Hooper, M. L., Melton, D. W., Thompson, S., & Smithies, O. (1987). Targetted correction of a mutant HPRT gene in mouse embryonic stem cells. *Nature, 330*(6148), 576-578. doi:10.1038/330576a0

Dubois, N. C., Craft, A. M., Sharma, P., Elliott, D. A., Stanley, E. G., Elefanty, A. G., . . . Keller, G. (2011). SIRPA is a specific cell-surface marker for isolating cardiomyocytes derived from human pluripotent stem cells. *Nat Biotechnol, 29*(11), 1011-1018. doi:10.1038/nbt.2005

Duca, L., Floquet, N., Alix, A. J., Haye, B., & Debelle, L. (2004). Elastin as a matrikine. *Crit Rev Oncol Hematol, 49*(3), 235-244. doi:10.1016/j.critrevonc.2003.09.007

Dufner-Almeida, L. G., do Carmo, R. T., Masotti, C., & Haddad, L. A. (2019). Understanding human DNA variants affecting pre-mRNA splicing in the NGS era. *Advances in genetics, 103*, 39-90. doi:10.1016/bs.adgen.2018.09.002

Egashira, T., Yuasa, S., Suzuki, T., Aizawa, Y., Yamakawa, H., Matsuhashi, T., . . . Fukuda, K. (2012). Disease characterization using LQTS-specific induced pluripotent stem cells. *Cardiovasc Res, 95*(4), 419-429. doi:10.1093/cvr/cvs206

Elliott, A. C., Smith, G. L., & Allen, D. G. (1989). Simultaneous measurements of action potential duration and intracellular ATP in isolated ferret hearts exposed to cyanide. *Circulation Research, 64*(3), 583-591.

Ellis, M. W., Luo, J., & Qyang, Y. (2019). Modeling elastin-associated vasculopathy with patient induced pluripotent stem cells and tissue engineering. *Cell Mol Life Sci, 76*(5), 893-901. doi:10.1007/s00018-018-2969-7

Engels, H., Bosse, K., Ehrbrecht, A., Zahn, S., Hoischen, A., Propping, P., . . . Reutter, H. (2002). Further case of Cantú syndrome: exclusion of cryptic subtelomeric chromosome aberrations. *Am J Med Genet, 111*(2), 205-209. doi:10.1002/ajmg.10560

Enkvetchakul, D., & Nichols, C. G. (2003). Gating mechanism of KATP channels: function fits form. *J Gen Physiol, 122*(5), 471-480. doi:10.1085/jgp.200308878

jgp.200308878 [pii]

Eoh, J. H., Shen, N., Burke, J. A., Hinderer, S., Xia, Z., Schenke-Layland, K., & Gerecht, S. (2017). Enhanced elastin synthesis and maturation in human vascular smooth muscle tissue derived from induced-pluripotent stem cells. *Acta Biomater, 52*, 49-59. doi:10.1016/j.actbio.2017.01.083

Evans, M. J., & Kaufman, M. H. (1981). Establishment in culture of pluripotential cells from mouse embryos. *Nature, 292*(5819), 154-156. doi:10.1038/292154a0

Evans, S. M., Yelon, D., Conlon, F. L., & Kirby, M. L. (2010). Myocardial lineage development. *Circ Res, 107*(12), 1428-1444. doi:10.1161/CIRCRESAHA.110.227405

Fahrenbach, J. P., Stoller, D., Kim, G., Aggarwal, N., Yerokun, B., Earley, J. U., . . . McNally, E. M. (2014). Abcc9 is required for the transition to oxidative metabolism in the newborn heart. *FASEB J, 28*(7), 2804-2815. doi:10.1096/fj.13-244459

Fan, Z., & Makielski, J. C. (1997). Anionic phospholipids activate ATP-sensitive potassium channels. *Journal of Biological Chemistry, 272*(9), 5388-5395.

Fatima, A., Xu, G., Shao, K., Papadopoulos, S., Lehmann, M., Arnaiz-Cot, J. J., . . . Saric, T. (2011). In vitro modeling of ryanodine receptor 2 dysfunction using human

induced pluripotent stem cells. *Cell Physiol Biochem, 28*(4), 579-592. doi:10.1159/000335753

Faury, G., Pezet, M., Knutsen, R. H., Boyle, W. A., Heximer, S. P., McLean, S. E., . . . Mecham, R. P. (2003). Developmental adaptation of the mouse cardiovascular system to elastin haploinsufficiency. *J Clin Invest, 112*(9), 1419-1428. doi:10.1172/JCI19028

Fhayli, W., Boyer, M., Ghandour, Z., Jacob, M. P., Andrieu, J. P., Starcher, B. C., . . . Faury, G. (2019). Chronic administration of minoxidil protects elastic fibers and stimulates their neosynthesis with improvement of the aorta mechanics in mice. *Cell Signal, 62*, 109333. doi:10.1016/j.cellsig.2019.05.018

Findlay, I. (1988). ATP4- and ATP.Mg inhibit the ATP-sensitive K+ channel of rat ventricular myocytes. *Pflugers Arch, 412*(1-2), 37-41.

Flagg, T. P., Charpentier, F., Manning-Fox, J., Remedi, M. S., Enkvetchakul, D., Lopatin, A., . . . Nichols, C. (2004). Remodeling of excitation-contraction coupling in transgenic mice expressing ATP-insensitive sarcolemmal KATP channels. *Am J Physiol Heart Circ Physiol, 286*(4), H1361-1369. doi:10.1152/ajpheart.00676.2003 00676.2003 [pii]

Flagg, T. P., Enkvetchakul, D., Koster, J. C., & Nichols, C. G. (2010). Muscle KATP channels: recent insights to energy sensing and myoprotection. *Physiol Rev, 90*(3), 799-829. doi:10.1152/physrev.00027.2009

Flagg, T. P., Kurata, H. T., Masia, R., Caputa, G., Magnuson, M. A., Lefer, D. J., . . . Nichols, C. G. (2008). Differential structure of atrial and ventricular KATP: atrial KATP channels require SUR1. *Circ Res, 103*(12), 1458-1465. doi:10.1161/CIRCRESAHA.108.178186

Flagg, T. P., & Nichols, C. G. (2001). Sarcolemmal K(ATP) channels in the heart: molecular mechanisms brought to light, but physiologic consequences still in the dark. *J Cardiovasc Electrophysiol, 12*(10), 1195-1198.

Foster, M. N., & Coetzee, W. A. (2016a). KATP Channels in the Cardiovascular System. *Physiological Reviews, 96*(1), 177-252. doi:10.1152/physrev.00003.2015

Foster, M. N., & Coetzee, W. A. (2016b). KATP Channels in the Cardiovascular System. *Physiol Rev, 96*(1), 177-252. doi:10.1152/physrev.00003.2015

Gahwiler, E. K. N., Motta, S. E., Martin, M., Nugraha, B., Hoerstrup, S. P., & Emmert, M. Y. (2021). Human iPSCs and Genome Editing Technologies for Precision Cardiovascular Tissue Engineering. *Front Cell Dev Biol, 9*, 639699. doi:10.3389/fcell.2021.639699

Garcia-Cruz, D., Mampel, A., Echeverria, M. I., Vargas, A. L., Castaneda-Cisneros, G., Davalos-Rodriguez, N., . . . Sanchez-Corona, J. (2011). Cantu syndrome and lymphoedema. *Clinical dysmorphology, 20*(1), 32-37. doi:10.1097/MCD.0b013e32833d015c

Garcia-Cruz, D., Sanchez-Corona, J., Nazara, Z., Garcia-Cruz, M. O., Figuera, L. E., Castaneda, V., & Cantu, J. M. (1997). Congenital hypertrichosis, osteochondrodysplasia, and cardiomegaly: further delineation of a new genetic syndrome. *American Journal of Medical Genetics, 69*(2), 138-151. doi:10.1002/(sici)1096-8628(19970317)69:2<138::aid-ajmg5>3.0.co;2-l

Giblin, J. P., Cui, Y., Clapp, L. H., & Tinker, A. (2002). Assembly limits the pharmacological complexity of ATP-sensitive potassium channels. *Journal of Biological Chemistry, 277*(16), 13717-13723.

Grange, D. K., Lorch, S. M., Cole, P. L., & Singh, G. K. (2006). Cantu syndrome in a woman and her two daughters: Further confirmation of autosomal dominant inheritance and review of the cardiac manifestations. *American journal of medical genetics. Part A, 140*(15), 1673-1680. doi:10.1002/ajmg.a.31348

Grange, D. K., Roessler, H. I., McClenaghan, C., Duran, K., Shields, K., Remedi, M. S., . . . van Haaften, G. (2019). Cantu syndrome: Findings from 74 patients in the International Cantu Syndrome Registry. *American journal of medical genetics. Part C, Seminars in medical genetics, 181*(4), 658-681. doi:10.1002/ajmg.c.31753

Gribble, F. M., & Ashcroft, F. M. (1999). Differential sensitivity of beta-cell and extrapancreatic K(ATP) channels to gliclazide. *Diabetologia, 42*(7), 845-848.

Gribble, F. M., & Reimann, F. (2003). Sulphonylurea action revisited: the post-cloning era. *Diabetologia, 46*(7), 875-891. doi:10.1007/s00125-003-1143-3

Gribble, F. M., Tucker, S. J., & Ashcroft, F. M. (1997a). The essential role of the Walker A motifs of SUR1 in K-ATP channel activation by Mg-ADP and diazoxide. *EMBO Journal, 16*(6), 1145-1152.

Gribble, F. M., Tucker, S. J., & Ashcroft, F. M. (1997b). The interaction of nucleotides with the tolbutamide block of cloned ATP-sensitive K+ channel currents expressed in Xenopus oocytes: a reinterpretation. *Journal of Physiology, 504*(Pt 1), 35-45.

Gribble, F. M., Tucker, S. J., Seino, S., & Ashcroft, F. M. (1998). Tissue specificity of sulfonylureas: studies on cloned cardiac and beta-cell K(ATP) channels. *Diabetes, 47*(9), 1412-1418.

Gros, L., Trapp, S., Dabrowski, M., Ashcroft, F. M., Bataille, D., & Blache, P. (2002). Characterization of two novel forms of the rat sulphonylurea receptor SUR1A2 and SUR1BDelta31. *Br J Pharmacol, 137*(1), 98-106. doi:10.1038/sj.bjp.0704836

Hambrock, A., Loffler-Walz, C., & Quast, U. (2002). Glibenclamide binding to sulphonylurea receptor subtypes: dependence on adenine nucleotides. *British Journal of Pharmacology, 136*(7), 995-1004. doi:10.1038/sj.bjp.0704801

Hambrock, A., Loffler-Walz, C., Russ, U., Lange, U., & Quast, U. (2001). Characterization of a mutant sulfonylurea receptor SUR2B with high affinity for sulfonylureas and openers: differences in the coupling to Kir6.x subtypes. *Mol Pharmacol, 60*(1), 190-199. doi:10.1124/mol.60.1.190

Hansen, A. M., Christensen, I. T., Hansen, J. B., Carr, R. D., Ashcroft, F. M., & Wahl, P. (2002). Differential interactions of nateglinide and repaglinide on the human beta-cell sulphonylurea receptor 1. *Diabetes, 51*(9), 2789-2795.

Harakalova, M., van Harssel, J. J., Terhal, P. A., van Lieshout, S., Duran, K., Renkens, I., . . . Cuppen, E. (2012). Dominant missense mutations in ABCC9 cause Cantu syndrome. *Nat Genet, 44*(7), 793-796. doi:10.1038/ng.2324

Hattori, F., Chen, H., Yamashita, H., Tohyama, S., Satoh, Y. S., Yuasa, S., . . . Fukuda, K. (2010). Nongenetic method for purifying stem cell-derived cardiomyocytes. *Nat Methods, 7*(1), 61-66. doi:10.1038/nmeth.1403

Hawes, J. Z., Cocciolone, A. J., Cui, A. H., Griffin, D. B., Staiculescu, M. C., Mecham, R. P., & Wagenseil, J. E. (2020). Elastin haploinsufficiency in mice has divergent effects on arterial remodeling with aging depending on sex. *Am J Physiol Heart Circ Physiol, 319*(6), H1398-H1408. doi:10.1152/ajpheart.00517.2020

Hayashi, A., Suzuki, T., Wachi, H., Tajima, S., Nishikawa, T., Murad, S., & Pinnell, S. R. (1994). Minoxidil stimulates elastin expression in aortic smooth muscle cells. *Arch Biochem Biophys, 315*(1), 137-141. doi:10.1006/abbi.1994.1482

Hew, Y., Grzelczak, Z., Lau, C., & Keeley, F. W. (1999). Identification of a large region of secondary structure in the 3'-untranslated region of chicken elastin mRNA with implications for the regulation of mRNA stability. *J Biol Chem, 274*(20), 14415-14421. doi:10.1074/jbc.274.20.14415

Hilgemann, D. W., & Ball, R. (1996). Regulation of cardiac Na+,Ca2+ exchange and KATP potassium channels by PIP2. *Science, 273*(5277), 956-959.

Hiraki, Y., Miyatake, S., Hayashidani, M., Nishimura, Y., Matsuura, H., Kamada, M., . . . Matsumoto, N. (2014). Aortic aneurysm and craniosynostosis in a family with Cantu syndrome. *American journal of medical genetics. Part A, 164A*(1), 231-236. doi:10.1002/ajmg.a.36228

Houdayer, C., Caux-Moncoutier, V., Krieger, S., Barrois, M., Bonnet, F., Bourdon, V., . . . Stoppa-Lyonnet, D. (2012). Guidelines for splicing analysis in molecular diagnosis derived from a set of 327 combined in silico/in vitro studies on BRCA1 and BRCA2 variants. *Human Mutation, 33*(8), 1228-1238. doi:10.1002/humu.22101

Houser, S. R., Margulies, K. B., Murphy, A. M., Spinale, F. G., Francis, G. S., Prabhu, S. D., . . . Translational, B. (2012). Animal models of heart failure: a scientific statement from the American Heart Association. *Circ Res, 111*(1), 131-150. doi:10.1161/RES.0b013e3182582523

Hu, Z. Y., Lin, P. T., Liu, J., & Liao, D. Q. (2008). Remifentanil induces L-type Ca2+ channel inhibition in human mesenteric arterial smooth muscle cells. *Can J Anaesth, 55*(4), 238-244. doi:10.1007/BF03021508

Huang, C. L. (2017). Murine Electrophysiological Models of Cardiac Arrhythmogenesis. *Physiol Rev, 97*(1), 283-409. doi:10.1152/physrev.00007.2016

Huang, Y., McClenaghan, C., Harter, T. M., Hinman, K., Halabi, C. M., Matkovich, S. J., . . . Nichols, C. G. (2018). Cardiovascular consequences of KATP overactivity in Cantu syndrome. *JCI insight, 3*(15). doi:10.1172/jci.insight.121153

Humphries, E. S., & Dart, C. (2015). Neuronal and Cardiovascular Potassium Channels as Therapeutic Drug Targets: Promise and Pitfalls. *J Biomol Screen, 20*(9), 1055-1073. doi:10.1177/1087057115601677

Hunter, M., & Giebisch, G. (1988). Calcium-activated K-channels of Amphiuma early distal tubule: inhibition by ATP. *Pflugers Archiv - European Journal of Physiology, 412*(3), 331-333.

Inagaki, N., Gonoi, T., Clement, J. P., Wang, C. Z., Aguilar-Bryan, L., Bryan, J., & Seino, S. (1996). A family of sulfonylurea receptors determines the pharmacological properties of ATP-sensitive K+ channels. *Neuron, 16*(5), 1011-1017.

Inagaki, N., Gonoi, T., Clement, J. P. t., Namba, N., Inazawa, J., Gonzalez, G., . . . Bryan, J. (1995). Reconstitution of IKATP: an inward rectifier subunit plus the sulfonylurea receptor. *Science, 270*(5239), 1166-1170.

Inagaki, N., Inazawa, J., & Seino, S. (1995). cDNA sequence, gene structure, and chromosomal localization of the human ATP-sensitive potassium channel, uKATP-1, gene (KCNJ8). *Genomics, 30*(1), 102-104.

Ishizaka, H., & Kuo, L. (1996). Acidosis-induced coronary arteriolar dilation is mediated by ATP-sensitive potassium channels in vascular smooth muscle. *Circ Res, 78*(1), 50-57. doi:10.1161/01.res.78.1.50

Isomoto, S., Kondo, C., Yamada, M., Matsumoto, S., Higashiguchi, O., Horio, Y., . . . Kurachi, Y. (1996). A novel sulfonylurea receptor forms with BIR (Kir6.2) a smooth muscle type ATP-sensitive K+ channel. *Journal of Biological Chemistry, 271*(40), 24321-24324.

Itzhaki, I., Maizels, L., Huber, I., Zwi-Dantsis, L., Caspi, O., Winterstern, A., . . . Gepstein, L. (2011). Modelling the long QT syndrome with induced pluripotent stem cells. *Nature, 471*(7337), 225-229. doi:10.1038/nature09747

Jahangir, A., & Terzic, A. (2005). K(ATP) channel therapeutics at the bedside. *J Mol Cell Cardiol, 39*(1), 99-112. doi:10.1016/j.yjmcc.2005.04.006

James, M. F., Rich, C. B., Trinkaus-Randall, V., Rosenbloom, J., & Foster, J. A. (1998). Elastogenesis in the developing chick lung is transcriptionally regulated. *Dev Dyn, 213*(2), 170-181. doi:10.1002/(SICI)1097-0177(199810)213:2<170::AID-AJA2>3.0.CO;2-D

Johnson, D. J., Robson, P., Hew, Y., & Keeley, F. W. (1995). Decreased elastin synthesis in normal development and in long-term aortic organ and cell cultures is related to rapid and selective destabilization of mRNA for elastin. *Circ Res, 77*(6), 1107-1113. doi:10.1161/01.res.77.6.1107

Jouen-Tachoire, T. R. H., Tucker, S. J., & Tammaro, P. (2021). Ion channels as convergence points in the pathology of pulmonary arterial hypertension. *Biochemical Society Transactions, 49*(4), 1855-1865. doi:10.1042/BST20210538

Jung, C. B., Moretti, A., Mederos y Schnitzler, M., Iop, L., Storch, U., Bellin, M., . . . Laugwitz, K. L. (2012). Dantrolene rescues arrhythmogenic RYR2 defect in a patient-specific stem cell model of catecholaminergic polymorphic ventricular tachycardia. *EMBO Mol Med, 4*(3), 180-191. doi:10.1002/emmm.201100194

Kakei M, N. A. S. T. (1985). Properties of adenosine-triphosphate-regulated potassium channels in guinea-pig ventricular cells. *Journal of physiology. 1985. 363: 441-462.*

Kanatsuka, H., Sekiguchi, N., Sato, K., Akai, K., Wang, Y., Komaru, T., . . . Takishima, T. (1992). Microvascular sites and mechanisms responsible for reactive hyperemia in the coronary circulation of the beating canine heart. *Circ Res, 71*(4), 912-922. doi:10.1161/01.res.71.4.912

Karagiannis, P., Takahashi, K., Saito, M., Yoshida, Y., Okita, K., Watanabe, A., . . . Osafune, K. (2019). Induced Pluripotent Stem Cells and Their Use in Human Models of Disease and Development. *Physiol Rev, 99*(1), 79-114. doi:10.1152/physrev.00039.2017

Karakikes, I., Ameen, M., Termglinchan, V., & Wu, J. C. (2015). Human induced pluripotent stem cell-derived cardiomyocytes: insights into molecular, cellular, and functional phenotypes. *Circ Res, 117*(1), 80-88. doi:10.1161/CIRCRESAHA.117.305365

Kattman, S. J., Witty, A. D., Gagliardi, M., Dubois, N. C., Niapour, M., Hotta, A., . . . Keller, G. (2011). Stage-specific optimization of activin/nodal and BMP signaling promotes cardiac differentiation of mouse and human pluripotent stem cell lines. *Cell Stem Cell, 8*(2), 228-240. doi:10.1016/j.stem.2010.12.008

Kinoshita, H., & Katusic, Z. S. (1997). Role of potassium channels in relaxations of isolated canine basilar arteries to acidosis. *Stroke, 28*(2), 433-437; discussion 437-438. doi:10.1161/01.str.28.2.433

Kisilevsky, E., Kohly, R. P., & Margolin, E. A. (2019). Dilated and tortuous retinal vessels as a sign of Cantu syndrome. *Ophthalmic Genet, 40*(5), 453-454. doi:10.1080/13816810.2019.1666415

Knutsen, R. H., Beeman, S. C., Broekelmann, T. J., Liu, D., Tsang, K. M., Kovacs, A., . . . Kozel, B. A. (2018). Minoxidil improves vascular compliance, restores cerebral blood flow, and alters extracellular matrix gene expression in a model of chronic vascular stiffness. *Am J Physiol Heart Circ Physiol, 315*(1), H18-H32. doi:10.1152/ajpheart.00683.2017

Ko, E. A., Han, J., Jung, I. D., & Park, W. S. (2008). Physiological roles of K+ channels in vascular smooth muscle cells. *J Smooth Muscle Res, 44*(2), 65-81. doi:10.1540/jsmr.44.65

Kobayashi, D., Cook, A. L., & Williams, D. A. (2010). Pulmonary hypertension secondary to partial pulmonary venous obstruction in a child with Cantu syndrome. *Pediatric pulmonology, 45*(7), 727-729. doi:10.1002/ppul.21215

Kolanowski, T. J., Antos, C. L., & Guan, K. (2017). Making human cardiomyocytes up to date: Derivation, maturation state and perspectives. *Int J Cardiol, 241*, 379-386. doi:10.1016/j.ijcard.2017.03.099

Koster, J. C., Knopp, A., Flagg, T. P., Markova, K. P., Sha, Q., Enkvetchakul, D., . . . Nichols, C. G. (2001). Tolerance for ATP-insensitive K(ATP) channels in transgenic mice. *Circ Res, 89*(11), 1022-1029.

Koster, J. C., Remedi, M. S., Dao, C., & Nichols, C. G. (2005). ATP and sulfonylurea sensitivity of mutant ATP-sensitive K+ channels in neonatal diabetes: implications for pharmacogenomic therapy. *Diabetes, 54*(9), 2645-2654. doi:54/9/2645 [pii]

Koster, J. C., Remedi, M. S., Masia, R., Patton, B., Tong, A., & Nichols, C. G. (2006). Expression of ATP-insensitive KATP channels in pancreatic beta-cells underlies a spectrum of diabetic phenotypes. *Diabetes, 55*(11), 2957-2964. doi:55/11/2957 [pii]

10.2337/db06-0732

Kucich, U., Rosenbloom, J. C., Abrams, W. R., Bashir, M. M., & Rosenbloom, J. (1997). Stabilization of elastin mRNA by TGF-beta: initial characterization of signaling pathway. *Am J Respir Cell Mol Biol, 17*(1), 10-16. doi:10.1165/ajrcmb.17.1.2816

Kuhner, P., Prager, R., Stephan, D., Russ, U., Winkler, M., Ortiz, D., . . . Quast, U. (2012). Importance of the Kir6.2 N-terminus for the interaction of glibenclamide and

repaglinide with the pancreatic K(ATP) channel. *Naunyn Schmiedebergs Arch Pharmacol, 385*(3), 299-311. doi:10.1007/s00210-011-0709-8

Kunzelmann, K., Pavenstadt, H., Beck, C., Unal, O., Emmrich, P., Arndt, H. J., & Greger, R. (1989). Characterization of potassium channels in respiratory cells. I. General properties. *Pflugers Archiv European Journal of Physiology, 414*(3), 291-296.

Kuo, A., Gulbis, J. M., Antcliff, J. F., Rahman, T., Lowe, E. D., Zimmer, J., . . . Doyle, D. A. (2003). Crystal structure of the potassium channel KirBac1.1 in the closed state. *Science, 300*(5627), 1922-1926. doi:10.1126/science.1085028

1085028 [pii]

Kähäri, V. M., Olsen, D. R., Rhudy, R. W., Carrillo, P., Chen, Y. Q., & Uitto, J. (1992). Transforming growth factor-beta up-regulates elastin gene expression in human skin fibroblasts. Evidence for post-transcriptional modulation. *Lab Invest, 66*(5), 580-588.

Lahti, A. L., Kujala, V. J., Chapman, H., Koivisto, A. P., Pekkanen-Mattila, M., Kerkela, E., . . . Aalto-Setala, K. (2012). Model for long QT syndrome type 2 using human iPS cells demonstrates arrhythmogenic characteristics in cell culture. *Dis Model Mech, 5*(2), 220-230. doi:10.1242/dmm.008409

Lan, F., Lee, A. S., Liang, P., Sanchez-Freire, V., Nguyen, P. K., Wang, L., . . . Wu, J. C. (2013). Abnormal calcium handling properties underlie familial hypertrophic cardiomyopathy pathology in patient-specific induced pluripotent stem cells. *Cell Stem Cell, 12*(1), 101-113. doi:10.1016/j.stem.2012.10.010

Landry, D. W., & Oliver, J. A. (1992). The ATP-sensitive K+ channel mediates hypotension in endotoxemia and hypoxic lactic acidosis in dog. *J Clin Invest, 89*(6), 2071-2074. doi:10.1172/JCI115820

Lazalde, B., Sanchez-Urbina, R., Nuno-Arana, I., Bitar, W. E., & de Lourdes Ramirez-Duenas, M. (2000). Autosomal dominant inheritance in Cantu syndrome (congenital hypertrichosis, osteochondrodysplasia, and cardiomegaly). *American Journal of Medical Genetics, 94*(5), 421-427.

Lederer, W. J., & Nichols, C. G. (1989). Nucleotide modulation of the activity of rat heart ATP-sensitive K+ channels in isolated membrane patches. *J Physiol, 419*, 193-211.

Lederer, W. J., Nichols, C. G., & Smith, G. L. (1989). The mechanism of early contractile failure of isolated rat ventricular myocytes subjected to complete metabolic inhibition. doi:papers2://publication/uuid/387EA704-0B1B-4579-A0AE-5311D29DF510

Lee, K. P. K., Chen, J., & MacKinnon, R. (2017). Molecular structure of human KATP in complex with ATP and ADP. *Elife, 6*. doi:10.7554/eLife.32481

Leon Guerrero, C. R., Pathak, S., Grange, D. K., Singh, G. K., Nichols, C. G., Lee, J. M., & Vo, K. D. (2016). Neurologic and neuroimaging manifestations of Cantu syndrome: A case series. *Neurology*. doi:10.1212/WNL.0000000000002861

Lescan, M., Perl, R. M., Golombek, S., Pilz, M., Hann, L., Yasmin, M., . . . Avci-Adali, M. (2018). De Novo Synthesis of Elastin by Exogenous Delivery of Synthetic Modified mRNA into Skin and Elastin-Deficient Cells. *Mol Ther Nucleic Acids, 11*, 475-484. doi:10.1016/j.omtn.2018.03.013

Levin, M. D., Singh, G. K., Zhang, H. X., Uchida, K., Kozel, B. A., Stein, P. K., . . . Nichols, C. G. (2016). KATP channel gain-of-function leads to increased myocardial L-type Ca2+ current and contractility in Cantu syndrome. *Proceedings of the National Academy of Sciences of the United States of America, 113*(24), 6773-6778. doi:10.1073/pnas.1606465113

Li, A., Knutsen, R. H., Zhang, H., Osei-Owusu, P., Moreno-Dominguez, A., Harter, T. M., . . . Nichols, C. G. (2013). Hypotension due to Kir6.1 gain-of-function in vascular smooth muscle. *J Am Heart Assoc, 2*(4), e000365. doi:10.1161/JAHA.113.000365

Li, P. Y., Zeng, X. R., Cheng, J., Wen, J., Inoue, I., & Yang, Y. (2013). Rhynchophylline-induced vasodilation in human mesenteric artery is mainly due to blockage of L-type calcium channels in vascular smooth muscle cells. *Naunyn Schmiedebergs Arch Pharmacol, 386*(11), 973-982. doi:10.1007/s00210-013-0888-6

Lian, X., Hsiao, C., Wilson, G., Zhu, K., Hazeltine, L. B., Azarin, S. M., . . . Palecek, S. P. (2012). Robust cardiomyocyte differentiation from human pluripotent stem cells via temporal modulation of canonical Wnt signaling. *Proceedings of the National Academy of Sciences of the United States of America, 109*(27), E1848-1857. doi:10.1073/pnas.1200250109

Light, P. E., Allen, B. G., Walsh, M. P., & French, R. J. (1995). Regulation of adenosine triphosphate-sensitive potassium channels from rabbit ventricular myocytes by protein kinase C and type 2A protein phosphatase. *Biochemistry, 34*(21), 7252-7257.

Light, P. E., Sabir, A. A., Allen, B. G., Walsh, M. P., & French, R. J. (1996). Protein kinase C-induced changes in the stoichiometry of ATP binding activate cardiac ATP-sensitive K+ channels. A possible mechanistic link to ischemic preconditioning. *Circ Res, 79*(3), 399-406. doi:10.1161/01.res.79.3.399

Lin, C. J., Hunkins, B. M., Roth, R. A., Lin, C. Y., Wagenseil, J. E., & Mecham, R. P. (2021). Vascular Smooth Muscle Cell Subpopulations and Neointimal Formation in Mouse Models of Elastin Insufficiency. *Arterioscler Thromb Vasc Biol, 41*(12), 2890-2905. doi:10.1161/ATVBAHA.120.315681

Lin, Y. F., Jan, Y. N., & Jan, L. Y. (2000). Regulation of ATP-sensitive potassium channel function by protein kinase A-mediated phosphorylation in transfected HEK293 cells. *Embo J, 19*(5), 942-955.

Liu, G. X., Hanley, P. J., Ray, J., & Daut, J. (2001). Long-chain acyl-coenzyme A esters and fatty acids directly link metabolism to K(ATP) channels in the heart.[see comment]. *Circulation Research, 88*(9), 918-924.

Loffler-Walz, C., Hambrock, A., & Quast, U. (2002). Interaction of K(ATP) channel modulators with sulfonylurea receptor SUR2B: implication for tetramer formation and allosteric coupling of subunits. *Mol Pharmacol, 61*(2), 407-414. doi:10.1124/mol.61.2.407

Loutzenhiser, R., Chilton, L., & Trottier, G. (1997). Membrane potential measurements in renal afferent and efferent arterioles: actions of angiotensin II. *Am J Physiol, 273*(2 Pt 2), F307-314. doi:10.1152/ajprenal.1997.273.2.F307

Ma, A., Gurnasinghani, S., Kirk, E. P., McClenaghan, C., Singh, G. K., Grange, D. K., . . . Nichols, C. G. (2019). Glibenclamide treatment in a Cantu syndrome patient with

a pathogenic ABCC9 gain-of-function variant: Initial experience. *American journal of medical genetics. Part A, 179*(8), 1585-1590. doi:10.1002/ajmg.a.61200

Ma, J., Guo, L., Fiene, S. J., Anson, B. D., Thomson, J. A., Kamp, T. J., . . . January, C. T. (2011). High purity human-induced pluripotent stem cell-derived cardiomyocytes: electrophysiological properties of action potentials and ionic currents. *Am J Physiol Heart Circ Physiol, 301*(5), H2006-2017. doi:10.1152/ajpheart.00694.2011

Maguire, E. M., Xiao, Q., & Xu, Q. (2017). Differentiation and Application of Induced Pluripotent Stem Cell-Derived Vascular Smooth Muscle Cells. *Arterioscler Thromb Vasc Biol, 37*(11), 2026-2037. doi:10.1161/ATVBAHA.117.309196

Mannhold, R. (2004). KATP channel openers: structure-activity relationships and therapeutic potential. *Med Res Rev, 24*(2), 213-266. doi:10.1002/med.10060

Martin, G. M., Kandasamy, B., DiMaio, F., Yoshioka, C., & Shyng, S. L. (2017). Anti-diabetic drug binding site in a mammalian KATP channel revealed by Cryo-EM. *Elife, 6*. doi:10.7554/eLife.31054

Martin, G. R. (1981). Isolation of a pluripotent cell line from early mouse embryos cultured in medium conditioned by teratocarcinoma stem cells. *Proc Natl Acad Sci U S A, 78*(12), 7634-7638. doi:10.1073/pnas.78.12.7634

Mathie, A., Veale, E. L., & Holden, R. G. (2021). Heterologous Expression of Ion Channels in Mammalian Cell Lines. *Methods Mol Biol, 2188*, 51-65. doi:10.1007/978-1-0716-0818-0_3

Matsa, E., Rajamohan, D., Dick, E., Young, L., Mellor, I., Staniforth, A., & Denning, C. (2011). Drug evaluation in cardiomyocytes derived from human induced pluripotent stem cells carrying a long QT syndrome type 2 mutation. *Eur Heart J, 32*(8), 952-962. doi:10.1093/eurheartj/ehr073

Matsuoka, T., Matsushita, K., Katayama, Y., Fujita, A., Inageda, K., Tanemoto, M., . . . Kurachi, Y. (2000). C-Terminal tails of sulfonylurea receptors control ADP-induced activation and diazoxide modulation of ATP-sensitive K(+) channels. *Circ Res, 87*(10), 873-880.

McClenaghan, C., Hanson, A., Sala-Rabanal, M., Roessler, H. I., Josifova, D., Grange, D. K., . . . Nichols, C. G. (2018). Cantu syndrome-associated SUR2 (ABCC9) mutations in distinct structural domains result in KATP channel gain-of-function by differential mechanisms. *The Journal of biological chemistry, 293*(6), 2041-2052. doi:10.1074/jbc.RA117.000351

McClenaghan, C., Huang, Y., Matkovich, S. J., Kovacs, A., Weinheimer, C. J., Perez, R., . . . Nichols, C. G. (2020). The Mechanism of High-Output Cardiac Hypertrophy Arising From Potassium Channel Gain-of-Function in Cantu Syndrome. *Function, 1*(1), zqaa004. doi:10.1093/function/zqaa004

McClenaghan, C., Huang, Y., Yan, Z., Harter, T., Halabi, C. M., Chalk, R., . . . Nichols, C. G. (2020). Glibenclamide reverses cardiovascular abnormalities of Cantu Syndrome driven by KATP channel overactivity. *J Clin Invest, (in press)*. doi:10.1172/JCI130571

McGowan, S. E., Jackson, S. K., Olson, P. J., Parekh, T., & Gold, L. I. (1997). Exogenous and endogenous transforming growth factors-beta influence elastin gene

expression in cultured lung fibroblasts. *Am J Respir Cell Mol Biol, 17*(1), 25-35. doi:10.1165/ajrcmb.17.1.2686

Mecham, R. P., Whitehouse, L. A., Wrenn, D. S., Parks, W. C., Griffin, G. L., Senior, R. M., . . . Voelkel, N. F. (1987). Smooth muscle-mediated connective tissue remodeling in pulmonary hypertension. *Science, 237*(4813), 423-426. doi:10.1126/science.3603030

Mehta, P. K., Mamdani, B., Shansky, R. M., Mahurkar, S. D., & Dunea, G. (1975). Severe hypertension. Treatment with minoxidil. *JAMA, 233*(3), 249-252.

Meisheri, K. D., Cipkus, L. A., & Taylor, C. J. (1988). Mechanism of action of minoxidil sulfate-induced vasodilation: a role for increased K+ permeability. *J Pharmacol Exp Ther, 245*(3), 751-760.

Miano, J. M., Zhu, Q. M., & Lowenstein, C. J. (2016). A CRISPR Path to Engineering New Genetic Mouse Models for Cardiovascular Research. *Arterioscler Thromb Vasc Biol, 36*(6), 1058-1075. doi:10.1161/ATVBAHA.116.304790

Miki, T., Minami, K., Shinozaki, H., Matsumura, K., Saraya, A., Ikeda, H., . . . Seino, S. (2005). Distinct effects of glucose-dependent insulinotropic polypeptide and glucagon-like peptide-1 on insulin secretion and gut motility. *Diabetes, 54*(4), 1056-1063. doi:10.2337/diabetes.54.4.1056

Miki, T., & Seino, S. (2005). Roles of KATP channels as metabolic sensors in acute metabolic changes. *Journal of Molecular & Cellular Cardiology, 38*(6), 917-925.

Moreau, C., Jacquet, H., Prost, A. L., D'Hahan, N., & Vivaudou, M. (2000). The molecular basis of the specificity of action of K(ATP) channel openers. *EMBO J, 19*(24), 6644-6651. doi:10.1093/emboj/19.24.6644

Moretti, A., Bellin, M., Welling, A., Jung, C. B., Lam, J. T., Bott-Flugel, L., . . . Laugwitz, K. L. (2010). Patient-specific induced pluripotent stem-cell models for long-QT syndrome. *N Engl J Med, 363*(15), 1397-1409. doi:10.1056/NEJMoa0908679

Nakashima, M., & Vanhoutte, P. M. (1995). Isoproterenol causes hyperpolarization through opening of ATP-sensitive potassium channels in vascular smooth muscle of the canine saphenous vein. *J Pharmacol Exp Ther, 272*(1), 379-384.

Nelson, M. T., Huang, Y., Brayden, J. E., Hescheler, J., & Standen, N. B. (1990). Arterial dilations in response to calcitonin gene-related peptide involve activation of K+ channels. *Nature, 344*(6268), 770-773.

Nelson, M. T., Patlak, J. B., Worley, J. F., & Standen, N. B. (1990). Calcium channels, potassium channels, and voltage dependence of arterial smooth muscle tone. *Am J Physiol, 259*(1 Pt 1), C3-18.

Nichols, A. J., Koster, P. F., & Ohlstein, E. H. (1990). The effect of diltiazem on the coronary haemodynamic and cardiac functional effects produced by intracoronary administration of endothelin-1 in the anaesthetized dog. *Br J Pharmacol, 99*(3), 597-601.

Nichols, C. G. (2006). KATP channels as molecular sensors of cellular metabolism. *Nature, 440*, 471-476.

Nichols, C. G., Koster, J. C., Enkvetchakul, D., & Flagg, T. P. (2006). KATP channels: From structure to disease. *Biological Membranes, 23*, 101-110.

Nichols, C. G., & Lederer, W. J. (1990a). The regulation of ATP-sensitive K+ channel activity in intact and permeabilized rat ventricular myocytes. *Journal of Physiology London, 423*(91), 91-110.
Nichols, C. G., & Lederer, W. J. (1990b). The role of ATP in energy-deprivation contractures in unloaded rat ventricular myocytes. *Canadian Journal of Physiology & Pharmacology, 68*(2), 183-194.
Nichols, C. G., Shyng, S. L., Nestorowicz, A., Glaser, B., Clement, J. P., Gonzalez, G., . . . Bryan, J. (1996). Adenosine Diphosphate As an Intracellular Regulator Of Insulin Secretion. *Science, 272*(5269), 1785-1787.
Nichols, C. G., Singh, G. K., & Grange, D. K. (2013). KATP channels and cardiovascular disease: suddenly a syndrome. *Circulation Research, 112*(7), 1059-1072. doi:10.1161/CIRCRESAHA.112.300514
Noma, A. (1983). ATP-regulated K+ channels in cardiac muscle. *Nature, 305*(5930), 147-148.
Noseda, M., Peterkin, T., Simoes, F. C., Patient, R., & Schneider, M. D. (2011). Cardiopoietic factors: extracellular signals for cardiac lineage commitment. *Circ Res, 108*(1), 129-152. doi:10.1161/CIRCRESAHA.110.223792
Novak, A., Barad, L., Zeevi-Levin, N., Shick, R., Shtrichman, R., Lorber, A., . . . Binah, O. (2012). Cardiomyocytes generated from CPVTD307H patients are arrhythmogenic in response to beta-adrenergic stimulation. *J Cell Mol Med, 16*(3), 468-482. doi:10.1111/j.1582-4934.2011.01476.x
Oh, J. E., Jung, C., & Yoon, Y. S. (2021). Human Induced Pluripotent Stem Cell-Derived Vascular Cells: Recent Progress and Future Directions. *J Cardiovasc Dev Dis, 8*(11). doi:10.3390/jcdd8110148
Olson, E. N. (2006). Gene regulatory networks in the evolution and development of the heart. *Science, 313*(5795), 1922-1927. doi:10.1126/science.1132292
Olson, W. K., Bansal, M., Burley, S. K., Dickerson, R. E., Gerstein, M., Harvey, S. C., . . . Berman, H. M. (2001). A standard reference frame for the description of nucleic acid base-pair geometry. *Journal of Molecular Biology, 313*(1), 229-237.
Ortiz, D., Gossack, L., Quast, U., & Bryan, J. (2013). Reinterpreting the action of ATP analogs on K(ATP) channels. *J Biol Chem, 288*(26), 18894-18902. doi:10.1074/jbc.M113.476887
Pagani, F., Buratti, E., Stuani, C., & Baralle, F. E. (2003). Missense, nonsense, and neutral mutations define juxtaposed regulatory elements of splicing in cystic fibrosis transmembrane regulator exon 9. *The Journal of biological chemistry, 278*(29), 26580-26588. doi:10.1074/jbc.M212813200
Parks, W. C. (1997). Posttranscriptional regulation of lung elastin production. *Am J Respir Cell Mol Biol, 17*(1), 1-2. doi:10.1165/ajrcmb.17.1.f135
Parrott, A., Lombardo, R., Brown, N., Tretter, J. T., Riley, L., & Weaver, K. N. (2020). Cantu syndrome: A longitudinal review of vascular findings in three individuals. *Am J Med Genet A, 182*(5), 1243-1248. doi:10.1002/ajmg.a.61521
Patsch, C., Challet-Meylan, L., Thoma, E. C., Urich, E., Heckel, T., O'Sullivan, J. F., . . . Cowan, C. A. (2015). Generation of vascular endothelial and smooth muscle cells

from human pluripotent stem cells. *Nat Cell Biol, 17*(8), 994-1003. doi:10.1038/ncb3205

Pennisi, A. J., Takahashi, M., Bernstein, B. H., Singsen, B. H., Uittenbogaart, C., Ettenger, R. B., . . . Fine, R. N. (1977). Minoxidil therapy in children with severe hypertension. *The Journal of pediatrics, 90*(5), 813-819.

Perlman, R. L. (2016). Mouse models of human disease: An evolutionary perspective. *Evol Med Public Health, 2016*(1), 170-176. doi:10.1093/emph/eow014

Pozzoli, U., & Sironi, M. (2005). Silencers regulate both constitutive and alternative splicing events in mammals. *Cellular and molecular life sciences : CMLS, 62*(14), 1579-1604. doi:10.1007/s00018-005-5030-6

Proks, P. (2013). Neonatal diabetes caused by activating mutations in the sulphonylurea receptor. *Diabetes & metabolism journal, 37*(3), 157-164. doi:10.4093/dmj.2013.37.3.157

Proks, P., de Wet, H., & Ashcroft, F. M. (2013). Molecular mechanism of sulphonylurea block of K(ATP) channels carrying mutations that impair ATP inhibition and cause neonatal diabetes. *Diabetes, 62*(11), 3909-3919. doi:10.2337/db13-0531

Proks, P., de Wet, H., & Ashcroft, F. M. (2014). Sulfonylureas suppress the stimulatory action of Mg-nucleotides on Kir6.2/SUR1 but not Kir6.2/SUR2A KATP channels: a mechanistic study. *J Gen Physiol, 144*(5), 469-486. doi:10.1085/jgp.201411222

Pu, J. L., Ye, B., Kroboth, S. L., McNally, E. M., Makielski, J. C., & Shi, N. Q. (2008). Cardiac sulfonylurea receptor short form-based channels confer a glibenclamide-insensitive K(ATP) activity. *Journal of Molecular & Cellular Cardiology, 44*, 188-200. Epub 2007 Sep 2029.

Pushp, P., Nogueira, D. E. S., Rodrigues, C. A. V., Ferreira, F. C., Cabral, J. M. S., & Gupta, M. K. (2021). A Concise Review on Induced Pluripotent Stem Cell-Derived Cardiomyocytes for Personalized Regenerative Medicine. *Stem Cell Rev Rep, 17*(3), 748-776. doi:10.1007/s12015-020-10061-2

Quamme, G. A., & Rabkin, S. W. (1990). Cytosolic free magnesium in cardiac myocytes: identification of a Mg2+ influx pathway. *Biochem Biophys Res Commun, 167*(3), 1406-1412. doi:10.1016/0006-291x(90)90679-h

Quayle, J. M., Nelson, M. T., & Standen, N. B. (1997). ATP-sensitive and inwardly rectifying potassium channels in smooth muscle. *Physiol Rev, 77*(4), 1165-1232. doi:10.1152/physrev.1997.77.4.1165

Quinn, K. V., Cui, Y., Giblin, J. P., Clapp, L. H., & Tinker, A. (2003). Do anionic phospholipids serve as cofactors or second messengers for the regulation of activity of cloned ATP-sensitive K+ channels? *Circ Res, 93*(7), 646-655. doi:10.1161/01.RES.0000095247.81449.8E

Ramratnam, M., Kenny, B., Kyle, J. W., Wiedmeyer, B., Hacker, T. A., Barefield, D. Y., . . . Makielski, J. C. (2018). Transgenic overexpression of the SUR2A-55 splice variant in mouse heart reduces infract size and promotes protective mitochondrial function. *Heliyon, 4*(7), e00677. doi:10.1016/j.heliyon.2018.e00677

Ran, F. A., Hsu, P. D., Wright, J., Agarwala, V., Scott, D. A., & Zhang, F. (2013). Genome engineering using the CRISPR-Cas9 system. *Nat Protoc, 8*(11), 2281-2308. doi:10.1038/nprot.2013.143

Reimann, F., Dabrowski, M., Jones, P., Gribble, F. M., & Ashcroft, F. M. (2003). Analysis of the differential modulation of sulphonylurea block of beta-cell and cardiac ATP-sensitive K+ (K(ATP)) channels by Mg-nucleotides. *J Physiol, 547*(Pt 1), 159-168. doi:10.1113/jphysiol.2002.031625
2002.031625 [pii]
Reimann, F., Gribble, F. M., & Ashcroft, F. M. (2000). Differential response of K(ATP) channels containing SUR2A or SUR2B subunits to nucleotides and pinacidil. *Mol Pharmacol, 58*(6), 1318-1325.
Ribalet, B., John, S. A., Xie, L. H., & Weiss, J. N. (2005). Regulation of the ATP-sensitive K channel Kir6.2 by ATP and PIP(2). *Journal of Molecular & Cellular Cardiology, 39*(1), 71-77.
Robertson, S. P., Kirk, E., Bernier, F., Brereton, J., Turner, A., & Bankier, A. (1999). Congenital hypertrichosis, osteochondrodysplasia, and cardiomegaly: Cantu syndrome. *American Journal of Medical Genetics, 85*(4), 395-402.
Rosser, E. M., Kaariainen, H., Hurst, J. A., Baraitser, M., Hall, C. M., Clayton, P., & Leonard, J. V. (1998). Three patients with the osteochondrodysplasia and hypertrichosis syndrome--Cantu syndrome. *Clinical dysmorphology, 7*(2), 79-85.
Scheuer, J. (1999). Catecholamines in cardiac hypertrophy. *Am J Cardiol, 83*(12A), 70H-74H. doi:10.1016/s0002-9149(99)00264-7
Schwach, V., & Passier, R. (2019). Native cardiac environment and its impact on engineering cardiac tissue. *Biomater Sci, 7*(9), 3566-3580. doi:10.1039/c8bm01348a
Scurr, I., Wilson, L., Lees, M., Robertson, S., Kirk, E., Turner, A., . . . Smithson, S. (2011). Cantu syndrome: report of nine new cases and expansion of the clinical phenotype. *American journal of medical genetics. Part A, 155A*(3), 508-518. doi:10.1002/ajmg.a.33885
Shen, M., Quertermous, T., Fischbein, M. P., & Wu, J. C. (2021). Generation of Vascular Smooth Muscle Cells From Induced Pluripotent Stem Cells: Methods, Applications, and Considerations. *Circ Res, 128*(5), 670-686. doi:10.1161/CIRCRESAHA.120.318049
Shi, N. Q., Ye, B., & Makielski, J. C. (2005). Function and distribution of the SUR isoforms and splice variants. *Journal of Molecular & Cellular Cardiology, 39*(1), 51-60.
Shiota, C., Larsson, O., Shelton, K. D., Shiota, M., Efanov, A. M., Hoy, M., . . . Magnuson, M. A. (2002). Sulfonylurea receptor type 1 knock-out mice have intact feeding-stimulated insulin secretion despite marked impairment in their response to glucose. *Journal of Biological Chemistry, 277*(40), 37176-37183.
Shyng, S., Ferrigni, T., & Nichols, C. G. (1997). Regulation of KATP channel activity by diazoxide and MgADP. Distinct functions of the two nucleotide binding folds of the sulfonylurea receptor. *J Gen Physiol, 110*(6), 643-654.
Shyng, S. L., & Nichols, C. G. (1998). Membrane phospholipid control of nucleotide sensitivity of KATP channels. *Science, 282*(5391), 1138-1141.
Slove, S., Lannoy, M., Behmoaras, J., Pezet, M., Sloboda, N., Lacolley, P., . . . Jacob, M. P. (2013). Potassium channel openers increase aortic elastic fiber formation and

reverse the genetically determined elastin deficit in the BN rat. *Hypertension, 62*(4), 794-801. doi:10.1161/HYPERTENSIONAHA.113.01379

Smeland, M. F., McClenaghan, C., Roessler, H. I., Savelberg, S., Hansen, G. A. M., Hjellnes, H., . . . van Haaften, G. (2019). ABCC9-related Intellectual disability Myopathy Syndrome is a KATP channelopathy with loss-of-function mutations in ABCC9. *Nature communications, 10*(1), 4457. doi:10.1038/s41467-019-12428-7

Smirnov, S. V., & Aaronson, P. I. (1992). Ca(2+)-activated and voltage-gated K+ currents in smooth muscle cells isolated from human mesenteric arteries. *J Physiol, 457*, 431-454. doi:10.1113/jphysiol.1992.sp019386

Spruce, A. E., Standen, N. B., & Stanfield, P. R. (1985). Voltage-dependent ATP-sensitive potassium channels of skeletal muscle membrane. *Nature, 316*(6030), 736-738. doi:10.1038/316736a0

Stegemann, J. P., Hong, H., & Nerem, R. M. (2005). Mechanical, biochemical, and extracellular matrix effects on vascular smooth muscle cell phenotype. *J Appl Physiol (1985), 98*(6), 2321-2327. doi:10.1152/japplphysiol.01114.2004

Sun, N., Yazawa, M., Liu, J., Han, L., Sanchez-Freire, V., Abilez, O. J., . . . Wu, J. C. (2012). Patient-specific induced pluripotent stem cells as a model for familial dilated cardiomyopathy. *Sci Transl Med, 4*(130), 130ra147. doi:10.1126/scitranslmed.3003552

Suzuki, M., Li, R. A., Miki, T., Uemura, H., Sakamoto, N., Ohmoto-Sekine, Y., . . . Nakaya, H. (2001). Functional roles of cardiac and vascular ATP-sensitive potassium channels clarified by Kir6.2-knockout mice. *Circ Res, 88*(6), 570-577.

Suzuki, M., Sasaki, N., Miki, T., Sakamoto, N., Ohmoto-Sekine, Y., Tamagawa, M., . . . Nakaya, H. (2002). Role of sarcolemmal K(ATP) channels in cardioprotection against ischemia/reperfusion injury in mice. *J Clin Invest, 109*(4), 509-516.

Swaminathan, R. (2003). Magnesium metabolism and its disorders. *Clin Biochem Rev, 24*(2), 47-66.

Tada, M., Takahama, Y., Abe, K., Nakatsuji, N., & Tada, T. (2001). Nuclear reprogramming of somatic cells by in vitro hybridization with ES cells. *Curr Biol, 11*(19), 1553-1558. doi:10.1016/s0960-9822(01)00459-6

Tajima, S., Hayashi, A., Suzuki, T., & Nishikawa, T. (1995). Stimulation of elastin expression by minoxidil in chick skin fibroblasts. *Arch Dermatol Res, 287*(5), 494-497. doi:10.1007/BF00373434

Takahashi, K., Tanabe, K., Ohnuki, M., Narita, M., Ichisaka, T., Tomoda, K., & Yamanaka, S. (2007). Induction of pluripotent stem cells from adult human fibroblasts by defined factors. *Cell, 131*(5), 861-872. doi:10.1016/j.cell.2007.11.019

Takahashi, K., & Yamanaka, S. (2006). Induction of pluripotent stem cells from mouse embryonic and adult fibroblast cultures by defined factors. *Cell, 126*(4), 663-676. doi:10.1016/j.cell.2006.07.024

Tao, X., Avalos, J. L., Chen, J., & MacKinnon, R. (2009). Crystal structure of the eukaryotic strong inward-rectifier K+ channel Kir2.2 at 3.1 A resolution. *Science, 326*(5960), 1668-1674. doi:326/5960/1668 [pii]

10.1126/science.1180310

Tapper, A. R., & George, A. L., Jr. (2003). Heterologous expression of ion channels. *Methods Mol Biol, 217*, 285-294. doi:10.1385/1-59259-330-5:285

Teramoto, N. (2006). Physiological roles of ATP-sensitive K+ channels in smooth muscle. *J Physiol, 572*(Pt 3), 617-624. doi:10.1113/jphysiol.2006.105973

Tohyama, S., Hattori, F., Sano, M., Hishiki, T., Nagahata, Y., Matsuura, T., . . . Fukuda, K. (2013). Distinct metabolic flow enables large-scale purification of mouse and human pluripotent stem cell-derived cardiomyocytes. *Cell stem cell, 12*(1), 127-137. doi:10.1016/j.stem.2012.09.013

Trillhaase, A., Maertens, M., Aherrahrou, Z., & Erdmann, J. (2021). Induced Pluripotent Stem Cells (iPSCs) in Vascular Research: from Two- to Three-Dimensional Organoids. *Stem Cell Rev Rep, 17*(5), 1741-1753. doi:10.1007/s12015-021-10149-3

Tsui, L. C., & Dorfman, R. (2013). The cystic fibrosis gene: a molecular genetic perspective. *Cold Spring Harb Perspect Med, 3*(2), a009472. doi:10.1101/cshperspect.a009472

Ueda, K., Inagaki, N., & Seino, S. (1997). MgADP antagonism to Mg2+-independent ATP binding of the sulfonylurea receptor SUR1. *J Biol Chem, 272*(37), 22983-22986.

Ueda, K., Komine, J., Matsuo, M., Seino, S., & Amachi, T. (1999). Cooperative binding of ATP and MgADP in the sulfonylurea receptor is modulated by glibenclamide. *Proc Natl Acad Sci U S A, 96*(4), 1268-1272.

Uhde, I., Toman, A., Gross, I., Schwanstecher, C., & Schwanstecher, M. (1999). Identification of the potassium channel opener site on sulfonylurea receptors. *The Journal of biological chemistry, 274*(40), 28079-28082. doi:10.1074/jbc.274.40.28079

Uosaki, H., Fukushima, H., Takeuchi, A., Matsuoka, S., Nakatsuji, N., Yamanaka, S., & Yamashita, J. K. (2011). Efficient and scalable purification of cardiomyocytes from human embryonic and induced pluripotent stem cells by VCAM1 surface expression. *PLoS One, 6*(8), e23657. doi:10.1371/journal.pone.0023657

van Bon, B. W., Gilissen, C., Grange, D. K., Hennekam, R. C., Kayserili, H., Engels, H., . . . Hoischen, A. (2012). Cantu syndrome is caused by mutations in ABCC9. *American journal of human genetics, 90*(6), 1094-1101. doi:10.1016/j.ajhg.2012.04.014

van Mil, A., Balk, G. M., Neef, K., Buikema, J. W., Asselbergs, F. W., Wu, S. M., . . . Sluijter, J. P. G. (2018). Modelling inherited cardiac disease using human induced pluripotent stem cell-derived cardiomyocytes: progress, pitfalls, and potential. *Cardiovasc Res, 114*(14), 1828-1842. doi:10.1093/cvr/cvy208

Vanoye, C. G., MacGregor, G. G., Dong, K., Tang, L., Buschmann, A. S., Hall, A. E., . . . Hebert, S. C. (2002). The carboxyl termini of K(ATP) channels bind nucleotides. *J Biol Chem, 277*(26), 23260-23270.

Vedovato, N., Cliff, E., Proks, P., Poovazhagi, V., Flanagan, S. E., Ellard, S., . . . Ashcroft, F. M. (2016). Neonatal diabetes caused by a homozygous KCNJ11 mutation demonstrates that tiny changes in ATP sensitivity markedly affect diabetes risk. *Diabetologia, 59*(7), 1430-1436. doi:10.1007/s00125-016-3964-x

von Scheidt, M., Zhao, Y., Kurt, Z., Pan, C., Zeng, L., Yang, X., . . . Lusis, A. J. (2017). Applications and Limitations of Mouse Models for Understanding Human Atherosclerosis. *Cell Metab, 25*(2), 248-261. doi:10.1016/j.cmet.2016.11.001

Wagenseil, J. E., Ciliberto, C. H., Knutsen, R. H., Levy, M. A., Kovacs, A., & Mecham, R. P. (2009). Reduced vessel elasticity alters cardiovascular structure and function in newborn mice. *Circ Res, 104*(10), 1217-1224. doi:10.1161/CIRCRESAHA.108.192054

Wagenseil, J. E., & Mecham, R. P. (2009). Vascular extracellular matrix and arterial mechanics. *Physiol Rev, 89*(3), 957-989. doi:10.1152/physrev.00041.2008

Wang, Y., Liang, P., Lan, F., Wu, H., Lisowski, L., Gu, M., . . . Wu, J. C. (2014). Genome editing of isogenic human induced pluripotent stem cells recapitulates long QT phenotype for drug testing. *J Am Coll Cardiol, 64*(5), 451-459. doi:10.1016/j.jacc.2014.04.057

Welch, C. L., & Chung, W. K. (2022). Channelopathy Genes in Pulmonary Arterial Hypertension. *Biomolecules, 12*(2). doi:10.3390/biom12020265

Welsh, D. G., Jackson, W. F., & Segal, S. S. (1998). Oxygen induces electromechanical coupling in arteriolar smooth muscle cells: a role for L-type Ca2+ channels. *Am J Physiol, 274*(6), H2018-2024. doi:10.1152/ajpheart.1998.274.6.H2018

Welsh, D. G., Nelson, M. T., Eckman, D. M., & Brayden, J. E. (2000). Swelling-activated cation channels mediate depolarization of rat cerebrovascular smooth muscle by hyposmolarity and intravascular pressure. *J Physiol, 527 Pt 1*, 139-148. doi:10.1111/j.1469-7793.2000.t01-1-00139.x

Wu, J., Cui, N., Piao, H., Wang, Y., Xu, H., Mao, J., & Jiang, C. (2002). Allosteric modulation of the mouse Kir6.2 channel by intracellular H+ and ATP. *Journal of Physiology, 543*(Pt 2), 495-504.

Xu, H., Cui, N., Yang, Z., Wu, J., Giwa, L. R., Abdulkadir, L., . . . Jiang, C. (2001). Direct activation of cloned K(atp) channels by intracellular acidosis. *Journal of Biological Chemistry, 276*(16), 12898-12902.

Yamada, M., Isomoto, S., Matsumoto, S., Kondo, C., Shindo, T., Horio, Y., & Kurachi, Y. (1997). Sulphonylurea receptor 2B and Kir6.1 form a sulphonylurea-sensitive but ATP-insensitive K+ channel. *Journal of Physiology, 499*(Pt 3), 715-720.

Yazawa, M., Hsueh, B., Jia, X., Pasca, A. M., Bernstein, J. A., Hallmayer, J., & Dolmetsch, R. E. (2011). Using induced pluripotent stem cells to investigate cardiac phenotypes in Timothy syndrome. *Nature, 471*(7337), 230-234. doi:10.1038/nature09855

Ye, B., Kroboth, S. L., Pu, J. L., Sims, J. J., Aggarwal, N. T., McNally, E. M., . . . Shi, N. Q. (2009). Molecular identification and functional characterization of a mitochondrial sulfonylurea receptor 2 splice variant generated by intraexonic splicing. *Circ Res, 105*(11), 1083-1093. doi:10.1161/CIRCRESAHA.109.195040

York, N. W., Parker, H., Xie, Z., Tyus, D., Waheed, M. A., Yan, Z., . . . Nichols, C. G. (2020). Kir6.1- and SUR2-dependent KATP over-activity disrupts intestinal motility in murine models of Cantu Syndrome. *JCI insight*. doi:10.1172/jci.insight.141443

Yu, J., Vodyanik, M. A., Smuga-Otto, K., Antosiewicz-Bourget, J., Frane, J. L., Tian, S., . . . Thomson, J. A. (2007). Induced pluripotent stem cell lines derived from human somatic cells. *Science, 318*(5858), 1917-1920. doi:10.1126/science.1151526

Zaragoza, C., Gomez-Guerrero, C., Martin-Ventura, J. L., Blanco-Colio, L., Lavin, B., Mallavia, B., . . . Egido, J. (2011). Animal models of cardiovascular diseases. *J Biomed Biotechnol, 2011*, 497841. doi:10.1155/2011/497841

Zaritsky, J. J., Eckman, D. M., Wellman, G. C., Nelson, M. T., & Schwarz, T. L. (2000). Targeted disruption of Kir2.1 and Kir2.2 genes reveals the essential role of the inwardly rectifying K(+) current in K(+)-mediated vasodilation.[see comment]. *Circulation Research, 87*(2), 160-166.

Zaritsky, J. J., Redell, J. B., Tempel, B. L., & Schwarz, T. L. (2001). The consequences of disrupting cardiac inwardly rectifying K(+) current (I(K1)) as revealed by the targeted deletion of the murine Kir2.1 and Kir2.2 genes. *J Physiol, 533*(Pt 3), 697-710. doi:10.1111/j.1469-7793.2001.t01-1-00697.x

Zhang, H., Hanson, A., de Almeida, T. S., Emfinger, C., McClenaghan, C., Harter, T., . . . Nichols, C. G. (2021). Complex consequences of Cantu syndrome SUR2 variant R1154Q in genetically modified mice. *JCI Insight, 6*(5). doi:10.1172/jci.insight.145934

Zhang, J., Klos, M., Wilson, G. F., Herman, A. M., Lian, X., Raval, K. K., . . . Kamp, T. J. (2012). Extracellular matrix promotes highly efficient cardiac differentiation of human pluripotent stem cells: the matrix sandwich method. *Circulation Research, 111*(9), 1125-1136. doi:10.1161/CIRCRESAHA.112.273144

Zhang, J., Wilson, G. F., Soerens, A. G., Koonce, C. H., Yu, J., Palecek, S. P., . . . Kamp, T. J. (2009). Functional cardiomyocytes derived from human induced pluripotent stem cells. *Circ Res, 104*(4), e30-41. doi:10.1161/CIRCRESAHA.108.192237

Zhang, M. C., Giro, M., Quaglino, D., & Davidson, J. M. (1995). Transforming growth factor-beta reverses a posttranscriptional defect in elastin synthesis in a cutis laxa skin fibroblast strain. *J Clin Invest, 95*(3), 986-994. doi:10.1172/JCI117808

Zhu, W., Mazzanti, A., Voelker, T. L., Hou, P., Moreno, J. D., Angsutararux, P., . . . Silva, J. R. (2019). Predicting Patient Response to the Antiarrhythmic Mexiletine Based on Genetic Variation. *Circ Res, 124*(4), 539-552. doi:10.1161/CIRCRESAHA.118.314050

Zingman, L. V., Alekseev, A. E., Bienengraeber, M., Hodgson, D., Karger, A. B., Dzeja, P. P., & Terzic, A. (2001). Signaling in channel/enzyme multimers: ATPase transitions in SUR module gate ATP-sensitive K+ conductance. *Neuron, 31*(2), 233-245.

Zwi, L., Caspi, O., Arbel, G., Huber, I., Gepstein, A., Park, I. H., & Gepstein, L. (2009). Cardiomyocyte differentiation of human induced pluripotent stem cells. *Circulation, 120*(15), 1513-1523. doi:10.1161/CIRCULATIONAHA.109.868885

Cardiovascular Electrophysiology and Pathogenic Consequences of Vascular K_{ATP} Channel Mutations, Hanson, B.A. 2014